ABSTRACT

Title of Thesis: Influence of the Air Gap in Firefighter Personal Protective Equipment on Skin Temperature in Pre-Flashover Thermal Exposures

Shaheer Ahmad
Masters of Science, 2022

Thesis directed by: Dr. James A Milke
Department of Fire Protection Engineering

Exposure to pre-flashover thermal conditions is typically considered as routine for many structural firefighters, and these low level thermal exposures pose a threat of burn injury. Skin burns occur as a result of prolonged exposure within these environments, and this hazard must be addressed to reduce the number of firefighters that fall victim to thermal injury. The incorporation of an air gap within firefighter personal protective equipment (PPE) was explored in this work to gain an understanding of the influence of the air gap on skin temperature in pre-flashover thermal exposures. The relationship between the air gap size and skin temperature was investigated both through experimental and numerical means. Experimental testing was conducted to measure the temperatures at a representative skin layer positioned underneath firefighter PPE with an incorporated air gap subject to thermal exposures consistent with pre-flashover conditions. Material property testing

was conducted for the same PPE-air gap assembly and the effective thermal properties for the bulk assembly were input into a computational model constructed with Fire Dynamics Simulator (FDS) to predict the temperatures at the equivalent skin position. The results show that the presence of an air gap within firefighter PPE prolongs the time to critical skin temperatures, and reduces the maximum temperatures reached at the skin surface. As the air gap thickness increases, the time to burn injury increases and the maximum temperatures at the skin decrease for both thermal exposures. These findings fundamentally suggest that the larger the air gap, the more thermal insulation is provided for the firefighter. Based on comparisons of the conduction-driven model with the experimental temperature data, the model was demonstrated to be accurate to within 15% of the experiments in the prediction of burn injury times for low heat flux exposures and small air gap sizes. The agreement of the model also confirms that the heat transfer is conduction-dominated for air gap sizes leading up to 6.35 mm, and transitions to alternative modes of heat transfer among larger air gap sizes.

Influence of the Air Gap in Firefighter Personal Protective Equipment on Skin Temperature in Pre-Flashover Thermal Exposures

by

Shaheer Ahmad

Thesis submitted to the Faculty of the Graduate School of the
University of Maryland, College Park in partial fulfillment
of the requirements for the degree of
Masters of Science
2022

Advisory Committee:
Dr. James A Milke, Chair/Advisor
Dr. Stanislav I Stoliarov, Professor/Committee
Dr. Matthew DiDomizio, UL FSRI/Defense Committee

Acknowledgements

I would like to thank Underwriters Laboratories Fire Safety Research Institute (UL FSRI) for sponsoring this research and selecting me for the UL FSRI fellowship as I pursued my Master of Science at the University of Maryland, College Park. Additionally, I would like to extend my gratitude to the entire UL FSRI team for their support throughout the course of my thesis, whether it be in technical expertise or general research guidance. Specifically, I would like to thank Dr. Matthew DiDomizio for his constant support on my advisory committee and Dr. Daniel Madrzykowski for his involvement during the start of this project.

I would also like to thank the University of Maryland's Department of Fire Protection Engineering for housing me over the duration of both my undergraduate and graduate career. Specifically, I would like to thank Professor James Milke for his guidance, support, and attentiveness as my primary advisor and committee chair. Additionally, I would like to thank Professor Stanislav Stoliarov for agreeing to be a member on my advisory committee.

I am extremely thankful for the unwavering support and care I have received from my friends and family throughout this journey. Thank you to my friends and fellow classmates for the emotional support and aid in alleviating the stresses of this lifestyle. The opportunities presented to me would not have been possible if not for the time, dedication, and effort put in by my parents, Imtiaz and Firzana Ahmad, and for that words cannot express how truly grateful I am.

Table of Contents

List of Tables

List of Figures

List of Abbreviations

ASTM	American Society for Testing and Materials
CFD	Computational Fluid Dynamics
CNC	Computer Numerical Controlled
CPVFD	College Park Volunteer Fire Department
CSV	Comma-Separated Value
DAQ	Data Acquisition
DelCo	Delaware County Emergency Services Training Center
ePTFE	Expanded Polytetrafluoroethylene
FDS	Fire Dynamics Simulator
FSRI	UL Fire Safety Research Institute
ISO	International Organization for Standardization
NFPA	National Fire Protection Association
NIST	National Institute Standards and Technology
PBI	Polybenzimidazole
PCPS	Protective Clothing Performance Simulator
PPE	Personal Protective Equipment
PTFE	Polytetrafluoroethylene
THB	Transient Hot Bridge
THL	Total Heat Loss
TPP	Thermal Protective Performance
UL	Underwriters Laboratories

Chapter 1: Introduction

1.1 Scope of the Problem

Firefighters may be exposed to thermal hazards on the fireground while completing structural firefighting tasks. While dangerous scenarios are not everyday occurrences, the risk of bodily harm remains an ongoing threat associated with the fire service. In this line of work, members of the fire service must employ the proper personal protective equipment (PPE) required to avoid sometimes fatal injuries that can occur when in close proximity to fires or otherwise dangerous thermal conditions.

Burn injuries have been a widespread problem for firefighters nationwide. From the years 2015 to 2017, it was estimated that there were 63,000 firefighter injuries that occurred annually; of these general injuries, 11% were caused from thermal burns alone [1]. Although these injuries may not encompass a wide percentage of the total number of injuries that firefighters may suffer both on and off the fireground, this still results in almost 7,000 firefighters being burned each year while on duty. Not only do burn injuries cause physical and mental trauma, but there are also economic hardships as well. Based on a 2019 study identifying the economic costs for firefighter injuries, burn injuries for firefighters have been calculated to result in an average total cost of approximately $1.34 billion [2]. This total is comprised

of direct and indirect costs including both medical costs to the victim as well as productivity losses for the affected firefighting unit. While improvements have been made in protective clothing and firefighter operating procedures in recent years, burn injuries are an ongoing issue that impacts thousands of fire service members with lasting damage.

The incorporation of an insulating air cavity within firefighter PPE has been explored as a solution in prolonging the time to burn injury and in turn reducing the number of burn injuries for firefighters. There is a need to better quantify and understand the significance of an air gap incorporated within firefighter PPE on skin temperatures under pre-flashover thermal exposures of an extended duration.

In this study, firefighter PPE was analyzed under specific conditions to provide a better understanding of the transfer of heat within the protective material both with and without an additional layer of insulation via air. The firefighter PPE in this analysis was focused on the incorporation of an air gap layer between the PPE and the wearer's undergarments. The PPE material was tested under low levels of thermal exposure to mimic frequently occurring firefighter burn injuries and produce new data on thermal conditions overlooked in prior firefighter PPE studies.

1.2 Background

1.2.1 Fire Environment

Understanding the fire environment is the first step in understanding the impact of an air gap within firefighter PPE. In this analysis, the fire environment is

defined as the surrounding conditions within a structure once a fire has occurred. Structural firefighters work within this fire environment and run the risk of injury via their presence in the hazardous space. The tenability of the fire environment is dependent on several factors such as the available fuel load, ventilation, and orientation of the space. These influential factors are what drive fire behavior and can lead to dangerous conditions for firefighters.

Most structure fires can be categorized as ventilation limited fires that portray fire behavior as a function of the available oxygen level within the space [3]. Typically at the start of a fire within a structure, the doors and windows are closed and the fire consumes the available oxygen to support combustion and grow in size. At this time, the typical fire environment within a structure consists of an untenable hot gas upper layer and a cool tenable lower layer of air towards the floor of the space [4]. As time progresses, the upper layer grows and banks down towards the floor until the oxygen in the room is depleted and the fire begins to decay. During this decay period, both the amount of heat released by the fire and the temperature in the structure decrease. Oxygen is reintroduced into the space once a vent, such as an initially closed door or window, is opened. The opening of a vent may be brought on by firefighters entering the structure or attempting to fight the fire. The reintroduction of oxygen can result in rapid fire growth and potentially lead to flashover conditions. Under flashover conditions, this partially tenable environment can transition into a well-mixed burning gas layer that encompasses the entirety of the room from the ceiling to the floor. In this new untenable environment, temperatures exceed 600°C and heat fluxes exposed to the surfaces within the compartment are between

60 to 200 kW/m^2. The fire is now a fully developed compartment fire capable of simultaneously igniting all potential fuel loads exposed.

Under typical firefighting operations, firefighters are not exposed to heat fluxes of the magnitude created post-flashover. The typical firefighter heat flux exposure falls between 1 to 6 kW/m^2, prior to flashover, with firefighter PPE exposure temperatures ranging between 50°C and 200°C, depending on the severity of the fire [5]. Although these thermal conditions are far below those of a flashover environment, they still pose a threat toward fully protected structural firefighters. Prior studies have found that skin burns occur more frequently at lower levels of radiant heat flux, typically ranging between 5 to 20 kW/m^2 and most burn injuries sustained by firefighters occur in low level fire environments [6]. Despite their low relative magnitude, these conditions cause burn injuries as a result of prolonged exposure, on the order of several minutes. It is important to note that these conditions are generally not strong enough to visibly degrade the exterior turnout gear fabric, meaning that firefighters can be burned with no perceptible indication that it is occurring, and that they should remove themselves from the hazardous environment. This scenario is the fire environment that will be focused upon within this study.

1.2.2 Personal Protective Equipment

Firefighter PPE is an important tool used to protect firefighters not only from thermal damage but from the risks of injury via cuts, abrasions, chemicals, and other hazardous materials. An important part of firefighter PPE is turnout gear.

The full structural turnout gear ensemble worn by firefighters from top to bottom consists of the hood, helmet, coat, gloves, trousers, and boots that each meet the protective standards established in NFPA 1971 [7]. In this study, the term PPE will represent structural firefighting protective clothing which accounts for the coat and trouser elements of the full ensemble, shown in Figure 1.1.

Figure 1.1: Structural Firefighting Coat and Trousers [8]

An additional specification defined in NFPA 1971 is that the coat and trouser elements of the turnout gear must consist of three unique layers of material that each serve a different purpose in protecting the user from the hazards faced in the field [7]. This composite system, in order from the outer most layer inward, is made up of an outer shell, moisture barrier, and thermal liner (composed of both a thermal barrier and face cloth), and each of these layers can be seen in Figure 1.2.

The first fabric layer, the outer shell, is located the furthest from the wearer

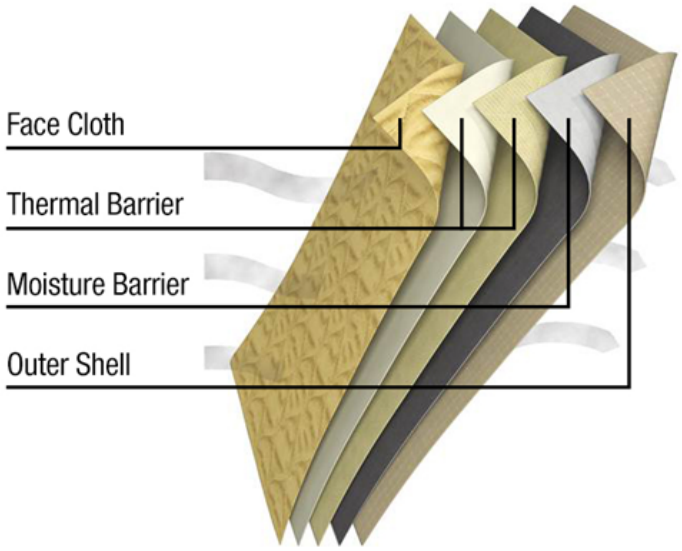

Figure 1.2: Turnout Gear Composite System of Materials [9]

and acts as a first line of defense, primarily focusing on direct flame and abrasion resistance [10]. This layer is typically made from performance blends of polybenzimidazole (PBI), Nomex®, and Kevlar® [10]. PBI is a thermoplastic with a relatively low coefficient of thermal expansion as well as a very high glass transition temperature indicating its excellent performance in high thermal conditions [11]. Nomex® is a synthetic fiber, trademarked by DuPont™, that is both heat and flame-resistant [12]. Kevlar® is also trademarked by DuPont and is not only heat-resistant but a strong synthetic fiber as well, making it an optimal choice to provide durability to firefighter gear [13]. These performance fabrics allow for turnout gear to withstand the hazardous surroundings firefighters face through tear resistance and flame protection.

The second layer within the turnout gear is the moisture barrier, which serves

as a partition that releases perspiration vapor from the body while simultaneously blocking liquids from penetrating inward toward the user [14]. In addition to liquids, this barrier also provides the wearer with resistance to chemicals and viral agents or pathogens [14]. The breathability of this layer helps in removing heat, through sweat moisture produced by the firefighter, which in turn prevents the body's core temperature from overheating to dangerous levels, also known as heat stress [15]. This middle layer is made up of a fabric substrate, using a blend of PBI and Nomex®, with a permeable film membrane made from expanded polytetrafluoroethylene (ePTFE) [10]. Once expanded, the polymer polytetrafluoroethylene (PTFE) becomes a versatile substance with a porous structure that has both a high thermal resistance as well as a high strength-to-weight ratio [16]. The use of these materials in this layer indicates the emphasis on the liquid resistance and absorptivity that wicks the moisture away from the body.

The third layer, the thermal liner, is the closest layer of material to the wearer and is used to reduce the amount of heat transferred from the hazardous firefighting environment to the body of the firefighter themselves [10]. Given the crucial role of this member in the composite system, insulation and thermal protection is a high priority of the fabric used. The thermal liner is made up of two sub-elements, the face cloth and batting [10]. The face cloth is primarily made from Nomex® and other aramid-based synthetic fibers, and is the surface exposed to the user that is fabricated to be comfortable enough to wear and conduct work in [17]. The batting or thermal barrier is typically made from a non-woven felt-like Nomex® material to provide an increased reduction in the heat transfer throughout this layer [18].

The batting fabric is either laminated or sewn into the face fabric to establish a comfortable element of thermal protection to bridge the PPE composite system to the user's skin or undergarments.

An additional element to note in the firefighter PPE system is the presence of a cotton undergarment. Cotton stationwear describes the standard uniforms worn by firefighters under their turnout gear when they are at the fire station. To depict the stationwear, a layer of cotton is incorporated into the PPE-air gap assembly to represent the stationwear shirt located on the interior surface of the air gap. In this analysis, cotton stationwear will be used to represent the user's skin as it can be assumed that the cotton and skin will be in direct contact with one another.

While firefighter PPE is typically designed to fit the individual user, turnout gear can often come across as bulky and obstructive in the range of mobility. There is a counterbalance that must be reached between creating large turnout gear to ensure the utmost protection for the firefighter, and reducing the size of the gear to allow for the firefighter to still be mobile enough to complete the necessary tasks at hand. Currently, there is no incorporated air gap within the structural firefighter turnout gear. That being said, air gaps do arise within the gear as a factor of the additional equipment worn by the wearer. While gaps may not be apparent under areas of compression or load-bearing gear, there is the possibility of an air gap to be formed at locations of slack within the gear, such as along the forearms or legs of the individual. While the incorporation of a manufactured air gap may result in furthering the lack of mobility of a firefighter, the influence of an air gap must be studied to understand if the advantages of the gap outweigh the potential drawbacks

of a more bulky ensemble. This is the motivation for the work conducted in this study.

1.2.3 Heat Transfer

Regardless of the effectiveness of firefighter PPE, burn injuries can still occur as a result of skin exposure to high temperatures or substantial levels of incident heat. Heat transfer is defined as the transfer of energy between two objects with differing temperatures [19]. For any material of finite mass, the specific heat capacity is a physical property that represents the amount of energy required to increase the temperature of that mass by one unit change. In a fire scenario, heat is transferred to firefighters from the fire and hot surroundings. There are three modes of heat transfer: conduction, convection, and radiation.

Conduction represents the transfer of heat through a solid material [19]. Heat flow via conduction is a function of the thermal conductivity, thickness, and temperature gradient within the solid in which the heat is being transferred through. The governing heat transfer equation for steady-state one-dimensional conductive heat flux is presented as Equation 1.1 with k representing the thermal conductivity of the material, L representing the thickness of the material, and the temperature difference of the indicated solid is depicted with ΔT [19]. The incorporated minus sign in this equation indicates that heat is being transferred from high to low temperatures from one side of the one-dimensional solid to the other. The thermal conductivity is a material property that describes how well a solid material transposes heat

throughout itself in the form of conduction [19].

$$\dot{q}''_{cond} = -\frac{k\Delta T}{L} \tag{1.1}$$

Convection represents the transfer of heat by fluid motion, which can be in either gas or liquid form [19]. This method of heat transfer can be interpreted by looking at the relationship between a solid surface, such as the flat surface of firefighter turnout gear, and a nearby gaseous fluid. The governing equation for convective heat flux is presented as Equation 1.2 with the convective heat transfer coefficient, h, and a temperature difference, ΔT [19].

$$\dot{q}''_{conv} = h\Delta T \tag{1.2}$$

The temperatures used in this equation equate to the difference between the temperature at the surface of the solid and the temperature of the surrounding fluid. Between the solid and the fluid, there are two forms of convection that can occur, forced convection and natural convection. Forced convection is the continuous fluid motion past the surface of the solid material, while natural convection is the motion of a fluid driven by buoyant flows and temperature differences when in contact with a solid surface [19]. These types of convection are denoted in the governing convective equation through the convective heat transfer coefficient, h, which can be represented through additional equations dependent on the conditions of the fluid flow and velocity as well as the shape of the solid surface. Forced convection for the gaseous medium of air is typically represented with a convective heat transfer

coefficient between 10 to 200 W/m^{2}K [20]. The typical convective heat transfer coefficient for the natural convection of air is between 5 and 25 W/m^{2}K [20].

Radiation represents the transfer of heat without the need for a physical medium, such as a gas or solid, and is the dominant form of heat transfer in well-developed fires [19]. Radiation is emitted from a hot surface or source and radiates to a cooler material seeking to fulfill the laws of thermal equilibrium. The governing equation for the total radiative heat flux from a surface is presented as Equation 1.3 [19].

$$\dot{q}''_{rad} = \varepsilon \sigma T^4 \tag{1.3}$$

The radiative heat flux is a function of the emissivity, ε, and the fourth power of the temperature of the heated surface of the source, T. The emissivity is a surface property of a material, which represents the ratio of the emissive power of the surface to the blackbody emissive power. The Stefan-Boltzmann constant, σ, is a fundamental constant theoretically derived to represent the radiative intensity, and is equal to 5.67×10^{-8} W/m^2 K^4.

Each of these modes of heat transfer are apparent in the fire environment and must be considered when assessing the heat transfer within firefighter PPE. A fire that occurs within a structure acts as a thermal source, emitting heat to its surroundings and toward firefighters within the space. For this analysis, the modes of heat transfer will be specified as they pertain to the journey of heat produced from the fire environment and absorbed by the firefighter to cause injury.

$$\dot{q}''_{cond} = \dot{q}''_{rad} + \dot{q}''_{conv} \tag{1.4}$$

The heat entering a firefighter's PPE can be represented by a net heat flux boundary condition shown in Equation 1.4. The exterior surface of the PPE is exposed to this total flux which is comprised of both radiation and convection. The radiative fraction of the total exposure is a factor of the radiative emissions from the flames itself, the hot gas upper layer, and the additional furnishings in the space. These furnishings, if not engulfed by flame through direct impingement, can be sources of radiation upon the temperature gradients established from their own increase in temperature. In addition to the radiation directed into the PPE, there is also radiation directed out of the PPE. This "re-radiation", although typically of a small magnitude, is equal to the radiation produced from the increased temperature of the outer shell of the PPE, as well as the reflected source radiation. The overall radiative component within the total exposure is a summation of the radiation being sent both into and out of the exterior surface. The convective fraction of the total exposure is a result of the natural convection and buoyant flows that add or remove heat from the surface.

The external heat flux exposures that will be used in this study, 5 and 10 kW/m^2, are each values that represent a total summation of the radiation, re-radiation, and convection along the outside of the PPE. The energy absorbed through the outer shell is transferred through the three layers of PPE, the outer shell, moisture barrier, and thermal liner, via conduction. These layers are in direct

contact with one another with the exception of the minuscule air gaps that may arise between the stitchings; these gaps were deemed negligible in this analysis. Upon reaching the face cloth of the thermal liner, the heat energy in this scenario will be confronted with the presence of an air gap of uniform thickness. The focus of this study is to better understand how the heat will be transferred from the firefighter PPE to the cotton stationwear across this air gap.

1.2.4 Burn Injuries

Burn injuries are classified into three different degrees of severity, depending on the nature and intensity of the burn. These classifications are derived according to the penetrated depth of injury to the victim's skin, and the temperature ranges to which these degrees occur are identified in Table 1.1. First degree burns occur when the victim's skin tissue exceeds a temperature of 44°C [21]. At this time the victim's outer layer of skin, the epidermis, is the only layer of skin affected and typical symptoms include the reddening of skin, dryness, and pain [21]. No blisters are formed from a first degree burn and long-term damage is rare [21]. Second degree burns occur when the victim's skin is exposed to temperatures greater than 55°C and the burn injury involves not only the epidermis but a portion of the dermis layer of skin as well [22]. The burn site in this degree of injury appears red and blistered and is often accompanied by pain and swelling [21]. Third degree burns occur at a temperature of 72°C when instantaneous thermal damage is likely [23]. This burn injury destroys both the epidermis and dermis layers of the victim's skin and may

also inflict damage on the victim's muscles, tendons, and bones [21]. There is a lack of sensation in the burn area as the nerve endings are severely damaged and the burn site may appear charred or white [21].

Table 1.1: Burn Injury Classification and Symptoms [21, 22]

Degree of Burn Injury	Temperature Range (°C)	Depth of Damage	Symptoms
First	$44 - 55$	• Epidermis	• Reddening of Skin • Dryness of Skin • Pain
Second	$55 - 72$	• Epidermis • Dermis	• Swelling of Skin • Formation of Blisters • Pain
Third	≥ 72	• Epidermis • Dermis • Tendons • Muscles • Bones	• Charring of Skin • White Discoloration • Lack of Sensation

A disclaimer should be made on the location of temperature measurement between the literature and this research. It should be noted that these criterium temperatures are measured at the basal layer under the epidermis of the skin, and

not at the skin surface. For this analysis however, the experimental and numerical temperatures obtained will be at the skin surface and assumed to represent the onset of injury. This assumption entails that the "times to burn injury" specified within this work are merely conservative estimates at which the skin surface will reach these temperatures as opposed to the actual times within the skin layer. Future work should consider the incorporation of a numerical skin model to properly quantify this relationship and take into account the human body's thermal regulatory processes such as blood circulation and perspiration.

1.3 Literature Review

1.3.1 Firefighter PPE Standard Testing

As previously mentioned, NFPA 1971 is the principal standard defining the minimum requirements needed for protective ensembles of structural and proximity fire fighting [7]. Not only are the necessary ensemble components prescribed in this standard, but the governing test methods for all of the components that make up the full PPE assembly are also detailed. The test methods employed by this standard are applicable to the establishment of the minimum performance requirements that these protective components should be able to withstand.

Of these tests, the Thermal Protective Performance (TPP) test provides the primary assessment used for overall PPE performance in regard to protecting the user from flash fire conditions. The TPP test is performed with the test apparatus and procedure specified in ISO 17492 [24], with an exposure heat flux of 84 $kW/m^2 \pm$

2 kW/m^2. The TPP test is meant to represent a controlled replication of flash fires that ignite and spread quickly at very high temperatures, rapidly consuming the combustible fuel in the surrounding environment. In the standard TPP test, the nominal air gap thickness is set as 6.35 mm, located between the PPE and human body. The TPP rating acquired from this test is derived from the intersecting point between the experimental temperature curve and the Stoll's curve [23] for skin burn predictions. Dividing the TPP rating in half produces the actual time to second degree burns in human tissue in a flashover environment. Multilayer protective garments that include the outer shell, moisture barrier, and thermal liner shall have an average TPP of at least 35.0, equivalent to 17.5 seconds before second degree burns can occur to human tissue. This test is designed to assess the thermal protection of the PPE assembly under short durations of intense flash fire conditions and ensure this equipment meets the necessary performance criteria to protect the wearer.

Another standard test included in NFPA 1971 is the total heat loss (THL) test. This test is designed to measure how well garments allow heat to escape from the body of the wearer [15]. The heat loss is measured through an assessment of the conductivity of the garment layers as well as sweat evaporation. The THL test is performed using the procedure and test apparatus of ASTM F1868 [25], under both wet and dry conditions. Heat flow is measured via a hot plate that mimics skin temperature control and provides information used to calculate a total heat loss value [15]. As mandated by NFPA 1971, the garment composite consisting of the outer shell, moisture barrier, and thermal liner shall have a THL of no less

than 205 W/m^2 [7]. The THL test opposes the intentions of the TPP test as it focuses on the evaporative cooling properties whereas the TPP test emphasizes the importance of thermal insulation. A balance must be made between these two standard requirements in order to produce the best PPE selection to provide thermal protection while alleviating the risk of heat stress.

1.3.2 Firefighter PPE Testing

The National Institute of Standards and Technology (NIST) has conducted a variety of testing to not only improve firefighter protective clothing, but also to better understand the fundamental heat transfer mechanisms as well. A test apparatus was built by NIST [26] to assess the properties of PPE over a wider range of thermal conditions that encompassed more than the short duration flash fire conditions established in NFPA 1971. The new bench scale test apparatus consisted of a vertical radiant panel and a pilot line burner allowing for firefighter garments to be exposed to heat flux conditions ranging from 1.5 kW/m^2 to over 50 kW/m^2 through both radiant panels and flame exposure. The newly designed apparatus also allowed for individual components of firefighter PPE to be evaluated for their own thermal protective properties, outside of the PPE assembly. Turnout gear mock-up assemblies, employing a constructed arrangement of an outer shell, moisture barrier, thermal liner, and exterior reflective trim, were created to be tested in this apparatus under varying conditions such as heat flux exposures, moisture content, and open and closed specimen backings. The data produced from this test apparatus provided

a greater insight on how different components of firefighter PPE perform in different thermal environments that firefighters may find themselves in.

In addition to radiant and flame exposure testing, NIST also conducted a series of thermal property measurements on the individual materials used in PPE assemblies [22]. The following thermal properties were acquired over a temperature range of 0°C to 100°C: thermal conductivity, specific heat capacity, absorptivity, reflectivity, and transmissivity. This temperature range both encompasses the temperatures at which burn injuries occur in human tissue and has a maximum temperature of 100°C, representing a value below the temperature of material degradation. These thermal properties were collected for ten different materials including three outer shell materials, five moisture barrier materials, one thermal liner, and one material representing the retro-reflective trim used on the exterior surface of the outer shell. Through the use of several test apparatuses, including a heat flow meter apparatus for thermal conductivity, thermal properties were acquired and used for further firefighter PPE research on a larger scale.

The vertical radiant panel bench scale test apparatus developed by NIST [26] was incorporated into an additional research project by NIST, comparing bench scale data to full scale testing [27]. The two scale test apparatuses were used to compare the experimental results between turnout gear material mock-ups and complete firefighter PPE ensembles. The mock-ups were created by stitching 305 × 305 mm (12 × 12 inch) garment specimens of each PPE layer in a fashion resembling the PPE composite orientation and were subjected to full scale apparatus testing in addition to the bench scale so that the data collected could be compared between

the two apparatus methods. From this data NIST identified the similarities in the peak temperatures obtained from both the bench scale and full scale testing for the turnout gear mock-up assemblies. Complete firefighter PPE ensembles were placed on manikins for the full scale testing, consisting of not only the coat and trousers, but the helmet, hood, gloves, and boots as well. In addition to the known objectives of this validation testing, NIST also reconfirmed the importance of air gaps to the transmission of heat through PPE, as differences were found between the temperature distributions obtained from the commercial firefighter ensembles and the constructed turnout gear mock-ups with open exposure. The experimental results acquired were also compared to temperature predictions from a heat transfer model developed by NIST [28–30] as an attempt to validate its results. While the heat transfer model did show good agreement among the temperature predictions of the outer surface of the mock-up bench scale assemblies, the measured and predicted temperatures differed within the material layers. Temperature differences were also found for the full scale ensemble tests as the model overpredicted the temperatures found within the layers of the measured test assemblies.

1.3.3 Firefighter PPE and Air Gaps

Firefighter PPE is a topic that has been studied throughout the years with the hopes of improving the clothing used by firefighters to keep themselves safe in the fire environment. The presence of air gaps within firefighter PPE is a specialized field of focus that has been experimentally tested through varying configurations of

PPE garments, layers, and thermal conditions. In addition to experimental testing, computational models have been developed by numerous researchers in the past to better understand and predict heat transfer through protective clothing. Over the years, the models have evolved to incorporate not only new methods of mathematical analysis but to also encompass different variables influential to the system's thermal protection, such as air gaps and the methods of heat transfer that traverse them.

Torvi and Dale [31] created the first numerical model for flame-resistant fabrics with a bench scale PPE system involving a single thermal fabric layer, an air gap, and a skin model. For the air gap in this system, both natural convection and thermal radiation were assessed and simplified to account for the heat distribution across the 6.35 mm air gap used. The numerical model was validated through experimental testing similar to the flash fire conditions of a TPP test and concluded that although the general agreement was very good between the results, simplified assumptions in the model created technical limitations on its accuracy.

Mell and Lawson [32] furthered the work done on modeling flash fire firefighter PPE heat transfer by creating a model that simulated the movement of heat through all three layers of firefighter turnout gear with the associated air gaps in between each layer, but stopped their analysis short of the larger air gap connecting the PPE to the skin model. Between these fabrics the air gaps were much smaller (approximately 1 millimeter), so heat transfer was modeled solely through thermal conduction. The numerical model was validated with experimental data acquired using the bench scale apparatus from [26] and demonstrated good agreement solely on the inner layers of the PPE assembly. Precision errors were apparent between

the model and the data on the exterior boundaries due to approximations made on the radiative properties such as transmissivity and reflectivity.

The next model created came from Chitrphiromsri and Kuznetsov [33], and not only included conductive and radiative heat transfer, but moisture transport as well. Their complete model focused on flash fire exposure to multilayer turnout gear with an air gap of 6.35 mm between the PPE and skin, and considered the textile materials to absorb moisture from the air and hold a gaseous mixture of both air and water vapor between the solid fibers of the garment. On the other side of the 6.35 mm air gap, a skin model was used to predict burn injuries through the use of previously defined thermal models and burn integrals [34, 35]. The air gap itself was modeled with all three forms of heat transfer, that being conduction, radiation, and natural convection. The garment materials were modeled using a simplified thermal radiative approach similar to that introduced by Torvi and Dale [31]. The numerical computations from this model were concluded to have the capabilities of estimating both the thermal response of the specified fabrics as well as predicting maximum flash fire exposure durations leading to second and third degree burns.

The addition of moisture transport to the heat transfer model was also being studied by NIST at this time. A computer software tool was developed by researchers at NIST and described through a series of reports [28–30] to predict and simulate the performance of protective clothing. In this numerical program, the heat transfer analysis stopped at the face cloth of the thermal liner layer, meaning no air gap was incorporated bridging the PPE to the wearer. The software simulator, Protective Clothing Performance Simulator (PCPS), was created through the

use of equations encompassing the behaviors of transient heat and moisture transfer through cloth fabrics. This software applied to multilayered fabric assemblies for PPE both with and without air gaps between the fabric layers. In the first report of this series [28], the numerical solver was created and compared to experimental data for both single layer and turnout coat ensembles under low radiant heat flux to primarily assess the agreement of temperatures through dry and wet conditions. The air gaps located between the thermal fabrics were of a thickness of 1 millimeter and modeled solely through conductive transport. The results found here were in good agreement with one another as peak temperatures were predicted by the model within 10% accuracy. The second report of this series [29] acts as a user's manual for PCPS, with information pertaining to the navigation, creation, and analysis of simulations in the computational solver by NIST. The third report in this series [30] assessed the transient response of heat and moisture transfer in single layer outer shell fabrics under TPP test conditions, imitating flash fire exposure. The experimental TPP test data was within 6% of the predicted TPP ratings from PCPS for two separate outer shell brand materials in this analysis. While good agreement was found between both the experimental data and the predicted values for both the TPP test and the radiant heat flux panel, as previously mentioned, the PCPS did not accurately predict the data under full scale fire conditions. This lack of agreement voids a complete numerical solver and provides areas for computational improvement.

Song and Barker [36] furthered the work done on the numerical heat transfer model for firefighter gear by shifting away from the bench top scale and constructing

a model to predict heat transfer on a manikin. In this research, a single layer of outer shell protective fabric was modeled to be worn by a manikin with an embedded air gap and exposed to flash fire conditions. The model was created to determine the manikin simulation's ability to predict not only surface heat flux but skin damage as well, through the use of bioheat models. The air gap in the fabric-air-skin system was modeled with radiative, conductive, and convective heat transport and its thickness was experimentally determined through the use of three-dimensional body scanning technology. This method, coupled with the manikin itself, allows for varying air gap sizes to be measured and numerically simulated over one's body and provides a representative idea of where natural air gaps form in the total PPE ensemble. The modeled results were validated through the use of the PyroMan manikin thermal protective clothing analysis system located at North Carolina State University and was exposed in short 3 to 4 second durations of flash fire flame contact and heat flux. Song and Barker concluded that the model predicted the heat transfer through single layer PPE and the resulting burn skin damage in flash fire exposures with good accuracy. It was noted in this work that the model was limited in its practical use given the lack of multilayer garments and moisture transport in the total PPE system.

In an additional study conducted by Song [37], the importance of air gaps in thermal protective clothing was reconfirmed through the use of flash fire manikin testing and a numerical model. Song's numerical model introduced in [36] was used in this analysis to determine an optimal threshold for air gap sizes within full thermal ensembles. Air gap distributions within a protective garment assembly were

identified on full scale manikins using a three-dimensional body scanning method, and the thermal insulation of these air gaps were then tested under severe thermal conditions for a short duration. For single layer garment testing, Song discovered an optimal air gap size between 7 to 8 millimeters. Below this 7 millimeter air gap size, Song concluded that the insulating value of the air gap increases as the air gap thickness increases [37]. The modes of heat transfer below this optimal size is driven by conductive and radiative transfer, as there is no boundary layer created for convection to take place. Upon surpassing 8 millimeters in thickness, the air gap no longer provides an increasing insulating value, as convection is hypothesized to occur in the space. Natural convection occurs as a result of the creation of a boundary layer in the now larger space. The boundary layer indicates that enough air is within the air gap to create fluid flow between the garment surfaces via a convective current, thus transferring an increased amount of heat back towards the skin.

Song et al. [38] continued the development of the numerical model in [36] by addressing and incorporating multilayer garments as well as moisture transport within the PPE system. In this assembly, there are three layers of turnout materials and an air gap separating the garments from the heat flux sensor. The air gap is also modeled by the three forms of heat transfer with the convective transfer to be considered as a function of natural convection in the enclosed space. More details on the development of this complete model and its parameters can be found in [33]. The predictions from the model were validated experimentally under multiple configurations including one-, two-, and multilayer systems, and with and without the

inclusion of a 6.35 mm air gap. The garment assemblies were tested in a TPP configuration under flash fire conditions similar to the standard test and the results allowed Song et al. to conclude multiple things about their model. This model can be used to predict the thermal response of protective clothing, the temperature and moisture distributions, and the influence of an air gap in reducing heat transfer under flash fire exposure.

In a more recent study by Ghazy and Bergstrom [39], a transient heat transfer model was developed for a protective clothing ensemble consisting of a single layer outer shell garment, an air gap, and the user's skin. Their model differs from the PPE air gap models that precede it due to the level of complexity involved within the heat transfer of the air gap itself. In prior studies, the numerical model developed focused primarily on the thermal behavior of either the skin or the PPE garment, with an approximate thermal assumption of conductive transfer, alone, being used for the air gap. Ghazy and Bergstrom introduced here a new numerical model that gives attention to the thermal capabilities of the air gap, accounting for both transient conduction and radiation to be transferred through the air medium. This model developed produced temperature distributions of the PPE assembly as well as the predicted time in which skin burn injuries would occur. The model was validated through experimental TPP testing, with the PPE assembly being exposed to a heat flux of 83 kW/m^2 as a combination of both radiative and convective heat transfer. This combined heat flux comes from localized flame contact onto the PPE fabric from the TPP apparatus. In this analysis, Ghazy and Bergstrom employed the nominal 6.35 mm air gap between the PPE and the exposed sensor. Upon

conducting this analysis, they discovered that their more realistic numerical model resulted in skin burn injury prediction times that were less than those obtained from simpler models that came before it.

Ghazy and Bergstrom continued their research by expanding the use of their model in various directions. They applied their model to multilayered PPE ensembles consisting of air gaps not only between the skin and the PPE, but with the inclusion of air gaps between each of the three layers of firefighter turnout gear as well, resulting in three air gaps in the total system [40]. These air gaps were modeled using the combined conduction-radiation heat transfer methods determined in [39] under flash fire exposure. Ghazy and Bergstrom also used their model to create an evolved model [41] whose purpose was to represent a halfway point between the two extremes of modeling air gaps; that being a simple approximate model and a sophisticated approach involving combined conduction and radiation. This new model simplified the conduction-radiation model as a means of reducing the complexity while maintaining a higher level of accuracy in air gap heat transfer within firefighter gear. Validation of this new model was completed and compared to the results of each of the preceding models, and Ghazy and Bergstrom concluded that the simplified combined model could act as a sufficient replacement for future use in PPE heat transfer.

The University of Maryland's Department of Fire Protection Engineering has also completed numerous research projects with a focus on firefighter PPE performance. The primary focus of this series of projects [42–46] surrounded the incorporation of a variable air gap being implemented into the PPE that would increase

in size through the use of shape-memory material, a material with the ability to reshape its figure when subjected to high temperatures. From this series, a study by Hendrickson [43] focused on creating a computer program to analyze the heat transfer through different layers of firefighter PPE with the inclusion of a variable air gap via effective conduction heat transfer. The program was used in addition to experimental data to validate the incorporation of an air gap creating shape-memory device within the PPE under low thermal exposure. While the computer program did predict temperature data in good agreement with the experimental tests for PPE without an air gap, the introduction of an air gap between the PPE and the user's skin invoked uncertainties between the model and the data. The computer model overpredicted the thermal insulation values for the variable air gap creating small yet differential errors.

Fu et al. [47] developed a numerical model building upon the prior work done pertaining to moisture transport. The heat and moisture transfer model created here was also applicable to low level thermal radiation instead of flash fire exposure, and focused solely on the PPE assembly, similar to NIST's PCPS program, with no air gap on the exterior side of the thermal liner. The air gaps among the PPE ensemble were considered to transfer heat through conductive and radiative means, and had a thickness of 1 millimeter. Fu et al. recognized the impacts of moisture on the overall temperature distributions and the influence of the local temperature to the PPE fabric's moisture evaporation and condensation behaviors concluded by [28], and incorporated these past findings into their own improved model. The model accounts for the moisture absorbed by external radiation for both the individual

fabric layers as well as the intermediate air gaps as well. When validating the numerical predictions to experimental data, Fu et al. exposed the PPE assembly, three fabric layers and two air gaps, to two levels of thermal radiation, 5 and 10 kW/m^2. These radiative heat fluxes were applied to the PPE for 600 seconds, followed by 150 seconds as a cool-down period for the fabric materials. The data obtained for temperature distributions and moisture content showed good agreement with their computational predictions indicating an accurate model was created for low thermal exposure in the presence of moisture for the multilayer garment system alone.

In summary, previous research has been conducted on the benefit of having air gaps that can act as thermal insulators between the protective garments and the user's skin under high thermal conditions such as flash fire exposure [31–33, 36, 39]. The conditions that are used to simulate flash fire exposure typically utilize high intensity heat fluxes, on the order of 80 – 83 kW/m^2, for a duration of a few seconds in order to represent the intense fire behavior that firefighters may be exposed to. Under these conditions, researchers have found that the methods of heat transfer through the air gap vary based on the size of the gap thickness. Some research has also been conducted at low heat flux [47], but there is a need to understand the influence of the air gap size on heat transfer within multilayer personal protective garments in this configuration. This research would not only provide an educational understanding on the importance of air gaps in PPE for firefighters and prolonging burn injuries, but it would also allow a better understanding of the methods of heat transfer applicable to an air gap under low level thermal exposures.

1.4 Research Objectives

To determine the influence of the air gap size on heat transfer within multilayer firefighter PPE for pre-flashover thermal exposures, four objectives were established:

- To assess if time to burn injury can be prolonged with inclusion of an air gap
- To explore the relationship between time to burn injury and air gap thickness
- To identify how the modes of heat transfer vary with air gap thickness
- To determine accuracy of the numerical model to predict time to burn injury

These objectives were achieved by two forms of analysis: experiments and numerical simulations. A cone heater apparatus was used to conduct the experimental temperature testing and achieve the first and second objectives. A numerical Fire Dynamics Simulator (FDS) model was constructed with experimental property inputs from a heat flow meter apparatus to predict these same temperatures and satisfy the third and fourth objectives.

Chapter 2: Methodology

This study involved two experimental test series. The first, denoted "Cone Heater", involved subjecting horizontally-oriented samples to constant thermal irradiation provided by a conically wound electric heating element. The second test series, denoted "Heat Flow Meter", placed horizontally-oriented samples between plates of constant temperature. Details of these two test series are provided in Section 2.3. Section 2.1 provides information on the materials used throughout, and Section 2.2 describes the preparation of the test samples used in these experiments. Section 2.4 contains the test matrices detailing all tests conducted in this study. Section 2.5 depicts the methodology of the one-dimensional heat transfer model used to validate the Cone Heater experiments.

2.1 Materials

The test specimens in this study were comprised of PPE, cotton stationwear, and an air gap spacer. The PPE garments consisted of the three fabric layers that make up turnout gear: the outer shell, moisture barrier, and thermal liner. TenCate Advance™ was chosen as the outer shell fabric for this assembly and can be seen in Figure 2.1(a). CROSSTECH® black moisture barrier was used for the interior

moisture barrier layer of the PPE multilayer system and is shown in Figure 2.1(b). The final layer in the PPE garments is the thermal liner, represented by TenCate Caldura® SL2i and depicted in Figure 2.1(c). These specific brands of the fabric layers were chosen for their own current use in firefighter PPE employed by fire service stations in and around Washington D.C. and the state of Maryland; see Appendix A.1. The cotton fabric used to represent the stationwear worn by firefighters underneath their PPE was taken from a 100% cotton Fruit of the Loom t-shirt.

The thermophysical properties for both the PPE and cotton fabrics are shown in Table 2.1. The thicknesses of each material were measured from the samples with a Carrera Precision Digital Caliper, having a precision of 0.01 mm. The thermal properties and the density of the PPE fabrics were obtained from previous FSRI studies involving these specific brands of firefighter PPE [48]. In this research, the density, thermal conductivity, and specific heat capacity were also experimentally measured using the Linseis Transient Hot Bridge (THB) method which acts as an enhancement to the Hot Wire and Transient Hot Strip Method (DIN EN 993-14, DIN EN 993-15) [48]. By comparison, NIST reported values ranging from 1090 to 2420 J/kg·K for the specific heat capacities of similar PPE fabrics [22]. The thermal and physical properties of the cotton fabric were taken from the *Fundamentals of Heat and Mass Transfer* textbook [19].

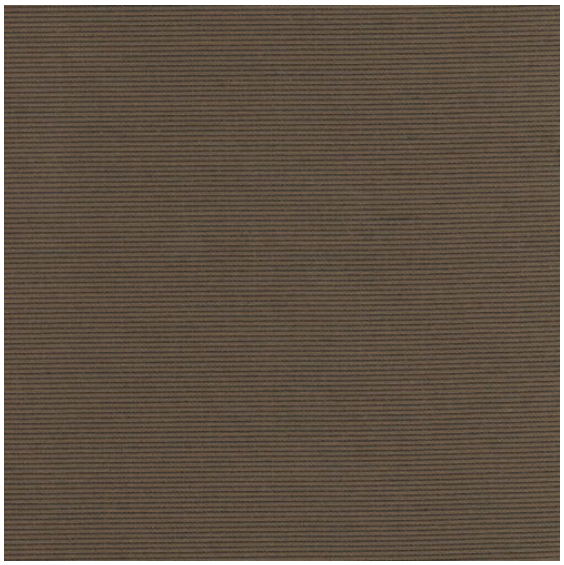

(a) TenCate Advance™ Outer Shell

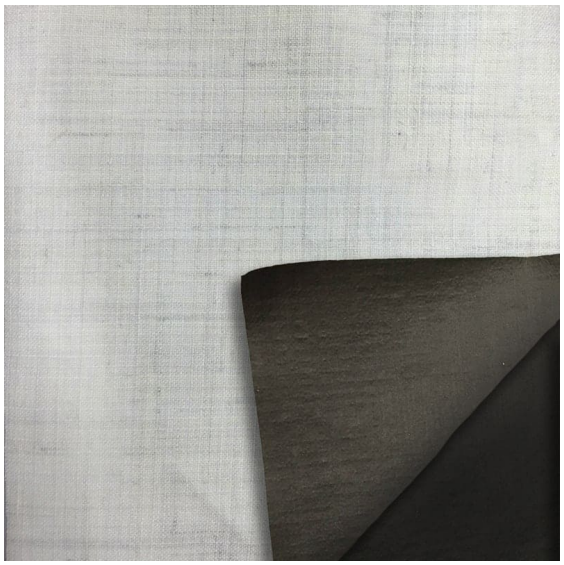

(b) CROSSTECH® Black Moisture Barrier

(c) TenCate Caldura® SL2i Thermal Liner

Figure 2.1: PPE Fabric Brands for Each Layer of the Assembled Turnout Gear

Table 2.1: PPE and Cotton Fabric Properties [48]

Fabric Layer and Brand	Thickness (m)	Density (kg/m^3)	Thermal Conductivity (W/m·K)	Specific Heat Capacity (J/kg·K)
Outer Shell: TenCate Advance™	5.00×10^{-4}	1.45×10^{3}	1.23×10^{-1}	107
Moisture Barrier: CROSSTECH®	3.20×10^{-4}	1.33×10^{3}	8.99×10^{-2}	152
Thermal Liner: TenCate Caldura® SL2i	1.00×10^{-3}	7.65×10^{2}	5.95×10^{-2}	168
Cotton Stationwear: Fruit of the Loom	4.50×10^{-4}	0.80×10^{2}	6.00×10^{-2}	1300

The material used to create the air gap spacers was SG-200 Fiberglass, an ultra-high-temperature and high-strength composite [49]. Manufactured by Röchling Glastic Composites, Inc. and obtained through McMaster-Carr, SG-200 Fiberglass withstands temperatures up to 210°C, has a thermal conductivity of 0.245 W/m·K, and is also easy to machine. This material was chosen for the spacer because it will not react nor deform under the conditions of this test, and because it is manufactured in fixed thickness sheets so that the air gap thicknesses may be controlled. Four thicknesses of the SG-200 Fiberglass material were acquired: 6.35 mm (0.25 inch), 12.7 mm (0.50 inch), 19.05 mm (0.75 inch), and 25.4 mm (1.00 inch). Each had a square area of 305 mm by 305 mm. The varying thickness fiberglass sheets were used to represent the different air gap sizes within the test assemblies. These sheets were used, with the assistance of a computer numerical controlled (CNC) machine, to fabricate the air gap spacers for these tests.

Fiberfrax® Duraboard 2600 ceramic fibreboard insulation was used in the Cone Heater test series. This material is a high-temperature insulating board made of polycrystalline wool and withstands temperatures up to approximately 1430°C [50]. The material and thermal properties of this insulation are shown in Table 2.2 [51]. The thermal properties are represented through temperature-dependent relations where the temperature, T, has units of °C.

Table 2.2: Ceramic Fibreboard Properties

Density (kg/m^3)	Thermal Conductivity (W/m·K)	Specific Heat Capacity (J/kg·K)
224	$(1.80 \times 10^{-4})\ T\ +0.043$	$145 \times \log(4.68\ T)$

2.2 Sample Preparation

2.2.1 Assembly Preparation

Two sets of assemblies were created for the experiments in this study — one set for the Cone Heater series and one set for the Heat Flow Meter series. The Cone Heater set consisted of five PPE sleeve assemblies, five cotton sleeve assemblies, and four fiberglass air gap spacers, with the dimensions of each of these materials being that of 101 mm by 101 mm (4 × 4 inch). The Heat Flow Meter set also had five PPE sleeve assemblies and four fiberglass air gap spacers, but these materials had dimensions of 203 mm by 203 mm (8 × 8 inch) and the cotton sleeve assembly set was removed. The cotton sleeve assemblies were tested only for the Cone Heater series as a baseline surrogate for the influence of an air gap, and there was not a need for the material properties of the cotton assemblies with the Heat Flow Meter experiments. The creation of the PPE sleeve assemblies, cotton sleeve assemblies, and fiberglass spacers for the individual sets will be detailed in this section.

The PPE sleeve assembly itself is assembled via the three PPE fabric layers being sewn together. From top to bottom, this consists of the outer shell, moisture barrier, and thermal liner. These layers are in direct contact with one another with the exception of the minuscule air gaps that may arise between the stitchings. Also sewn into these arrangements is the cotton stationwear fabric, attached to the bottom surface of the thermal liner. In order to attach the cotton stationwear while also providing a space of the intended air gap, the cotton fabric samples were sewn

to the PPE garments on two out of the four sides of the square samples to create a fabric sleeve that would allow the air gap spacer to be inserted within. The PPE sleeve assemblies for both the Cone Heater and Heat Flow Meter sets can be seen in Figures 2.2(a) and 2.2(b), respectively.

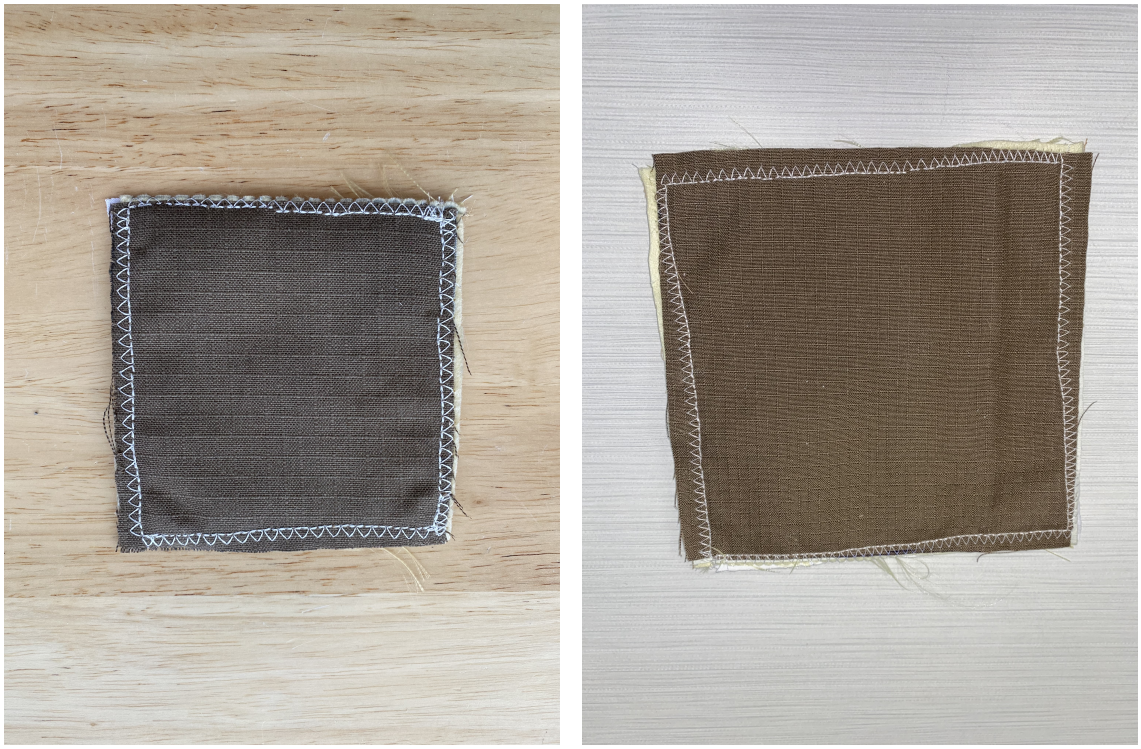

(a) Cone Heater PPE Sleeve Assembly (b) Heat Flow Meter PPE Sleeve Assembly

Figure 2.2: PPE Sleeve Assemblies for the Cone Heater and Heat Flow Meter Series

Cotton sleeve assemblies were created as baseline surrogates to be used interchangeably with the air gap spacers as well for the Cone Heater experiments. These 100% cotton sleeve assemblies consisted of one layer of cotton on either side of the air gap to characterize the behavior of a growing air gap size, with no PPE involved. The two layers of cotton fabric were stitched in a similar fashion, on two of the four sides of the square area, to allow for the insertion of the air gap spacer. The data produced from the cotton sleeve assemblies was to be used as a reference

or baseline to gauge the relationship between heat transfer and the thickness of the incorporated air gap. The cotton sleeve assemblies for the Cone Heater set can be seen in Figure 2.3.

Figure 2.3: Cotton Sleeve Assembly for the Cone Heater Series

The air gap spacer was designed as a square ring to allow for an open air gap space in the center of the spacer while also maintaining support on the outer frame of the sleeve assembly system. The four fiberglass pieces of varying thicknesses were machined to produce the two spacer area sizes, both of which were designed to be machined from the same 305 mm by 305 mm fiberglass slab. The air gap spacer was designed using Autodesk Fusion 360 for both sets of test specimens. For the Cone Heater spacers, a hollow interior square area of 55.9 mm by 55.9 mm was machined out of the square. For the Heat Flow Meter spacers, a hollow interior square area of

157.5 mm by 157.5 mm was removed. The AutoDesk Fusion 360 drawing for one of the 305 mm by 305 mm fiberglass slabs, the 25.4 mm spacer thickness, is depicted in Figure 2.4. The Autodesk Fusion 360 files were then used with a CNC machine to precisely drill through the fiberglass material and create the exact shapes needed for the spacers. A total of eight spacers were machined from the fiberglass slabs to be used for the sleeve assemblies of the two test series sets. The final cut 25.4 mm thick fiberglass air gap spacer for both sets are depicted in Figures 2.5(a) and 2.5(b), respectively.

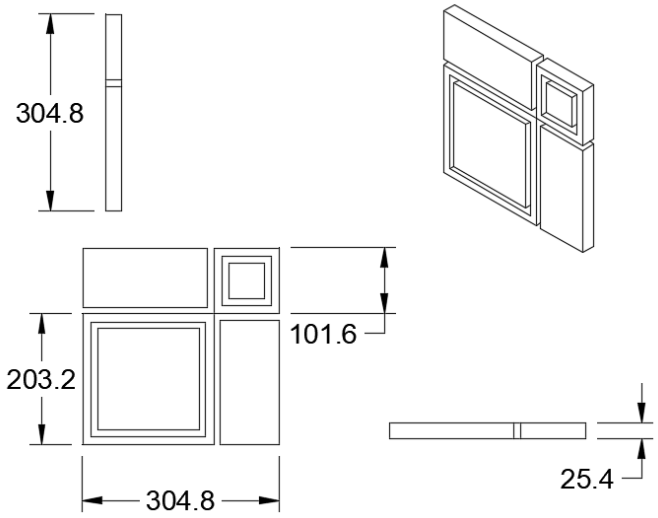

Figure 2.4: Autodesk Fusion 360 Air Gap Spacer Design for the 25.4 mm Fiberglass

2.2.2 Assembly Schematics

The PPE sleeve assemblies are graphically depicted in Figure 2.6 with a side profile schematic showing the orientation of each of the layers once the air gap has been inserted. This schematic applies to both the Cone Heater set as well as the Heat Flow Meter set as the only difference between the two PPE sets are the

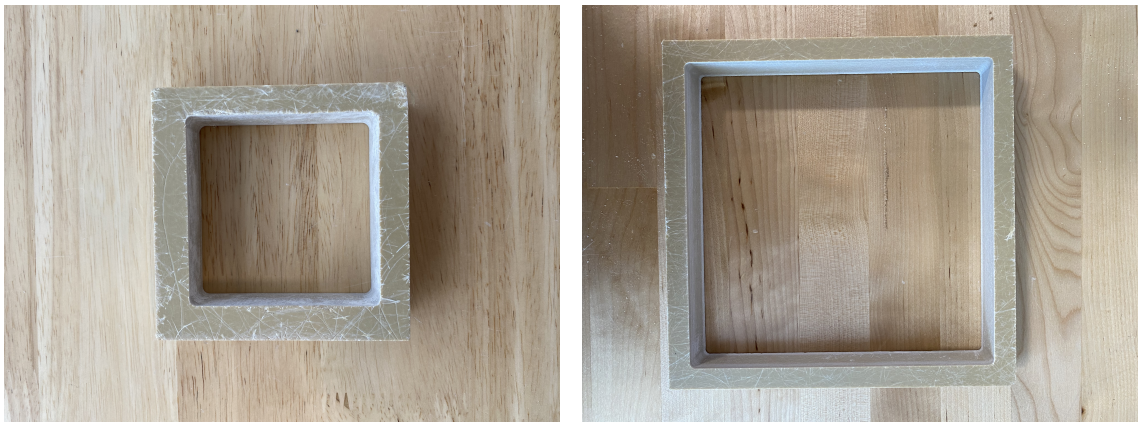

(a) Cone Heater Air Gap Spacer (b) Heat Flow Meter Air Gap Spacer

Figure 2.5: Fiberglass Air Gap Spacers for the Cone Heater and Heat Flow Meter Series

dimensions and the overall layer orientation remains the same. The cotton sleeve assembly schematic is depicted in Figure 2.7. Among these schematics, the air gap is the only layer that changes, as the thickness of the air gap is dependent on the test trial being conducted. The remaining fabric layers for both the PPE and cotton assemblies remain the same throughout all tests.

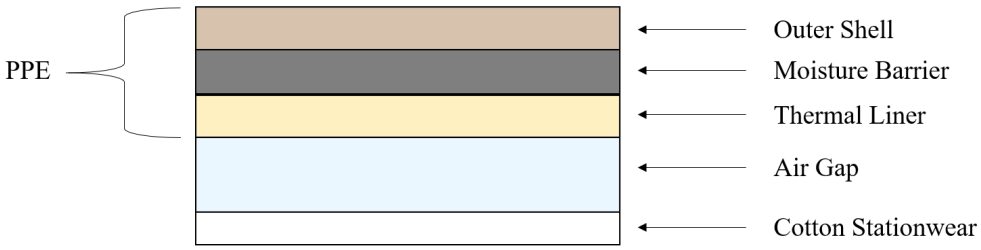

Figure 2.6: Schematic for the PPE Sleeve Assembly

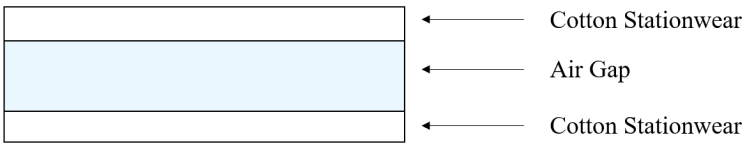

Figure 2.7: Schematic for the Cotton Sleeve Assembly

2.3 Test Instruments and Procedures

2.3.1 Cone Heater Experiments

2.3.1.1 Overview

The temperature data used to assess the value of an air gap between firefighter PPE and the wearer was obtained using thermocouples and a cone heater from a mass loss calorimeter. This testing was conducted at the UL FSRI Laboratory at the Delaware County Emergency Training Site (DelCo) in Delaware County, PA. Inside the DelCo lab space, the ambient temperature was between 19.3 and 25.3°C with a relative humidity ranging from 21.8 to 33.7%. The mass loss calorimeter used in these tests was a *Deatak Mass Loss Calorimeter Model MLC-5* and can be seen in Figure 2.8. The cone heater from this apparatus was set to provide exposures of thermal irradiation at 5 and 10 kW/m^2 for each sample, and these pre-flashover total heat fluxes were chosen for their use in prior work [47]. This apparatus used sample holders that were 101 mm by 101 mm, which is why the Cone Heater sleeve assembly set was used for these tests.

The MLC-5 cone heater was used to produce two constant radiation-dominated

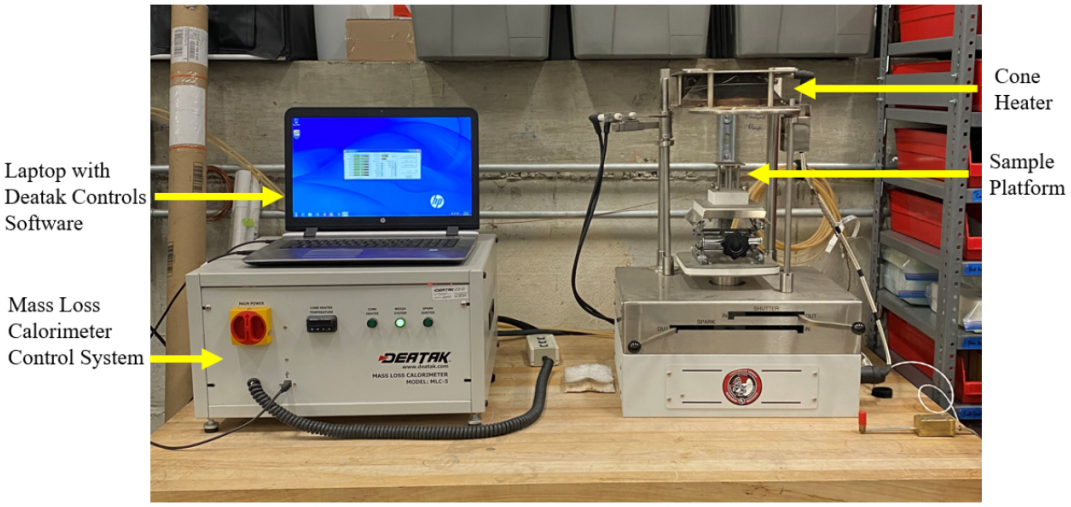

Figure 2.8: Deatak Mass Loss Calorimeter Model MLC-5

thermal exposures, calibrated to 5 and 10 kW/m^2 total heat flux. The heat flux on the exposed surface area of the sample was assumed to be uniform within the central 50 mm by 50 mm area and decreased in uniformity along the edges and corners when located 25 mm below the heater [52]. This was satisfactory for these experiments as the temperatures were measured along the centerline of the assembly via thermocouple placement. These heat fluxes were determined using a water-cooled *Medtherm 64-series Schmidt-Boelter* heat flux gauge, Figure 2.9, having an outer diameter of 12.7 mm, and calibrated to a full-scale output of 10 mV for an irradiance of 45 kW/m^2.

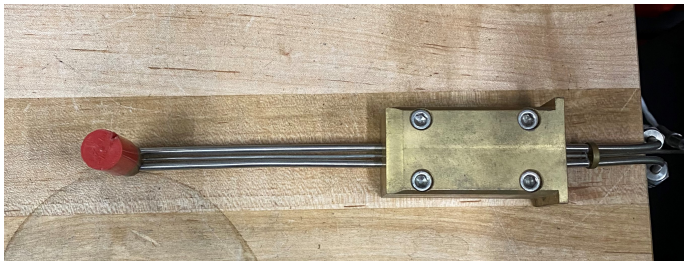

Figure 2.9: Medtherm 64-Series Schmidt-Boelter Heat Flux Gauge

Figure 2.10: Type K Self-Adhesive 30 Gauge Thermocouple [53]

A type K 24 gauge bead-welded thermocouple was located under the insulative backing of the assembly. Type K 40 gauge butt-welded thermocouples were used within the PPE, cotton garments, and air gap of the assembly, with the exception of type K self-adhesive 30 gauge thermocouples used along the bottom of the PPE garments. This self-adhesive 30 gauge thermocouple consisted of an adhesive pad that could be used to stick to surfaces, as shown in Figure 2.10. The thermocouple temperature data was recorded with a *Keysight 34972A LXI Data Acquisition / Switch Unit*, or DAQ system, seen in Figure 2.11.

2.3.1.2 Preparation

In addition to the sleeve assemblies, air gap spacers, and thermocouples, insulation was also implemented for the MLC-5 apparatus testing to minimize heat transfer at the boundaries of samples, and promote one-dimensional heat transfer through the depth of samples. Ceramic fibreboard was used as the insulation along the bottom of the sleeve assemblies and ceramic fibre batt insulation was wrapped around the sides of the entire assembly. The ceramic fibreboard was cut into 101 mm by 101 mm squares, each with a thickness of 12.7 mm and these pieces of insu-

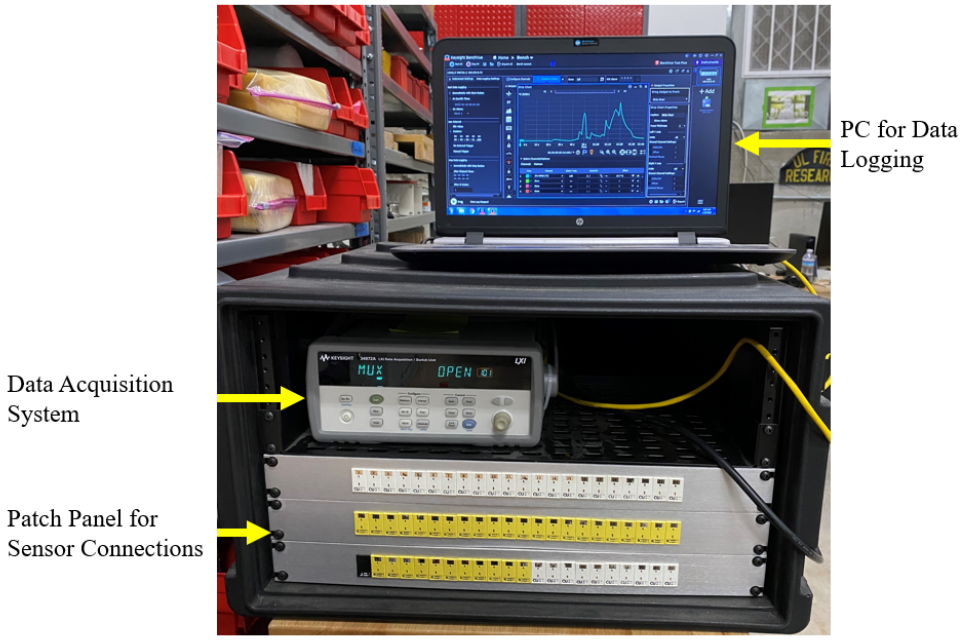

Figure 2.11: Keysight 34972A LXI Data Acquisition / Switch Unit

lation were oven dried for two days at 105°C, see Figure 2.12(a). Once the ceramic fibreboard squares were removed from the oven, they were placed in airtight plastic containers with Drierite (a calcium sulfate based desiccant) to absorb the moisture from the air and maintain the low humidity conditions. The stitched 101 mm by 101 mm PPE and cotton sleeve assemblies, with their associated fiberglass spacers, were also dried out for two days using the same method to reduce any potential interference via moisture content in the fabrics. In addition to the ceramic fibreboard squares, the ceramic fibre batt was cut and prepared to be wrapped around the sample holder, and tied off with 18 gauge steel wire, as shown in Figure 2.12(b)

Immediate preparation prior to testing consisted of assembling the sample holders and thermocouple placement. Two sample holders were assembled simul-

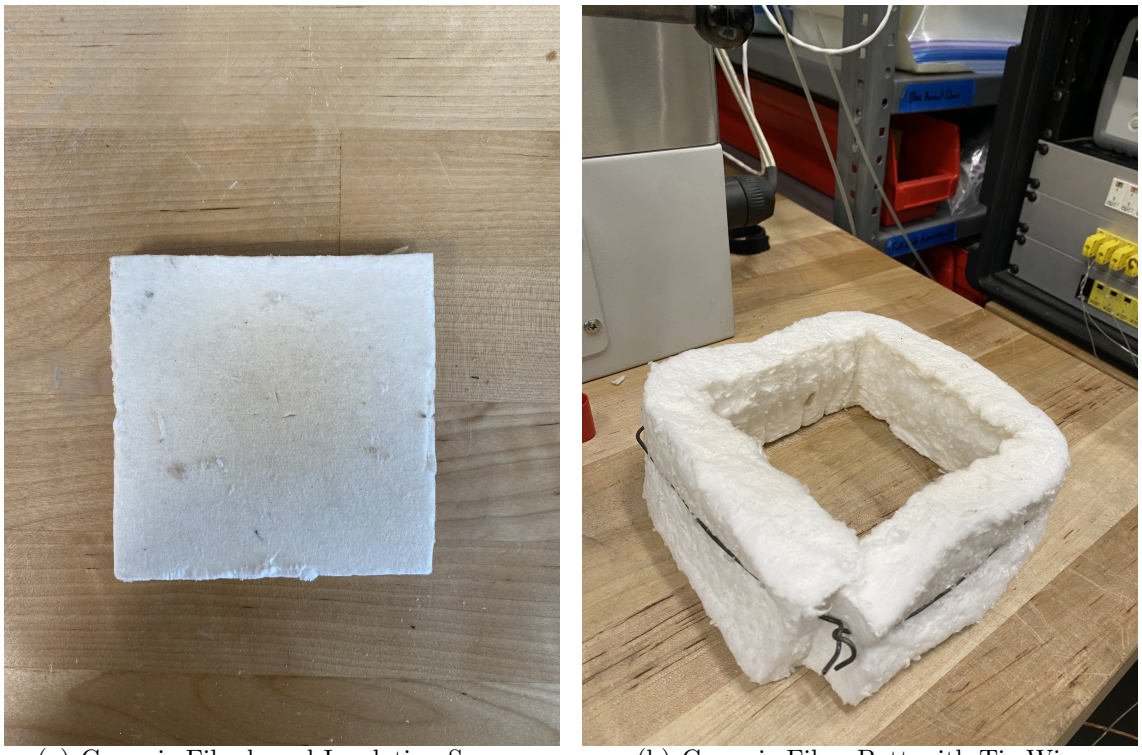

(a) Ceramic Fibreboard Insulation Square (b) Ceramic Fibre Batt with Tie Wire

Figure 2.12: Ceramic Fibreboard Insulation Square and Ceramic Fibre Batt Insulation Assembly

taneously so that tests could be conducted with the apparatus back to back while allowing post-test samples to cool down in a timely fashion. The sample holder itself consisted of a 101 × 101 × 25.4 mm square pan with an open top surface and a handle for placement purposes [54] as shown in Figure 2.13.

Ceramic fibreboard insulation was the first to be placed into the sample holder. Two 12.7 mm thick ceramic fibreboard squares were placed into the holder, and the 24 gauge thermocouple was inserted between the two squares, which were firmly pressed into one another to ensure that the thermocouple measured the temperature at the midpoint of the material and was not exposed to the surrounding air. The bottom ceramic fibreboard square with the 24 gauge thermocouple can be seen in

Figure 2.13: MLC-5 Sample Holder

Figure 2.14 upon removing the top insulative square. The total thickness of ceramic fibreboard was 25.4 mm, completely filling the depth of the sample holder. The PPE and cotton sleeve assemblies were placed on top of the insulation and enclosed within ceramic fibre batt. The components of the entire PPE assembly are identified in Figure 2.15 and consist of, from left to right, the ceramic fibreboard square, sample holder, PPE sleeve assembly, and ceramic fibre batt. Both the PPE and cotton completely assembled sample holders can be seen in Figure 2.16.

Depending on the thickness of the air gap spacer and the sleeve assembly being used, the thermocouple placements and types varied. For the samples being tested with a 0.0 mm air gap (no air gap), one 40 gauge thermocouple was placed below the fabric being tested. The thermocouple orientation for this configuration is shown in Figure 2.17. The fabric itself was stapled into the ceramic fibreboard insulation to ensure that the thermocouple was not exposed to an air gap between the fabric and insulation below. The 0.0 mm PPE stapled sample can be seen in Figure 2.18. For the non-zero air gap thickness sleeve assemblies, additional thermocouples were

(a) Without Top Ceramic Fibreboard Square (b) With Top Ceramic Fibreboard Square

Figure 2.14: Sample Holder with Ceramic Fibreboard Insulation Squares

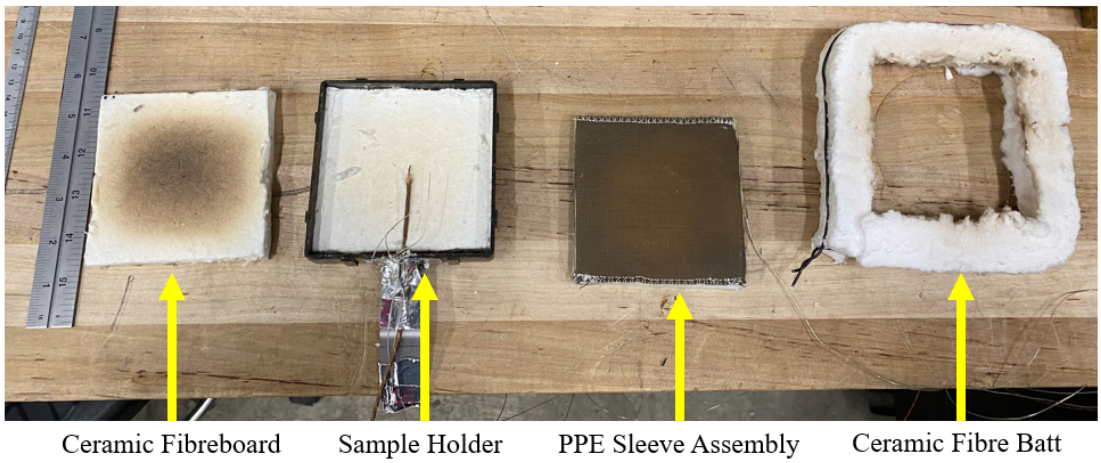

Figure 2.15: PPE Sample Holder Components

incorporated between the fabric layers and in the air gap itself.

For the cotton sleeve assemblies, three additional 40 gauge thermocouples were included in the sample holder. Once the cotton sleeve assembly was secured onto

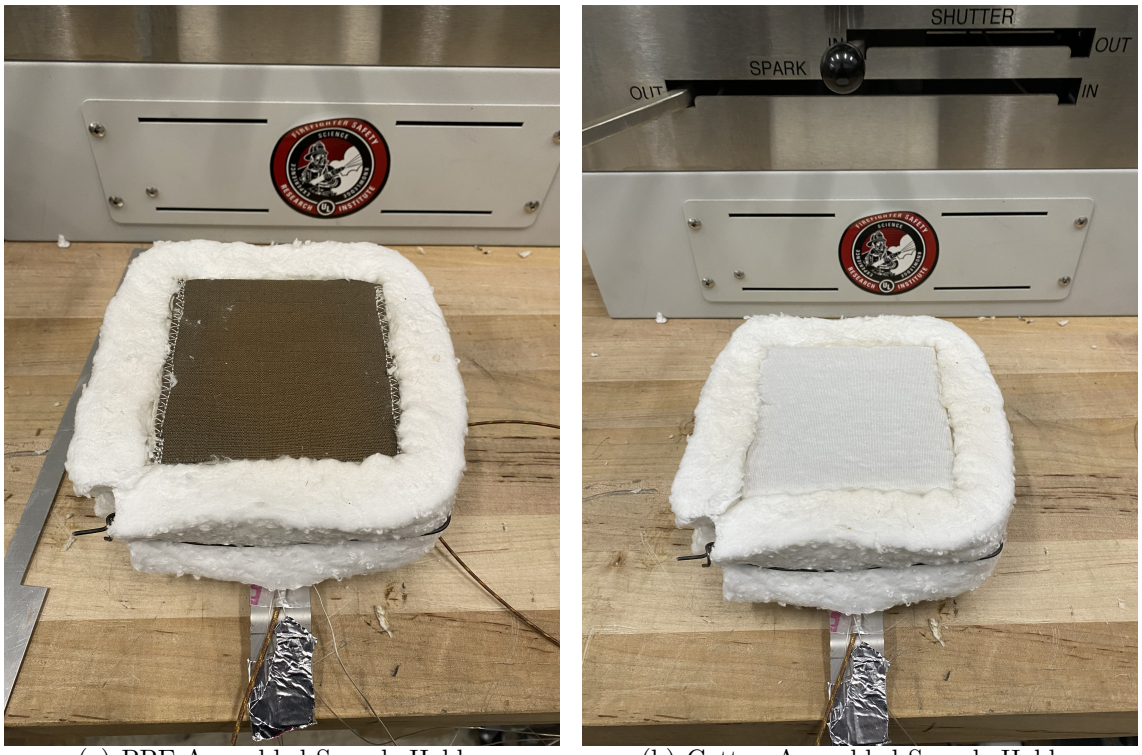

(a) PPE Assembled Sample Holder (b) Cotton Assembled Sample Holder

Figure 2.16: PPE and Cotton Assembled Sample Holders

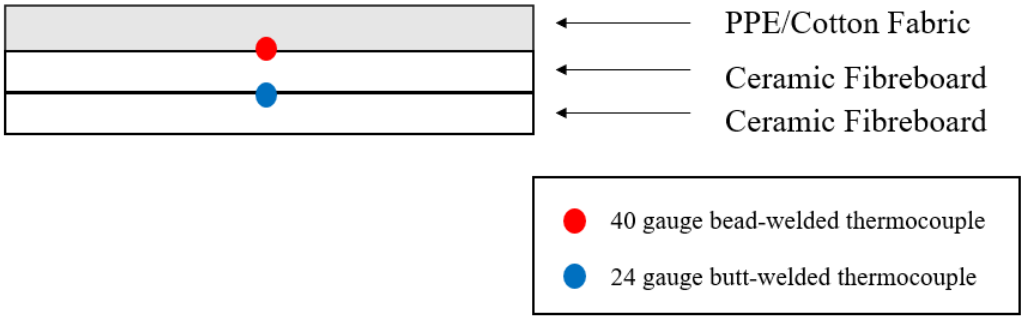

Figure 2.17: Thermocouple Schematic for Assemblies with No Air Gap

the desired air gap spacer, it was placed on the insulation-filled sample holder. One 40 gauge thermocouple was inserted between the insulation and bottom layer of the cotton sleeve and another was placed on the underside of the top layer of the cotton sleeve. The third 40 gauge thermocouple was used for determining the

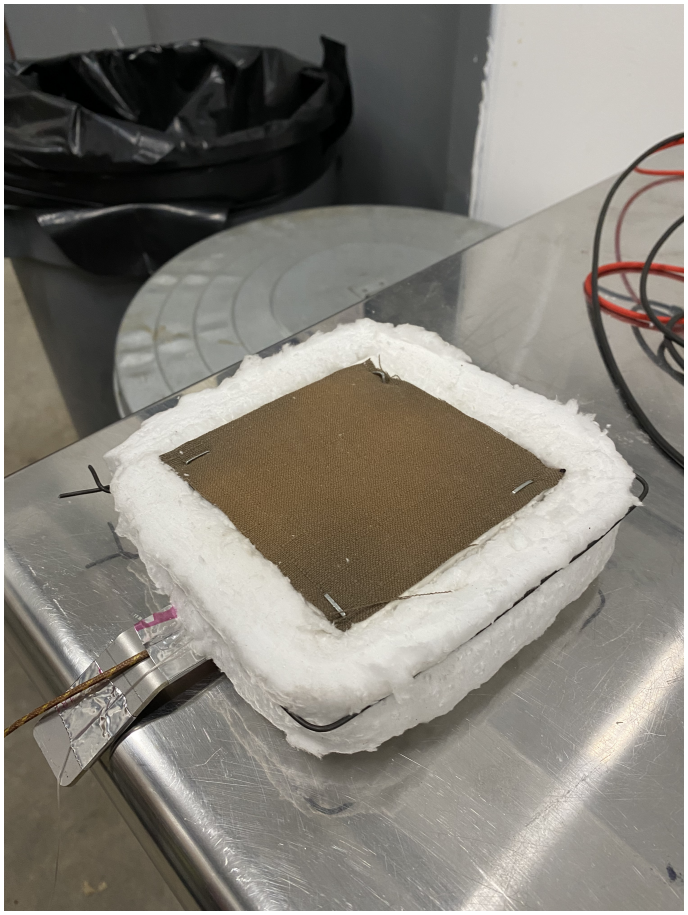

Figure 2.18: Stapled PPE Sample with No Air Gap

temperature of the air gap and was placed in the center of the air gap space by feeding the thermocouple through a small hole drilled into the fiberglass spacer. This thermocouple orientation, summing to four total thermocouples, was used for the 6.35, 12.7, 19.05, and 25.4 mm air gaps tests for the cotton sleeve assemblies. The thermocouple orientation for this configuration is shown in Figure 2.19.

For the PPE sleeve assemblies, four additional thermocouples were included in the sample holder in addition to the 24 gauge thermocouple in the insulation. Upon securing the PPE sleeve assembly to the air gap spacer, it was placed onto the insulation-filled sample holder and 40 gauge thermocouples were placed on the

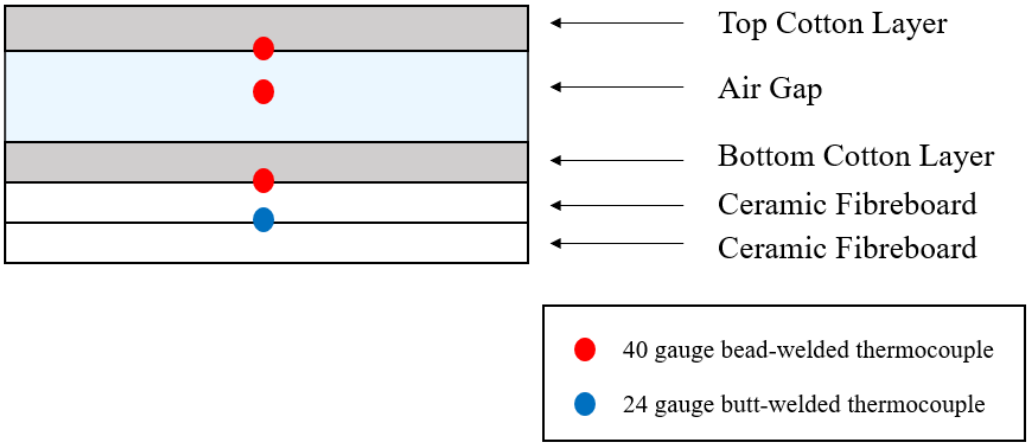

Figure 2.19: Thermocouple Schematic for Cotton Sleeve Assembly with an Air Gap

bottom surface of the cotton stationwear, in the air gap space using a drilled hole, and fed into the space between the top outer shell layer and the moisture barrier of the PPE garment. The fourth thermocouple was placed at the bottom of the three-layered PPE garment in between the thermal liner and the air gap itself. Because there was no surface for the thermocouple to be sandwiched between on the air gap side, a 30 gauge self-adhesive thermocouple pad was attached to the back surface of the thermal liner material. This allowed the thermocouple to read the temperatures reached on the backside of the PPE garment prior to an influence from the air gap. The thermocouple schematic for this configuration is shown in Figure 2.20 and the actual thermocouple placements are depicted in Figure 2.21. In Figure 2.21, Figure 2.21(a) depicts the three 40 gauge thermocouples to be placed under the cotton stationwear, into the air gap, and under the outer shell of the PPE, and the 24 gauge thermocouple placed under the insulation. Figure 2.21(b) shows the additional self-adhesive thermocouple pad placed on the bottom surface

of the thermal liner layer of the PPE. Figure 2.21(c) depicts the thermocouple wiring and orientation for four out of the five thermocouples used with the 24 gauge thermocouple being hidden from view under the insulation. This thermocouple orientation, summing to five total thermocouples, was used for the 6.35, 12.7, 19.05, and 25.4 mm air gap tests for the PPE sleeve assemblies.

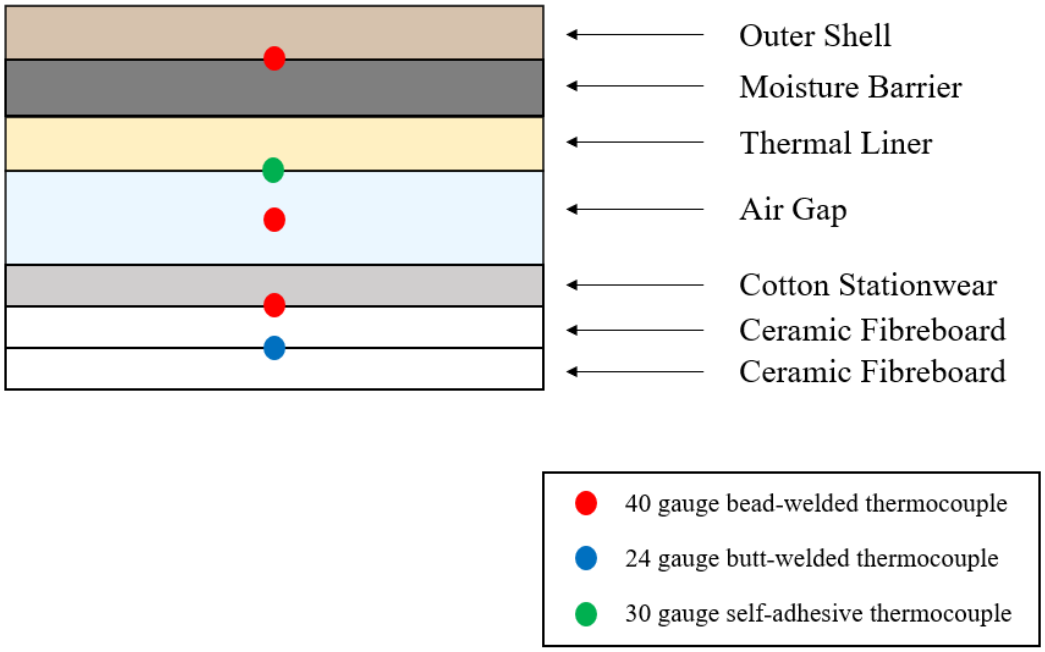

Figure 2.20: Thermocouple Schematic for PPE Sleeve Assembly with an Air Gap

Once the thermocouples were placed for each test, the entire assembly was secured in place using the ceramic fibreboard batting insulative frame.

2.3.1.3 Procedure

To begin testing, the MLC-5 apparatus was calibrated to produce 5 kW/m^2 from the cone heater. Prior to turning on the heater, the sample holder was adjusted to match the height of the heat flux gauge holder, located 25.4 mm below the cone

(a) 40 Gauge and 24 Gauge Thermocouples

(b) Thermocouple Pad on Thermal Liner

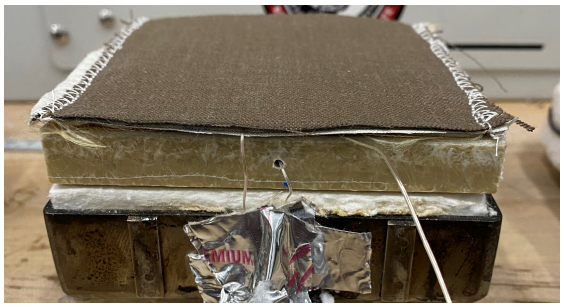

(c) Inserted Thermocouple Wiring

Figure 2.21: Thermocouple Orientations and Placement for the PPE Assembly

heater. Once the test sample had been prepared, the sample holder was placed onto the sample platform and manually adjusted so that the top surface of the test sample was also 25.4 mm below the cone heater to ensure that the heat flux being exposed to the test sample was equal to that being recorded by the heat flux gauge during the calibration. The sample platform height was manually readjusted for each air gap thickness size tested to maintain a distance of 25.4 mm between the

top of the test sample and the cone heater.

To calibrate the cone heater, the heat flux gauge was positioned and the heater was turned on. The calibrate feature on the MLC-5 system allowed for the user to manually input the desired heat flux and the apparatus would gradually alter the cone heater temperature to equal the target heat flux at 25.4 mm below the heater opening. For the 5 and 10 kW/m^2 heat fluxes, a heater temperature of 345°C and 450°C were required, respectively. Once the specified heat flux was reached, the calorimeter's heat shutter was closed and the heat flux gauge was removed to allow for the sample holder to be placed on the stand upon the beginning of the test.

(a) Prior to Apparatus Placement (b) After Apparatus Placement

Figure 2.22: PPE Assembled Sample Holder Prior To and After Placement in the MLC-5 Apparatus

Upon proper calibration and sample preparation, testing was begun for each of the PPE and cotton assemblies. Prior to placing the sample holder onto the apparatus stand, the DAQ system was turned on and a timer was initiated simul-

taneously. The sample holder was then placed onto the apparatus stand where the heat shutter was still closed, shielding the sample from the heater. Figure 2.22 shows the sample holder before and after being placed in the MLC-5 apparatus. The shutter was opened after 60 seconds had elapsed during the test, to allow for a uniform standard initiation of heat exposure amongst all tests. This also allowed the operator of the test time to place the sample holder onto the stand and to confirm that the thermocouples were transmitting properly to the DAQ. Upon the opening of the heat shutter, the test was run and the specimen exposed for 600 seconds, similar to prior work [47]. After 600 seconds had passed, the heat shutter was closed and the specimen entered the cool down period, lasting 180 seconds. The DAQ system remained on during the cool down period to record the temperatures after the removal of the heat source. Once 180 additional seconds had passed, the DAQ system was turned off and the sample holder was removed from the apparatus sample holder stand. The sample holder was then disassembled to allow for the PPE or cotton specimens and the air gap spacer to cool prior to the following test. The thermocouple data was exported from the DAQ system to a comma-separated value (CSV) text file. This procedure was repeated for each of the sleeve assemblies for the intended number of trials.

2.3.1.4 Limitations

One of the primary limitations of the cone heater experiments is the repetition of exposure to the samples prepared. For each air gap thickness, only one PPE sleeve

assembly and one cotton sleeve assembly was made to be used for both the 5 and 10 kW/m^2 heat fluxes. While this is not a concern for the 5 kW/m^2 tests, the PPE sleeve assemblies that underwent the 10 kW/m^2 tests exhibited some amount of decomposition. Although the samples were allowed a sufficient amount of time to return to their initial ambient conditions, the potential for varied results still remain given the effects of the initial heat flux exposure to the PPE or cotton fabrics. The same limitations apply to the fiberglass spacers used, as only one spacer was created to be used for both the PPE and cotton sleeve assemblies as well as for each of the two heat fluxes. The thermocouples used throughout the assembly are listed by the manufacturer to carry a tolerance value of ± 2°C. The placement of the thermocouples themselves also provides a possibility for error, primarily in the air gap. The thermocouples threaded between the layers are secured in place by the weight and fit of the fabrics however, for the thermocouple measuring the air gap temperature, the exact vertical location of the thermocouple in the air gap cavity varies, which in turn results in discrepancies of the recorded temperatures given that there is a temperature gradient across the vertical distance.

2.3.2 Heat Flow Meter Experiments

2.3.2.1 Overview

Obtaining the effective thermal conductivities and specific heat capacities of the constructed PPE sleeve assemblies benefit this study in two key ways. The values of the parameters, themselves, can provide insight on the ability of the entire

sleeve-air gap system to transfer heat from one end to the other in a one-directional scale through the increase or reduction of the property values in the presence of an air gap of predefined thickness. This property data was also valuable in this research as it provided experimental property inputs for the sleeve assemblies as a whole in the FDS simulated heat transfer models.

In order to determine the effective thermal properties of the PPE sleeve assemblies with the incorporated air gap, a *TA Instruments FOX 200 Heat Flow Meter* was used, located in the UL FSRI Laboratory in Columbia, MD. The Heat Flow Meter sleeve assemblies were tested in the apparatus under ambient environment conditions with an average temperature of 21°C and an average relative humidity of 27%. The heat flow meter apparatus operates in accordance with ASTM C518 and ISO 8301 [55] and utilizes Fourier's Law of Heat Conduction, Equation 2.1, to produce outputs of thermal conductivity, k, measured in W/m·K. The heat flow meter apparatus also produces values for determining the specific heat capacities of specified samples. The apparatus itself outputs volumetric heat capacities, C, with units J/m^3·K, using Equation 2.2. These volumetric heat capacities can be used to calculate the specific heat capacities for each assembly through a volume-density relation.

$$\dot{q}'' = -\frac{k\Delta T}{L} \tag{2.1}$$

$$Q'' = LC\Delta T \tag{2.2}$$

The closed apparatus can be seen in Figure 2.23(a) and the interior of the machine, where the assemblies were placed, can be seen in Figure 2.23(b). The PPE sleeve assemblies fit within the available sample size space of 203 × 203 mm which allowed for the intended sample to completely fill the apparatus space and ensured a lack of movement along the ends of the machine interior. The apparatus was set to automatically adjust its thickness to match that of the sample within and ensure no additional gaps were located between the top and bottom plates of the device. The temperature sensors are located in the center of the apparatus and encompass a 76 × 76 mm square area. This is fortunate for the PPE assembly testing of this study, as the sensors will focus on the conductivity and heat capacity at the center of the material assemblies with negligible interference from the surrounding fiberglass spacer ring frame.

(a) Closed FOX 200 Apparatus (b) Open FOX 200 Apparatus

Figure 2.23: TA Instruments FOX 200 Heat Flow Meter Apparatus

2.3.2.2 Measurement Theory

As previously mentioned, the governing equation, Equation 2.1, for conductive heat flux on a one-dimensional object is used by the heat flow meter to output a thermal conductivity, k, for the inserted assembly. In this testing scenario, L is the automatically adjusted thickness determined by the apparatus in m, $\dot{q}''$ is the steady state conductive heat flow in W/m^2, and ΔT is the difference between the temperatures of the top and bottom plates, T_2 and T_1, in K. Once the sample assembly has been inserted into the apparatus and adjusted for its thickness, a defined steady state heat flux, $\dot{q}''$, flows from the bottom plate to the top plate through the center of the sample. In order to solve for the only unknown parameter, k with units W/m·K in Equation 1.1, a temperature gradient must be established and maintained throughout the duration of the test. For this testing, four temperature set point ranges were defined and held for the top and bottom plates and these are specified in Table 2.3. This range of temperature set points allows for calculated thermal conductivities to be produced at both the top and bottom plates and are averaged to result in the final conductivity obtained for each test or sample.

Table 2.3: FOX 200 Thermal Conductivity Plate Temperatures

Test	Top Plate Temperature	Bottom Plate Temperature
1	5°C	25°C
2	10°C	30°C
3	20°C	40°C
4	30°C	50°C

For the volumetric heat capacities, the governing equation, Equation 2.2, was

used by the heat flow meter to output a parameter, C, as a function of temperature, heat flow, and thickness. The volumetric heat capacity is an intensive property that measures the heat capacity per unit volume. In this testing scenario, Q'', in J/m^2, is the total heat flow per square area from the time at which one temperature arrangement reaches equilibrium until the next temperature arrangement reaches equilibrium. Equilibrium is considered to be reached when the temperature of one plate is equal to the temperature of the other plate. For these tests, both the top and bottom plates are held at the same temperature set points and for the total five tests conducted, the temperature values are shown in Table 2.4. The temperature difference between two of these temperature arrangements is denoted as ΔT, in K, in Equation 2.2 and L is the automatically adjusted thickness determined by the apparatus, in m. The volumetric heat capacity for the tested sample is the final output quantity for the four intermediate temperatures between the five temperature set point arrangements for these experiments.

Table 2.4: FOX 200 Volumetric Heat Capacity Plate Temperatures

Test	Top Plate Temperature	Bottom Plate Temperature
1	5°C	5°C
2	15°C	15°C
3	25°C	25°C
4	35°C	35°C
5	45°C	45°C

The specific heat capacity is an additional intensive material property that indicates the amount of heat required per unit mass to increase the temperature by one unit change. To convert the volumetric heat capacities into specific heat

capacities, the output values from the heat flow meter apparatus were divided by the density of the PPE assembly, as shown in Equation 2.3. The specific heat capacity, c_p, is in units of J/kg·K and the density, ρ, is in kg/m^3.

$$c_p = \frac{C}{\rho} \tag{2.3}$$

The density for each PPE sleeve assembly was calculated using Equation 2.4 which requires the mass and volume of the effective assembly. The mass of each assembly was measured using a Sartorius Laboratory Balance, having a precision of 0.01 g. The volume of each assembly was measured using both a metric ruler in addition to a Carrera Precision digital caliper to obtain values on the length, width, and thickness of the assemblies, each of which are in units m. The densities calculated and shown in Table 2.5 were used to produce the specific heat capacities for each PPE sleeve assembly.

$$\rho = \frac{m}{V} \tag{2.4}$$

Table 2.5: Calculated Densities for PPE-Air Gap Assemblies

Air Gap Thickness (mm)	Density (kg/m^3)
0.0	261
6.35	345
12.7	493
19.05	405
25.4	410

2.3.2.3 Limitations

The associated thermo-physical properties of the effective material are considered to be constant in this analysis although in reality, both the thermal conductivity and specific heat capacity are temperature-dependent properties. The measurements for these parameters are beyond the range of the heat flow meter employed here. Thermal conductivity, as referred to in Fourier's one-dimensional law, is an intrinsic property of an isothermal homogeneous anisotropic material. The model being adopted in this study is a composite specimen comprised of layered materials and air. This assembly represents an "effective" solid material to which the derived thermal conductivity applies. This model greatly limits the utility of the calculated thermal conductivity. For one, given that the samples are asymmetric, the result is only appropriate in the direction of heat transfer tested. For the Heat Flow Meter apparatus in this arrangement, the heat flows from the bottom to the top plate or from the top of the PPE down to the cotton stationwear. Another limitation for both the thermal conductivity and the specific heat capacity is that the results are only appropriate for the temperature range tested, as the maximum test temperature set point conducted produces parameters at 40°C contrary to the experiments of the Cone Heater series which were conducted at elevated temperatures. Finally, and most importantly, these values are only applicable to steady-state measurements, not for transient measurements.

2.4 Testing Matrices

The test matrices for the Cone Heater series at heat fluxes 5 kW/m^2 and 10 kW/m^2 are shown in Figures 2.24 and 2.25, respectively. In total, 34 tests were conducted with the PPE and cotton sleeve assemblies. The PPE sleeve assemblies were tested in duplicate for each of the five air gap thicknesses at each heat flux exposure resulting in 20 complete tests. The cotton sleeve assemblies were also tested for each of the five air gap thicknesses and heat flux exposures except these assemblies were only tested once, equaling 10 tests. An additional four tests were conducted on the outer shell fabric alone, with no air gap, to provide a comparative reference of the heat transferred to the thermocouple through solely the top layer of the PPE. These four additional tests included two trials of the outer shell fabric being exposed to the 5 kW/m^2 flux and two trials of the outer shell fabric being exposed to the 10 kW/m^2.

Cone Heater Series					
Exposure Flux	5 kW/m^2				
Material Assembly	Outer Shell		Cotton	PPE	
Trial	1	2	1	1	2
Air Gap Thickness (mm)					
0.00					
6.35					
12.70					
19.05					
25.40					

Figure 2.24: Test Matrix for the 5 kW/m^2 Flux Cone Heater Series

The test matrix for the Heat Flow Meter series is shown in Figure 2.26. Both

Cone Heater Series					
Exposure Flux	10 kW/m^2				
Material Assembly	Outer Shell		Cotton	PPE	
Trial	1	2	1	1	2
Air Gap Thickness (mm)					
0.00					
6.35					
12.70					
19.05					
25.40					

Figure 2.25: Test Matrix for the 10 kW/m^2 Flux Cone Heater Series

the thermal conductivity and volumetric specific heat capacity for the PPE assemblies were tested in triplicate to quantify and understand the variability, as it may play a more significant role when these values are used within the simulated model. For both material property tests, each of the five air gap thickness sleeve assemblies were used, resulting in a total of 30 tests overall.

Heat Flow Meter Series						
Material Property	Thermal Conductivity			Volumetric Specific Heat Capacity		
Trial	1	2	3	1	2	3
Air Gap Thickness (mm)						
0.00						
6.35						
12.70						
19.05						
25.40						

Figure 2.26: Test Matrix for the Heat Flow Meter Series

2.5 One-Dimensional Heat Transfer Model

2.5.1 Overview

A one-dimensional heat transfer model was created to represent the configurations of the Cone Heater series using FDS and the material property data from the Heat Flow Meter series. FDS is a computational fluid dynamics (CFD) model of fire-driven fluid flow used to solve practical fire protection engineering problems in addition to studying the fundamental principles of fire dynamics and heat transfer. The simulations produced from this software would not only validate the experimental Cone Heater data but also provide a better understanding into the methods of heat transfer apparent within the PPE-air gap system. The goal of the simulations was to obtain a temperature-time curve at the depth below the cotton stationwear, where the hypothetical skin layer would be located. The temperature-time curve produced from the FDS simulation with the heat flow meter thermal property inputs would ideally match that of the experimental curves produced from the Cone Heater series. Simulations were run using FDS for the PPE sleeve assemblies for all air gap sizes and under both levels of heat flux exposure. The cotton sleeve assemblies were not included in the configurations modeled with FDS as the purpose of the cotton experiments were to solely gain a qualitative understanding of the air gap's influence.

FDS is an open-source software, developed by NIST, that is available to the public and can be accessed on the internet through the NIST website. FDS is pro-

grammed to numerically solve a form of the Navier-Stokes equations for low-speed, thermally-driven flow [56]. In addition to modeling fluid flow, this software has the capability of modeling heat transfer through solid phase materials via predefined thermophysical properties. While the majority of the capabilities of FDS focus on combustion-based problems, it also can be used to model heat transfer problems with an external radiant source. These functions of both solid phase heat transfer and an external radiant heat source are the primary reason that FDS was chosen for this study. To use the FDS software, scenario parameters were specified within an input text file that is then read by the software, which outputs results of the simulation to a data file.

2.5.2 FDS Input File

The FDS model was designed to simulate a similar configuration to the Cone Heater series experiments, with an external heat flux being exposed to the horizontal top layer of an effective PPE sleeve assembly with an insulative backing. The simulations began at ambient temperatures between 20 and 25°C, depending on the ambient temperatures of the associated experimental tests, and ran over a total duration of 840 seconds. The mesh was made up of 27 cells in a $3 \times 3 \times 3$ grid with a uniform cell size of 0.1 m.

The model was designed to run in a single mesh for solid phase heat transfer only, meaning that FDS would consider a single solid surface to consist of multiple layers of varying materials that of which can be specified through their own unique

properties. The heat transferred through the normal direction of this surface from top to bottom is considered to act solely as a function of conduction, as indicated by the solid phase transient conduction equations specified within the FDS Technical Reference Guide [57]. The FDS conduction model has been validated; see Chapter 11 in the FDS Verification Guide [58].

In solid phase simulations, the numerical accuracy and stability are dependent on node spacing, mesh cell sizes, time resolution, and the number of cells within a single layer [56]. Given that FDS solves the one-dimensional heat transfer equation numerically, node spacing has a stronger influence in the simulation over grid resolution, which is used for gas phase computations. Node spacing within a solid phase computation has a default stretch factor value of one, indicating a perfectly uniform mesh. The mesh cell size also has a default value of one which represents the largest cell size available for configuration. The default number of cells within a layer is 1000, which can be reduced depending on the complexity of the model. Given that the scenario for this model is computing heat transfer within a single surface in the absence of combustion or a pyrolysis reaction, the default values for the number of cells, mesh cell size, and stretch factor were deemed appropriate. The time resolution for this model was not kept at the default value of two, but instead changed to one. This change forces the solid phase solution to be calculated and updated at every time step instead of every two time steps with the initial time step being set to 0.01 seconds.

There were two materials defined within the solid surface of this model, the effective PPE assembly and the ceramic fibreboard insulation. Three material prop-

erties were specified for each of these layers, that being the thermal conductivity, specific heat capacity, and density. The additional thermal and physical properties of the materials, such as the radiative emissivity and absorption factors, were taken as the default FDS values. As indicated by the experimental property inputs of the Heat Flow Meter series, the PPE assembly with its respective fabric layers and air gap was modeled as a single effective solid material. The thermal conductivity and specific heat capacity inputs were taken for each air gap size assembly from the experimental data in Table 3.1. The densities of each air gap assembly are shown in Table 2.5 and were measured using the procedure outlined in Section 2.3.2 detailing the conversion from volumetric specific heat capacity for the Heat Flow Meter series. The ceramic fibreboard insulation material was defined with the thermal and physical properties identified in Table 2.2. The temperature-dependent property equations for the insulation were implemented into the input file using the ramp FDS function for material properties at intervals of 25°C from 0°C to 300°C, and the associated thermal conductivity and specific heat capacity values at each temperature were specified to be entered in the model.

The surface conditions were defined to reflect not only the materials within the depth of the surface but the external radiant and convective exposure conditions as well. The material layers included in the surface are the PPE assembly, at its respective thickness to the air gap size, and two layers of ceramic fibreboard insulation below it, each at a thickness of 12.7 mm to mimic the insulative backing of the Cone Heater experiments. The thicknesses of the entire PPE assembly for each air gap size were measured and output from the heat flow meter apparatus and

are shown in Appendix A.2. As previously mentioned, the radiative properties, such as emissivity, for the effective assembly were taken as the default FDS values and in-depth absorption was neglected for this model. For the respective input file of each exposure condition, the external flux was denoted as 5 or 10 kW/m^2. Associated with these external exposures were the convective heat transfer coefficients relative to the orientation and ambient environment of the test. The convective heat transfer coefficients were estimated using the natural convection Nusselt correlations for a horizontal plate in the *Fundamentals of Heat and Mass Transfer* text [19]. The exact correlation used for both heat flux exposures depicted the upper surface of a cold plate, shown in Equation 2.5.

$$Nu_L = 0.52{Ra_L}^{1/5} \tag{2.5}$$

The Rayleigh number, Ra_L, was calculated with the thermal properties of air [19], taken at a film temperature averaged between the hot gas temperature from the heater and the ambient surface temperature of the outer shell fabric. The hot gas temperature for the 5 kW/m^2 exposure was 345°C and 450°C for the 10 kW/m^2 exposure, and the ambient surface temperature was 20°C. The convective heat transfer coefficients were estimated to be 7.05 W/m^{2}K for the 5 kW/m^2 exposure and 7.30 W/m^{2}K for the 10 kW/m^2 exposure. Given that these values are estimates, the convective heat transfer coefficient is an additional source of uncertainty for the model.

The external heat flux exposure was initiated after 60 seconds to mimic the

opening of the heat shutter in the Cone Heater tests. The 5 and 10 kW/m^2 heat fluxes were exposed to the effective PPE assembly for 600 seconds before the external flux was turned off, similar to the closing of the shutter. The simulation was set to run for the additional 180 seconds to gain an understanding of the temperature behavior during the cool down period within FDS. These openings and closings of the external flux were modeled using a ramp FDS function for the surface properties that was set to initiate a full fraction of the flux at the 60 second mark and to remove it exactly at 660 seconds.

The mesh was configured to apply these surface and material properties through the use of boundary conditions, or vents. The default six vents are located along each exterior boundary of the mesh and the vent conditions can be set to meet the desired specifications of the simulation. For the configurations of these tests, the minimum boundary in the Z-direction was defined with the surface conditions detailed above. The remaining five vents were set to reflect passive openings to the outside or ambient environment. A single device in FDS was defined and placed below the PPE assembly using a depth parameter equivalent to the thickness of the entire assembly. This device resembled that of a thermocouple and was designed to record the interior temperature throughout the duration of the simulation. The temperature data output from this device creates the temperature-time curve used for comparison.

Input files were created and run for each air gap thickness and both heat flux exposures equating to a total of 10 FDS simulations. An example of the input file for the PPE assembly with a 6.35 mm air gap under the 5 kW/m^2 exposure is shown

in Appendix A.4.

2.5.3 Limitations

The overall PPE-air gap system is modeled as an "effective" solid material that conducts heat through its heterogeneous composition to the thermocouple located on the far surface. The assumption of one-dimensional heat transfer through both the fabric layers as well as the air gap is met with opposition of the realistic non-uniformity of irradiance and conduction. In reality, the potential for heat to dissipate laterally in the system is still apparent regardless of insulation on the exterior boundaries. The effective conduction model constructed here neglects both radiation and convection within the air gap cavity and the effective properties from the heat flow meter are valid only for steady state conditions. The model is also limited by the assumption of non-decomposition of the samples themselves. The thermal decomposition of the samples are not considered in this study even though it can be assumed that mass loss will be apparent in the PPE fabrics at the exposed exterior surface. It should also be noted that moisture transport is neglected for the current model.

The simple conduction-driven model is satisfactory for this work given its assumed capabilities in validating the experimental data of the PPE assembly with no air gap, and representing the conduction-dominant air cavities within the selected air gap sizes.

Chapter 3: Experimental Results

3.1 Cone Heater Series

3.1.1 Cone Heater Results

Prior to the primary tests with the PPE sleeve assemblies, tests were conducted for the outer shell fabric as well as the cotton sleeve assemblies. The outer shell fabric tests were used as a comparative measure of the temperatures recorded through one layer of PPE fabric. This was done to ensure that the temperatures recorded under the top layer of the PPE for the PPE sleeve assembly tests was equivalent to that recorded for the top outer shell layer alone. Additionally, these tests ensured that the thermocouples and DAQ system were functioning properly prior to PPE sleeve assembly exposure. The temperature data of the outer shell fabric tests for each heat flux are in Appendix B.1. Cotton sleeve assemblies were also tested in the cone heater and these tests were conducted to gain a qualitative understanding of the influence of an air gap to cotton clothing in general, with no PPE involved. Given that these tests were run with the intent of merely observing the thermal phenomenon, only one trial of testing was conducted for each of the air gap sizes. The data produced by the cone heater for each air gap thickness and heat flux of the

cotton baseline surrogates is located in Appendix B.2. From this data it is apparent that the inclusion of an air gap reduces the temperatures reached on the backside of the air gap thus qualitatively confirming the existence of an insulating factor. For the remainder of the Cone Heater results and analysis, the primary focus will be on the PPE sleeve assemblies.

As previously mentioned, the PPE sleeve assemblies were tested in duplicate to characterize the repeatability of these experiments in the cone heater. Two trials was deemed satisfactory in determining the repeatability of the tests for the purposes of this study. From the two trials of PPE sleeve assembly data for each air gap size, an average temperature curve was calculated with additional curves representing the maximum and minimum temperature values at each point in time. From here onward for the plots of this report, the average temperature of the two trials at each layer in the assembly is denoted with a solid colored line matching the associated label in the legend. The maximum and minimum curves are denoted on the same plots in the respective colors of their average temperature curve, but are distinguished via their lighter dashed lines instead.

3.1.1.1 5 kW/m^2 Exposure

The temperature-time plot for the PPE sleeve assembly with a 0.0 mm air gap under the 5 kW/m^2 heat flux is shown in Figure 3.1. On this figure, the temperature data from the thermocouples located below the PPE-stationwear and the insulation are shown. The curves provide evidence of the key events that took place during

the Cone Heater series, such as the opening and closing of the heat shutter at 60 and 660 seconds, respectively. The temperature data below the PPE and cotton stationwear shows a steep increase in temperature from the ambient environment, 22°C, once the shutter has been opened. The temperature continues to increase for the duration of the exposure and reaches a maximum temperature of 192°C prior to the shutter being closed, at which time the temperature drops. The following cool down period lasts 180 seconds and by the end of the experiment the temperature has dropped back down to 96°C. For the temperature data under the insulation, the curve steadily rises throughout the test ending at 85°C.

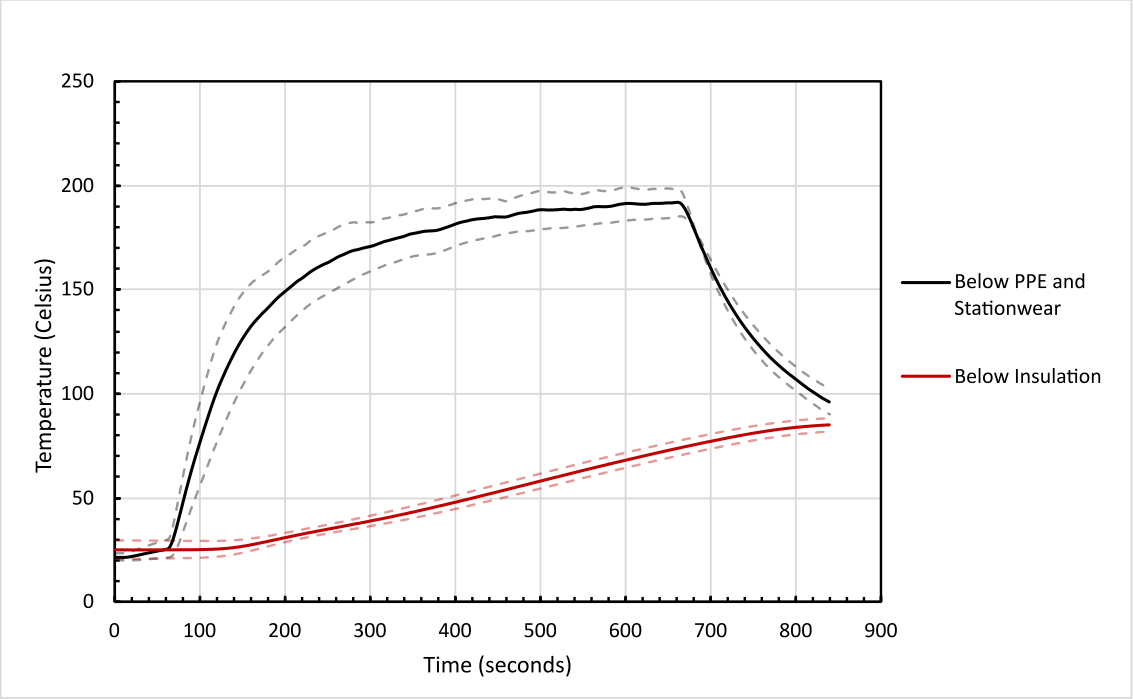

Figure 3.1: Temperature versus Time for the PPE Sleeve Assembly with a 0.0 mm Air Gap at 5 kW/m^2 Heat Flux

For the temperature-time plot of the PPE sleeve assembly with a 6.35 mm air gap under 5 kW/m^2 exposure, shown in Figure 3.2, the general trends remain

the same however, there are now five curves of temperature data. Within this plot, "Below Outer Shell" refers to the thermocouple temperature data recorded by the thermocouple under the top outer shell fabric, "Below Thermal Liner" refers to the thermocouple pad on the back surface of the thermal liner, "Air Gap" refers to the thermocouple within the air gap cavity, "Below Stationwear" refers to the thermocouple under the cotton stationwear, and "Below Insulation" refers to the thermocouple located under the ceramic fibreboard.

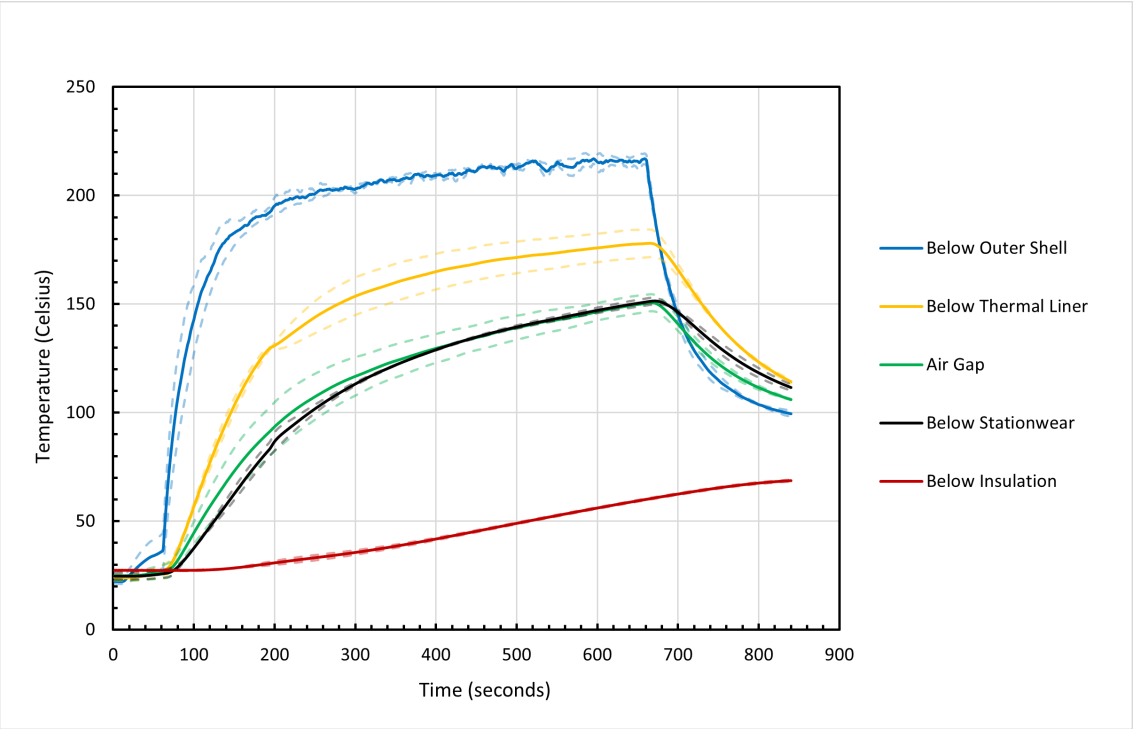

Figure 3.2: Temperature versus Time for the PPE Sleeve Assembly with a 6.35 mm Air Gap at 5 kW/m^2 Heat Flux

In this plot, the opening and closing of the shutter at 60 and 660 seconds, respectively, is noticeable on four of the five curves with the exception of the insulation. At the thermocouples above the insulation, an increase denotes the time at which the thermocouple for each depth position begins to respond to the external

heat. For the "Below Outer Shell" curve, the significant temperature increase begins at 60 seconds and reaches a maximum temperature at the end of exposure of 217°C. It should be noted that there is an initial rise in temperature prior to the 60 second initiation due to heat propagating through the heat shutter of the apparatus. The temperature curve for this data drops back down to 100°C during the cool down period. For the "Below Thermal Liner" curve, while there is an increase in temperature post opening of the shutter, it is delayed beyond that of the "Below Outer Shell" curve. The duration of exposure for this curve leads to a maximum temperature of 178°C and after the cool down period the temperature is at 114°C. It is important to note that there is a slight delay in this reduction during the cool down period, as the "Below Thermal Liner" curve drops after the "Below Outer Shell" curve. For the following "Air Gap" curve, the same trends mimic that of the "Below Thermal Liner" curve, but to a lesser extent. There is a further delay in the steep increase after the shutter is opened and the maximum temperature reached throughout the duration of the exposure is 150°C. The final temperature at the end of the cool down period for this curve is 106°C. For the "Below Stationwear" curve, there is a further delay behind the "Air Gap" curve in the increase in temperature however, the increase in temperature itself over the exposure duration is observed to be essentially the same as the "Air Gap" curve. The curves themselves overlap for a significant amount of time and the "Below Stationwear" curve reaches a maximum temperature of 151°C prior to the cool down period. The final temperature after the cool down period is greater for the "Below Stationwear" curve than the "Air Gap" curve with the "Below Stationwear" at 112°C. The final curve on the plot

is the "Below Insulation" curve and while it does not match that of the trends of the four previous curves, it does resemble the insulation curve of the 0.0 mm air gap plot. The "Below Insulation" curve increases gradually throughout the entire duration of the test with no variations in behavior at key events. This steady rise in temperature begins at the ambient temperature of 27°C and ends at 69°C.

The remaining temperature-time plots for the 12.7 mm, 19.05 mm, and 25.4 mm air gap assemblies under the 5 kW/m^2 heat flux are shown in Appendix B.3.1. These plots are of the same design as the 6.35 mm plot, with the five thermocouple temperature curves labeled and colored in the same fashion. The trends for these plots all demonstrate the same behavior for each of the respective curves in regard to their position and relation to the key events within the experiments. The primary difference between each of these graphs and their individual curves are the magnitudes of the temperatures reached. As the air gap thickness increases, the maximum temperatures reached for all five curves decreases. It is also important to note that there is a slight fluctuation in the temperature data during the cool down period of the "Below Outer Shell" curve in the 12.7 mm air gap plot, which is a result of thermocouple damage that occurred at the end of the experiment.

Through visual observation, the PPE sleeve assemblies only showed signs of heat flux exposure on the top outer shell surface for the 5 kW/m^2 flux. There was a slight discoloration of the outer shell fabric which can be seen in Figure 3.3. This discoloration occurred as a result of the entire duration of exposure and represent the minimal thermal degradation that took place during the experiment.

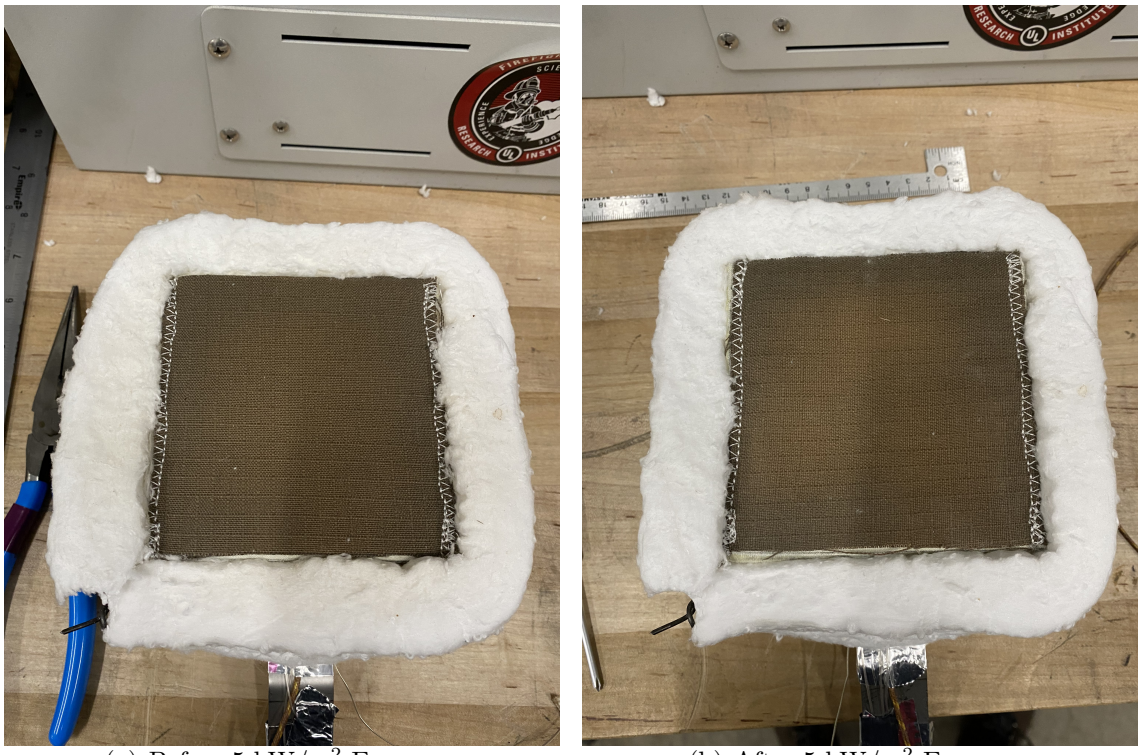

(a) Before 5 kW/m^2 Exposure (b) After 5 kW/m^2 Exposure

Figure 3.3: Top Surface of the Outer Shell Fabric Before and After the 5 kW/m^2 Heat Flux

3.1.1.2 10 kW/m^2 Exposure

The temperature-time plot for the PPE sleeve assembly with a 0.0 mm air gap under the 10 kW/m^2 heat flux is shown in Figure 3.4. On this figure, the temperature data is also from the thermocouples located below the PPE-stationwear and the insulation, similar to Figure 3.1. In this plot the curves also provide evidence of the key events that took place during the Cone Heater series, such as the opening and closing of the heat shutter at 60 and 660 seconds, respectively. The temperature data below the PPE and cotton stationwear shows an increase in temperature, once the shutter is opened, from 22°C to 275°C over the entire exposure duration. The temperature then drops during the 180 second cool down period ending at 180°C.

The behavior of the temperature data below the insulation is similar to the 5 kW/m^2 exposure as it continuously increases throughout the entire experiment however, the maximum temperature reached is much greater, ending at a temperature of 128°C.

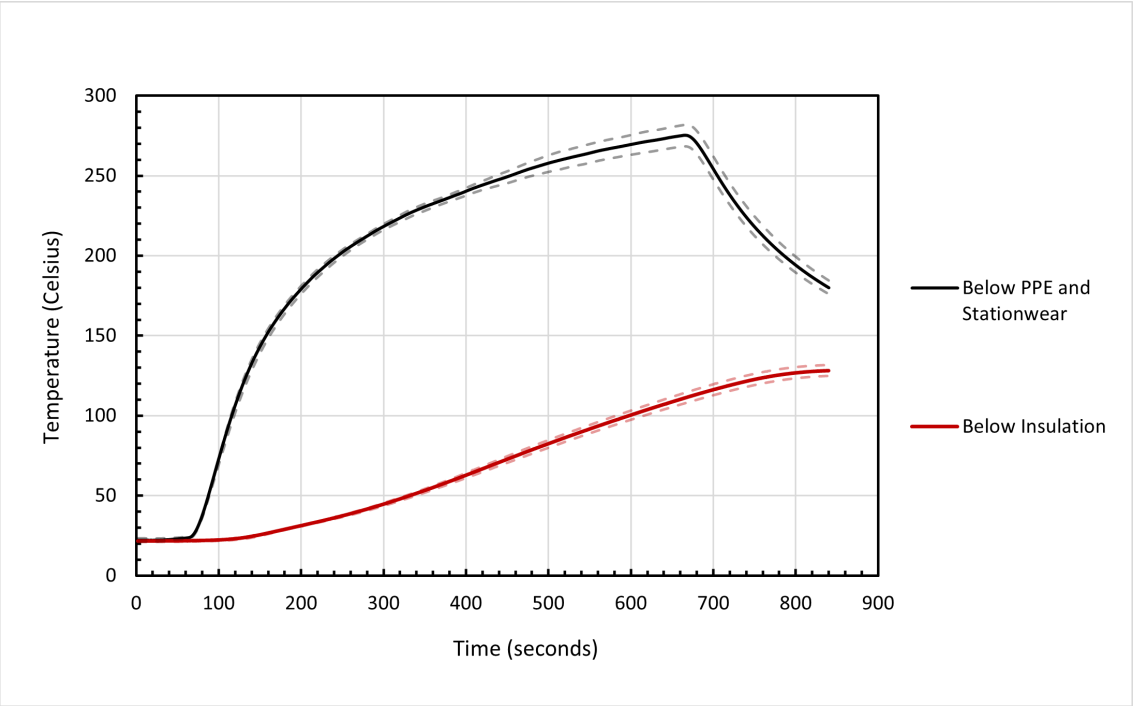

Figure 3.4: Temperature versus Time for the PPE Sleeve Assembly with a 0.0 mm Air Gap at 10 kW/m^2 Heat Flux

For the temperature-time plot of the PPE sleeve assembly with a 6.35 mm air gap under the 10 kW/m^2 exposure, shown in Figure 3.5, the behavior is similar to the 5 kW/m^2 exposure plot but is instead at elevated temperatures and times. The five curves portrayed on the plot share the same labels depicting their position within the depth of the entire PPE sleeve assembly. The "Below Outer Shell" curve still depicts an increase at the opening of the shutter and then reaches a maximum temperature of 304°C, until the shutter is closed. The temperature then drops down to 126°C at the end of the cool down period. For the "Below Thermal

Liner" curve, there is still a delayed increase in temperature behind the "Below Outer Shell" curve and the increasing data reaches a maximum temperature of 252°C prior to the cool down period, leaving the curve to end at 152°C. For the "Air Gap" and "Below Stationwear" data, they are still closely related however, the "Air Gap" curve is initiated sooner than the "Below Stationwear" curve and also reaches a maximum temperature less than that of the "Below Stationwear" line. The maximum temperatures of the "Air Gap" and "Below Stationwear" curves are 215°C and 220°C, respectively. The decreasing behavior holds true throughout the cool down period to produce final temperatures of 142°C and 151°C for the "Air Gap" and "Below Stationwear" curves, respectively. The "Below Insulation" follows the same continuous increasing behavior to reach a final temperature of 94°C.

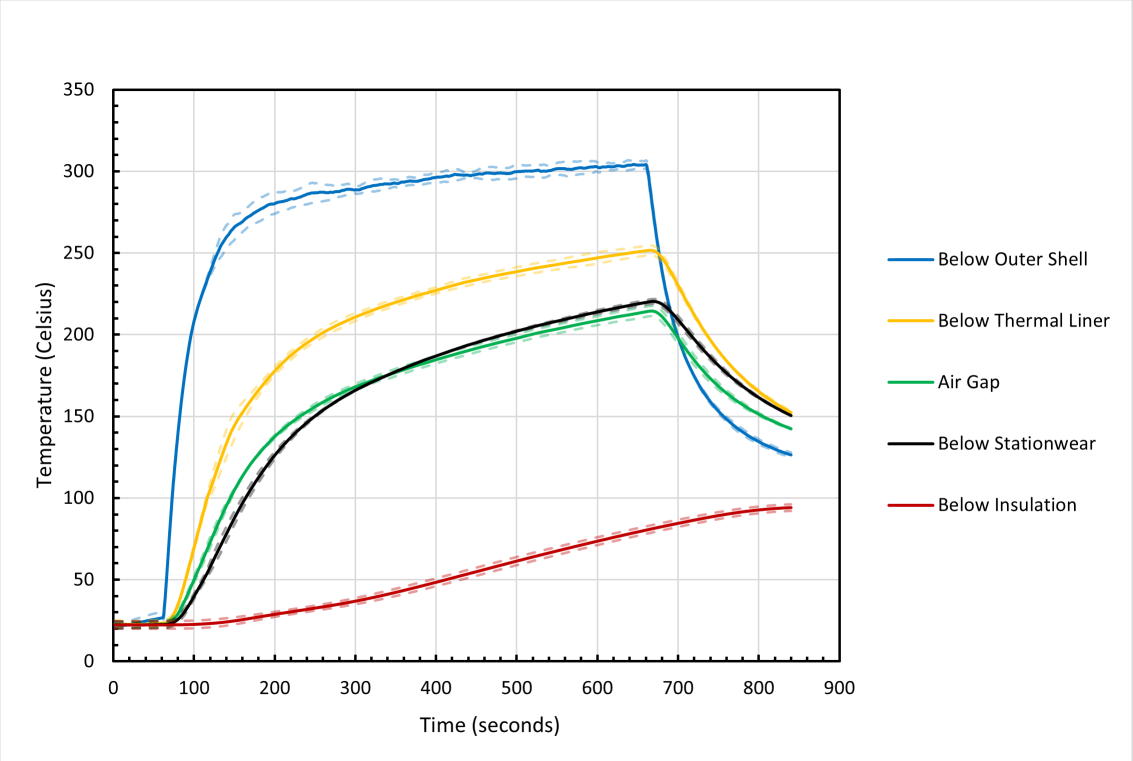

Figure 3.5: Temperature versus Time for the PPE Sleeve Assembly with a 6.35 mm Air Gap at 10 kW/m^2 Heat Flux

The remaining temperature-time plots for the 12.7 mm, 19.05 mm, and 25.4 mm air gap assemblies under the 10 kW/m^2 heat flux are shown in Appendix B.3.2. These plots follow the same design as the plots that precede them, with the five thermocouple temperature curves labeled and colored in the same fashion. The trends for each of these plots depict the same shape and once again the temperatures are the primary indicators of varying results as a function of the air gap size.

For the 10 kW/m^2 heat flux, there was significantly more visible thermal degradation apparent to the PPE sleeve assemblies. In Figure 3.6, the outer shell fabric is shown before and after the 10 kW/m^2 exposure. Here it can be seen that there is a lightening of the fabric throughout majority of the top surface, and along the center area above the air gap there is a dark discoloration and to the touch, there was an increase in the fabric's stiffness. The heat effect is not only at the top surface for the 10 kW/m^2 heat flux as there is material degradation apparent throughout the fabric layers and fiberglass spacer as well. In Figure 3.7, the fiberglass spacer can be seen with a green-black heat stained pattern along the ring and the bottom cotton layer of the fabric sleeve is darkened at the center as well. The visual damage made apparent here indicates that the degradation and discoloration brought on by the heat was transmitted throughout the entirety of the PPE material over the test duration.

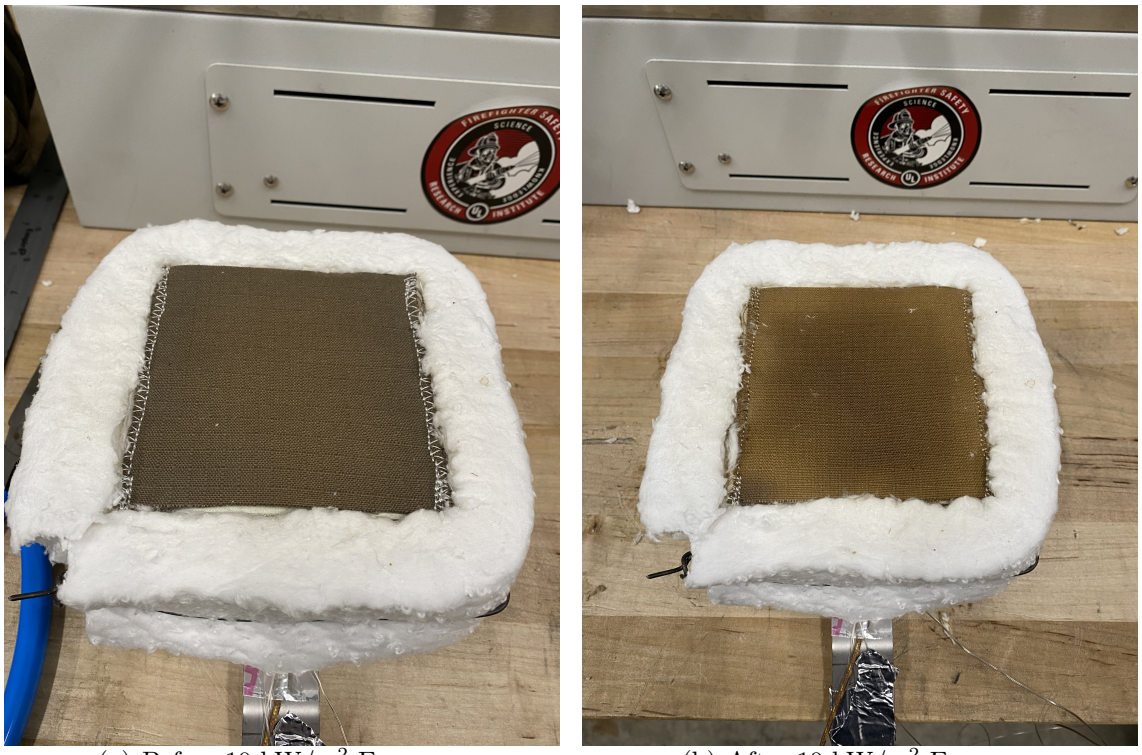

(a) Before 10 kW/m^2 Exposure (b) After 10 kW/m^2 Exposure

Figure 3.6: Top Surface of the Outer Shell Fabric Before and After the 10 kW/m^2 Flux

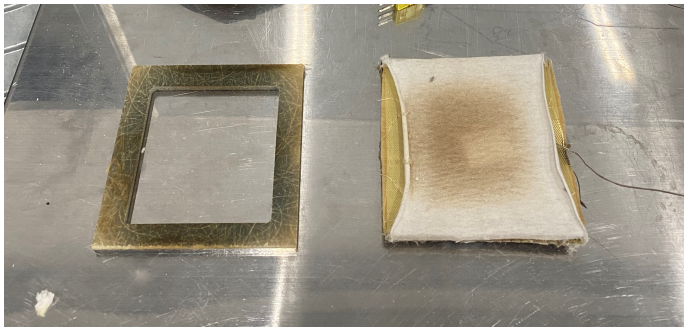

Figure 3.7: Visual Discoloration on the Fiberglass Spacer and Cotton Stationwear for the 6.35 mm Assembly After the 10 kW/m^2 Exposure

3.1.2 Discussion of Cone Heater Results

3.1.2.1 Analysis

From the obtained temperature data, insight is provided on the thermal lag and maximum temperatures reached as a function of the depth in the PPE assembly. For both the 5 and 10 kW/m^2 heat fluxes, the behavior of the measurements in both the plots without an air gap as well as the plots with an air gap were relatively similar in that the thermocouples above the insulation demonstrated behavior to align with the key events of the experiment, that being the opening and closing of the heat shutter. The "Below Insulation" data in all plots demonstrated the same increasing trends throughout the entirety of the experiment indicating behavior impervious to the key events. In addition to this, the thermal lag for the measurements below the insulation are much larger than the measurements above the insulation, as shown by the large delay in a temperature response. From these observations it can be concluded that while the bottom of the assembly is not adiabatic given the temperature increase, the intense thermal lag and unresponsiveness of the data to key events indicates a reasonable approximation for an insulated boundary at the bottom of the assembly.

For the measurements above the insulation, the "Below Outer Shell" temperature data was of the largest magnitude among all plot conditions, which is justifiable given its proximity to the external heat source. The governing trend that is reconfirmed from this data is that as the depth from the exposed surface increases, the

maximum temperature decreases. This is made apparent for the measurements in all air gap thicknesses and heat flux exposures. The exception to this statement is visible between the "Air Gap" and "Below Stationwear" data at each air gap thickness. For these measurements, although the "Air Gap" location is positioned closer to the exposed surface than the "Below Stationwear" location, its maximum temperature is less than that of the "Below Stationwear". The explanation for this deviation in the trend is because the temperature of the "Air Gap" is the gaseous temperature of the air within the cavity as opposed to the temperature reading of the solid cotton stationwear fabric in the "Below Stationwear" data. Excluding the "Air Gap" temperatures from the comparison, the maximum temperatures of the solid materials from top to bottom in the assembly maintain the trend. In addition to the magnitude of the temperatures, the time at which a temperature increase is observed also depends on the relative position to the source. This relationship detailing the thermal lag entails that as the depth from the exposed surface increases, the time to response also increases. This is shown in the plots by the delay times of the thermocouple positions and their associated measurements at the opening of the heat shutter. For both heat flux exposures and all air gap thicknesses, the order of thermal response to the external source remains "Below Outer Shell", "Below Thermal Liner", "Air Gap", "Below Stationwear", and "Below Insulation".

When focusing on the impact of the air gap to the temperature data, the initial observations of the gap influence can be seen via the "Below Thermal Liner" and "Below Stationwear" measurements. These two locations reside on either side of the air gap and directly represent the temperature difference as an effect of the

potentially insulating air gap. Looking at any of the PPE assemblies with an air gap, it can be seen that the temperature, at any point in time during the exposure, of the "Below Stationwear" data is less than the temperature of the "Below Thermal Liner" data. This indicates that the incorporation of an air gap into the assembly reduces the transfer of heat, either by the properties of the air itself or by the mere extension of the position of the receiver from the source, and thus reduces the hazardous temperatures reached at the point of interest. This is additionally supported by the temperatures of the 0.0 mm assembly with no air gap. Under the same exposure and testing conditions, the maximum temperature below the PPE and stationwear of the 0.0 mm assembly is larger than any of the temperatures below the stationwear for any of the four air gap assemblies.

The thermal degradation observed on the assemblies reflects the expected behavior for each heat flux. It has been noted in prior work that visible degradation is typically not seen on firefighter PPE at 5 kW/m^2 exposures [6], and this observation holds true for the current data as minimal thermal degradation was seen. For the 10 kW/m^2 heat flux, significant thermal decomposition was seen and these thermal effects influence the heat transfer properties. The degradation of the materials implies the presence of energetic reactions that directly correlate with the breakdown of the materials affecting the heat flow through the fabric.

3.1.2.2 Application

While the benefit of an air gap is made clear amongst the differences in the maximum temperatures within the assembly, the scope of these temperatures are not practical for a real-world application. A firefighter is not concerned with what is happening at temperature conditions that exceed 72°C. At this temperature, third degree burns would have already occurred and irreparable damage would have been inflicted on the wearer. To answer the question on whether the time to burn injury can be prolonged with the inclusion of an air gap, further analysis of the temperature data must be conducted.

The temperature curves produced from the Cone Heater experiments provide relevant information at multiple depths within the PPE-air gap system however, the layer of interest for this analysis is the "Below Stationwear" data. This data represents the temperature at the hypothetical skin layer of the PPE-air gap system and can be used to provide a conservative estimate of the time to burn injury for the wearer. The times to burn injury were obtained for each air gap thickness through the "Below Stationwear" data for the 5 kW/m^2 heat flux and are shown within Figure 3.8. The black arrow shown above the plot entails that the true quantity of the third degree time to burn injury for the 25.4 mm thickness is 507 seconds as it was not graphically shown for the sake of visual clarity for the data of smaller magnitude. In this plot, the times corresponding to the representative skin temperature reaching these critical values are found as the times when the "Below Stationwear" temperatures reach 44°C for first degree burns, 55°C for second degree

burns, and 72°C for third degree burns. The times obtained here do not correspond with the actual burn times but instead represent a potential time to burn injury as they are expected to be a reasonable approximation that is appropriate for this analysis.

From this data it can be observed that the time to burn injury increases as the air gap thickness increases. The time to first degree burn shows the smallest changes in time as a function of the air gap thickness whereas the time to third degree burn depicts the largest difference in time. The time to third degree burn with a 25.4 mm air gap is shown as being five times the time to third degree burn with no air gap at all. From this data it can be seen that the time to burn injury is prolonged with the inclusion of an air gap, and that the relative size of the air gap also has influence as well.

The times to burn injury for each air gap thickness for the 10 kW/m^2 heat flux were also obtained from the "Below Stationwear" curves and are shown within Figure 3.9. From this data it is shown that for majority of the cases, the time to burn injury increases as the air gap thickness increases. The time to third degree burn increases as the air gap thickness increases holding true to the trends of the 5 kW/m^2 exposure. For the first and second degree times to burn injury, there is an increase in time between the 0.0 mm and 6.35 mm thicknesses however, between the 6.35 mm and 12.7 mm, there is a slight decrease in the time to burn injury. This reverts back to the governing trend from the 12.7 mm to the 25.4 mm thicknesses as the times to burn injury once again continue to increase with the thicknesses. The decrease in the time to burn injury between the 6.35 mm and 12.7 mm thicknesses is a factor

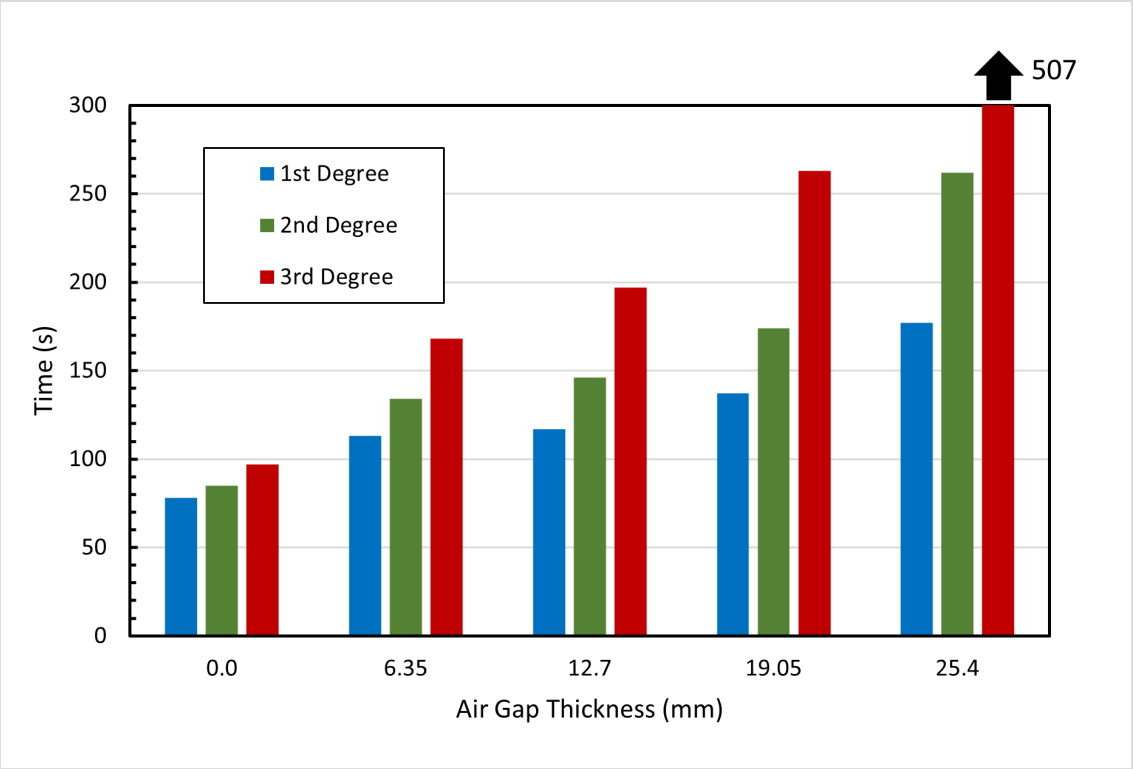

Figure 3.8: Time to Burn Injury versus Air Gap Thickness at 5 kW/m^2 Heat Flux

of experimental error among the preliminary air gap tests. Minor discrepancies in the initial ambient temperatures below the stationwear for the 12.7 mm thickness tests are indicators of premature burn injury times for the first and second degrees. Although this provides uncertainty in the quantitative accuracy of the burn times, it should be restated that this deviation is only apparent for the 10 kW/m^2 flux and that the remaining data mimics the same trends of the 5 kW/m^2 flux. Given that this is a conservative estimate of the time to burn injury with the influence of an air gap, the qualitative takeaways are still valid.

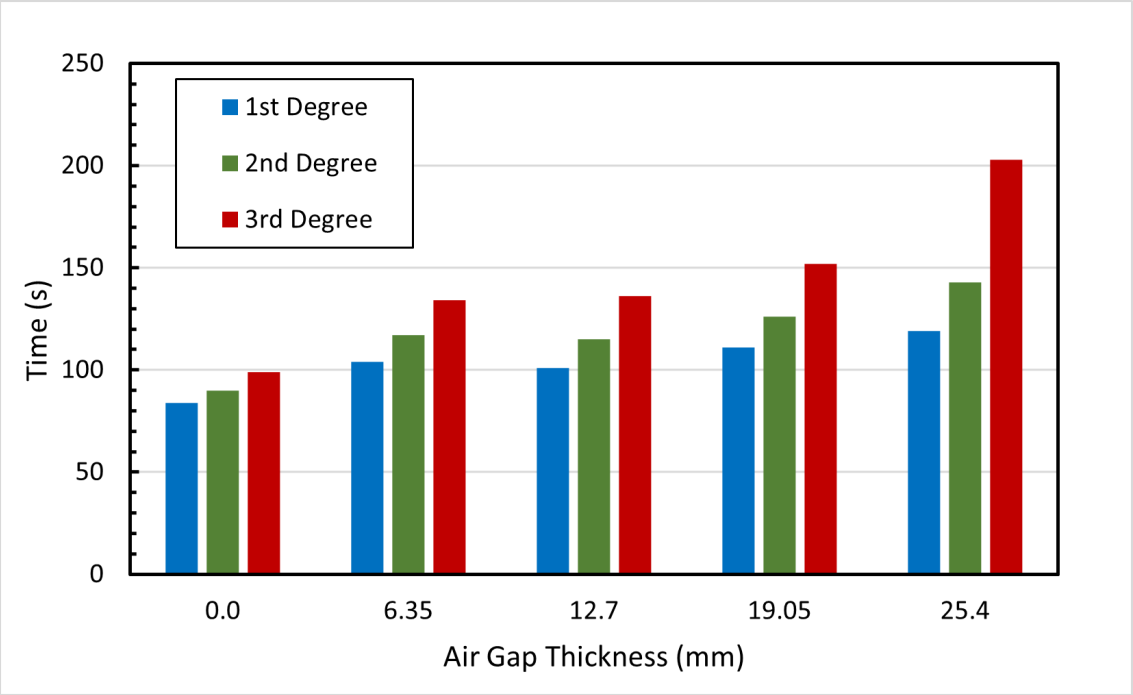

Figure 3.9: Time to Burn Injury versus Air Gap Thickness at 10 kW/m^2 Heat Flux

3.1.2.3 Takeaways

From the experimental Cone Heater data, it can be seen that the presence of an air gap does prolong the time to burn injury. Burn injury is brought on by increasing temperatures so by default, this also states that the presence of an air gap reduces the magnitude of temperatures reached on the opposing side of the air gap from the source. This hold true for both the 5 and 10 kW/m^2 exposures. In addition to its mere presence, the thickness of the air gap also has an influence on the temperatures and associated burn injury times. From this data it can be seen that the increase in the air gap thickness from 6.35 mm to 25.4 mm corresponds to a decrease in the maximum temperatures reached below the cotton stationwear and an increase in the times to burn injury. So conceptually, while it may not

be practical to be implemented within firefighter PPE, the 25.4 mm thick air gap provides the largest duration of time prior to the onset of first degree burn for the firefighter under both 5 and 10 kW/m^2.

3.2 Heat Flow Meter Series

3.2.1 Heat Flow Meter Results

Values for the thermal conductivity of the PPE assemblies were output at four mean temperatures, 15°C, 20°C, 30°C, and 40°C. Given that the simulations to be created with FDS are to mimic that of the conditions of the Cone Heater, the property values at the highest temperature, 40°C, were taken and used as the inputs in the model. Three quantities were produced for each air gap thickness and the average thermal conductivity for each thickness was calculated and reported in Table 3.1 along with its two standard errors.

Values for the volumetric heat capacity of the effective assemblies were output at four mean temperatures, 10°C, 20°C, 30°C, and 40°C. The volumetric heat capacity for the triplicate tests were also taken at the 40°C temperature given that it was relatively the closest temperature to that of the exposure temperatures in the Cone Heater experiments. These three volumetric heat capacity values for each thickness were averaged and reported with their two standard errors, shown in Appendix A.3. The averaged quantities were then converted using the densities of the effective PPE assemblies, shown in Table 2.5, to produce the specific heat capacities for each air gap thickness. This data, showing the average specific heat capacities

with their respective two standard errors, is in Table 3.1.

Table 3.1: Measured Effective Thermal Properties for PPE-Air Gap Assemblies

Air Gap Thickness (mm)	Thermal Conductivity (W/m·K)	Specific Heat Capacity (J/kg·K)
0.0	$4.45 \times 10^{-2} \pm 9.75 \times 10^{-4}$	1360 ± 37.9
6.35	$4.32 \times 10^{-2} \pm 3.64 \times 10^{-4}$	347 ± 5.51
12.7	$5.18 \times 10^{-2} \pm 4.98 \times 10^{-4}$	165 ± 1.93
19.05	$6.14 \times 10^{-2} \pm 1.13 \times 10^{-4}$	172 ± 9.43
25.4	$7.32 \times 10^{-2} \pm 2.53 \times 10^{-4}$	166 ± 1.99

3.2.2 Discussion of Heat Flow Meter Results

3.2.2.1 Analysis

From the data produced, it can be seen that both the thermal conductivity and specific heat capacity values change between the assemblies indicating a correlation between these effective thermal properties and the gap thickness. Materials with a high thermal conductivity value more readily transfer heat through their bulk. In order to slow the transfer of heat to a firefighter's skin, as is the intention of the PPE assembly, the overall thermal conductivity of the PPE assembly should be minimized. Additionally, the specific heat capacity should be maximized to slow the transfer of heat through the bulk as well. As is seen by the data produced from the heat flow meter testing, the effective thermal conductivity of the PPE assembly generally increases as a function of the increasing air gap thickness. The exception is that the effective thermal conductivity values decrease from the 0.0 mm to the 6.35 mm thickness assemblies prior to increasing from the 6.35 mm air gap to the 25.4 mm

air gap. In reality, the thermal conductivity should be decreasing with respect to the increasing air gap thickness to better symbolize the insulating capabilities however, it is reasoned that the increasing thermal conductivities are directly correlated with the thickness. As seen in Fourier's law 3.1, the heat flux and temperature difference remain constant at steady state between the varying assembly tests, implying that the thermal conductivity must increase with the increasing thickness.

$$\dot{q}''_{cond} = -\frac{k\Delta T}{L} \tag{3.1}$$

While assumptions can be made about the reasonings behind the unexpected trends of the measured data, the true physical meaning of these effective values is not clear. This is because the assumed heat transfer model used by the heat flow meter apparatus only applies to solids and is not capable of properly quantifying the insulative capabilities of the embedded air gap. The same limitations apply to the effective specific heat capacities that are shown to decrease as a function of the increasing thickness from this data.

The experimental property values in Table 3.1 are reported with their two standard errors to provide insight on the uncertainty in both quantities. The two standard errors depict 95% confidence intervals to quantify the variability of the material properties. To minimize the uncertainty and variability within a data set, a small interval of standard error is desired. From the table it can be seen that the standard error is relatively small for all air gap thicknesses indicating a low level of uncertainty in the data.

3.2.2.2 Comparison

The Heat Flow Meter series results produces thermal property data for each effective PPE assembly. From the individual property data of the PPE and cotton fabrics, shown in Table 2.1, effective thermal properties can also be calculated through a series of equations [57]. To calculate the effective properties of the entire assembly, the properties of each individual layer must be known, including the air gap positioned within. The thermal properties of air were taken at an ambient temperature of 300 K [19], and are shown in Table 3.2.

Table 3.2: Thermal and Physical Properties of Air

Density (kg/m^3)	Thermal Conductivity (W/m·K)	Specific Heat Capacity (J/kg·K)
1.16	2.63×10^{-2}	1.01×10^{3}

To calculate the effective thermal conductivity of the entire assembly, Equation 3.2 was used and represents the thermal resistance for steady state conduction [57]. To produce an effective thermal conductivity in W/m·K, L_{total} is the total thickness of the assembly in m, L is the thickness of each respective layer in m, and k is the thermal conductivity of each layer in W/m·K. The L_{total} was taken as a summation of the individual thicknesses from Table 2.1 in addition to each thickness of the air gap assemblies.

$$k_{eff} = \frac{L_{total}}{L_1/k_1 + L_2/k_2 + ... + L_n/k_n} \tag{3.2}$$

To calculate the effective specific heat capacity in J/kg·K, a mass-weighted average was used, shown in Equation 3.3 [57]. In this equation, c_p represents the specific heat capacity for each individual material in J/kg·K and ρ represents the individual densities.

$$c_{p_{eff}} = \frac{c_{p_1} L_1 \rho_1 + c_{p_2} L_2 \rho_2 + ... + c_{p_n} L_n \rho_n}{L_1 \rho_1 + L_2 \rho_2 + ... + L_n \rho_n} \tag{3.3}$$

Using these equations and the physical and thermal properties from Table 2.1 and Table 3.2, the effective thermal properties were calculated for each air gap assembly size and are shown in Table 3.3.

Table 3.3: Calculated Effective Thermal Properties for PPE-Air Gap Assemblies

Air Gap Thickness (mm)	Thermal Conductivity (W/m·K)	Specific Heat Capacity (J/kg·K)
0.0	7.11×10^{-2}	163
6.35	3.15×10^{-2}	166
12.7	2.91×10^{-2}	169
19.05	2.82×10^{-2}	172
25.4	2.77×10^{-2}	175

When comparing the two sets of quantities, it can be seen that the magnitudes of the properties for all air gap sizes are the same throughout, indicating a relatively accurate execution of the equations and techniques used in the manual calculations. While the process in acquiring these values may have been accurate, the parameters themselves for the measured and calculated properties do differ significantly. For the measured data, the thermal conductivities generally increase in magnitude as the air gap size increases whereas for the calculated thermal conductivities, the values

decrease in magnitude as the air gap size increases. The same inverse relationship occurs for the specific heat capacities as the measured values decrease with respect to an increasing thickness while the calculated values increase with respect to an increasing gap thickness. Throughout all the property data there is only one instance of an equivalent parameter, that being the specific heat capacity of the 19.05 mm thickness.

As previously denoted, a minimal thermal conductivity and a larger specific heat capacity is desired for the purposes of prolonging the transfer of heat throughout the assembly. From the calculated material properties, these trends are apparent as a function of the increasing air gap size. The data calculated varies from measured data as these values better represent the physical meaning of the incorporated air gap and the influence of the individual properties of each layer within the bulk assembly. The equations used within these calculations more accurately depict the qualitative benefits of the larger air gap size and reflect general opinions on the values themselves. From the calculated effective thermal conductivities, it can be seen that the values approach the thermal conductivity of air, shown in Table 3.2, which is logically assumed to occur given that the percent composition of the air within the assembly increases as a function of the larger air gap.

There are limitations to these equations that prevent these quantities from being accepted as the true quantitative values of the effective thermal properties. To start, the individual properties for both the fabrics as well as the air were taken from the literature which raises the concern of uncertainties that may not be accounted for within these calculations. The properties of air taken from the text were also taken

as constant properties at an assumed ambient temperature whereas in reality these properties are typically temperature dependent and would change when exposed to heat. It should also be noted that both of these equations are a form of an assumed average of which case limitations apply that may result in the output values being inaccurate.

The presence of air itself is one of the governing limitations for these calculations and directly impacts the thermal resistance equation used. The primary intent of this equation is for solid phase materials and not the inclusion of a gaseous cavity. The use of this equation makes a simplified assumption for the solid-phase heat transfer within the gap rather than accounting for the molecular benefits of having a gaseous space capable of delaying the physical heat transfer mechanisms for insulative purposes. The incorporation of the air gap, with its gaseous thermal and physical properties, in this conduction equation is the leading assumption in any discrepancies of these calculations.

3.2.2.3 Takeaways

From the experimental Heat Flow Meter data, thermal property trends can be observed on the influence of an increasing air gap within a PPE assembly. For the effective thermal conductivity, it is apparent that the presence of an air gap reduces the conductivity of the effective PPE assembly when compared to the same assembly with no air gap. This implies that the presence of an air gap leads to a reduction in the overall thermal conductivity providing a form of insulation. This material

behavior however, does not hold as the air gaps increase in size. This differs from the behavior of the Cone Heater results, which indicate that the larger the air gap size, the greater the thermal insulation. The variations between these data trends implies instrument limitations with the heat flow meter apparatus as the expected trends are observed when conducting manual calculations of the effective thermal properties with respect to the air gap size.

While the results produced in this series do provide insight on the influence of an air gap on the thermal behavior of the effective assemblies, the properties were also measured experimentally for the one-dimensional heat transfer model. Based on the relatively small error values within this data, these constant thermal property parameters were deemed sufficient in their usage as inputs in the FDS simulations.

Chapter 4: Modeled Results

4.1 FDS Model Results

4.1.1 Model Validation Results

4.1.1.1 5 kW/m^2 Exposure

The temperature-time plot shown in Figure 4.1 depicts the temperature data from both the experimental results in addition to the temperature data simulated by the FDS model for a 0.0 mm air gap under the 5 kW/m^2 heat flux. In this figure, the temperature data denoted as "Experimental" is taken as the "Below Stationwear" curve defined in Section 3.1.1. The temperature data denoted as "Model" is the produced temperature data from the thermocouple device within the associated FDS model of these conditions. The key events of the opening and closing of the heat shutter are visibly seen as the increase of temperature and the decrease in temperature, respectively. From this plot it can be seen that there is general agreement among the two curves for the duration of the exposure. From the initial increase and throughout the duration of exposure, the two curves demonstrate virtually the same behavior. The slight deviations in temperature within the curve begin to occur at the end of the experiment during the cool down period.

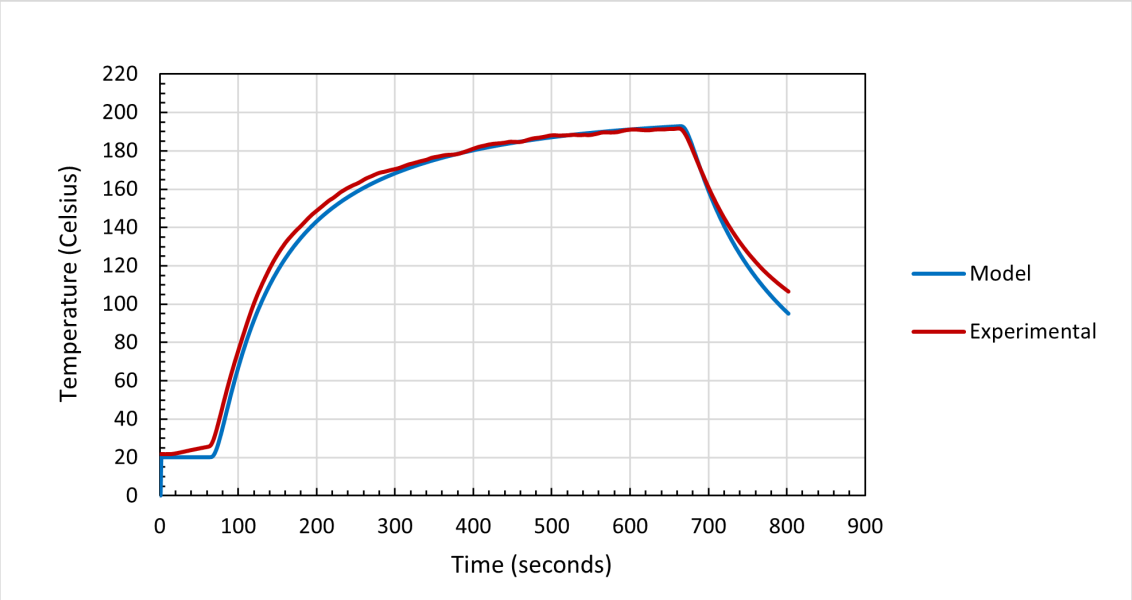

Figure 4.1: Temperature versus Time for the Model and Experimental Data for the PPE Sleeve Assembly with a 0.0 mm Air Gap Exposed to a 5 kW/m^2 Heat Flux

4.1.1.2 10 kW/m^2 Exposure

The simulated data produced by FDS for the 10 kW/m^2 exposure of the 0.0 mm assembly differs in behavior than that of the assembly under the 5 kW/m^2 exposure. In the 5 kW/m^2 exposure 0.0 mm plot, the curve shows good agreement between the model and experimental data for almost the entire duration of the tests. For the 10 kW/m^2 heat flux with 0.0 mm air gap, Figure 4.2 shows that the model predicts a similar general response; however, it overestimates the entirety of the temperature data until the cool down period is initiated, at which time the modeled curve falls below the experimental. A significant difference in the two curves was established halfway through the exposure length and this difference decreased with time as the exposure period came to an end. Both the model and the experimental curves approach a similar temperature equivalent to approximately 285°C indicating

the effective properties used are suitable for steady state but not representative within the transient heating stage.

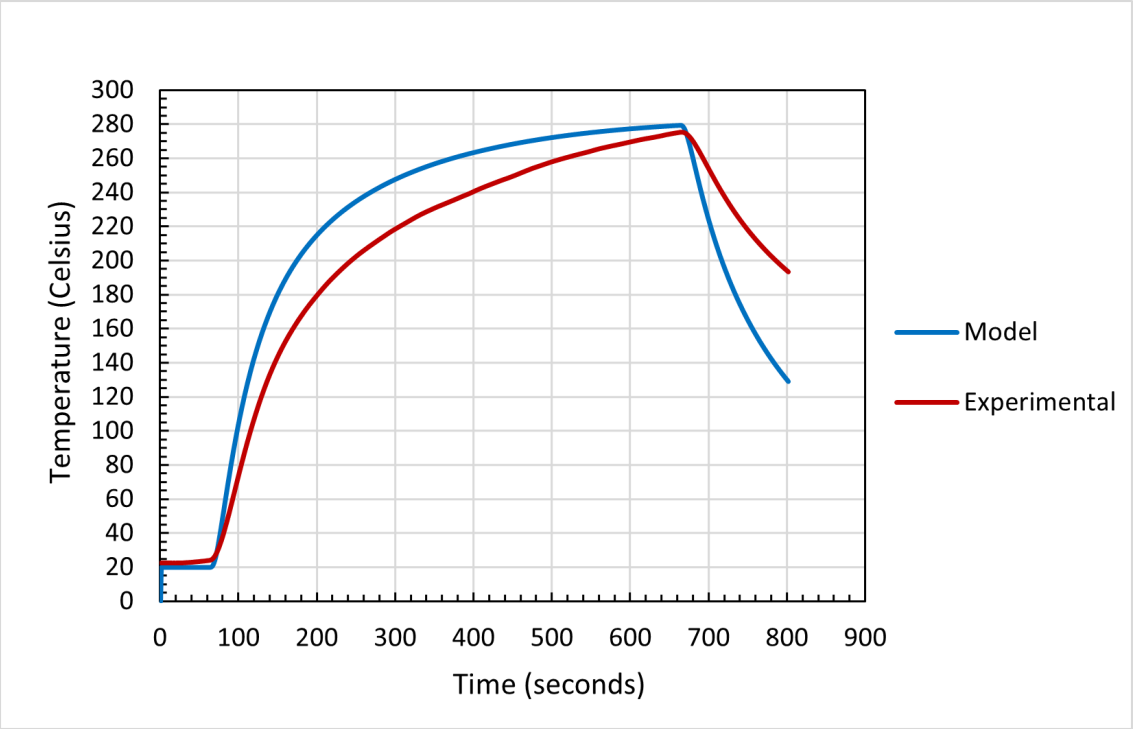

Figure 4.2: Temperature versus Time for the Model and Experimental Data for the PPE Sleeve Assembly with a 0.0 mm Air Gap Exposed to a 10 kW/m^2 Heat Flux

4.1.2 Model Comparison Results

4.1.2.1 5 kW/m^2 Exposure

The temperature-time plots for all PPE sleeve assembly thicknesses under the 5 kW/m^2 heat flux exposure are shown in Figure 4.3. These plots are of the same design as the 0.0 mm plot, with the two temperature curves distinguished by their methods of acquisition. When assessing the agreement between the data as a function of the increasing air gap size, for the 5 kW/m^2 flux, there is relatively good

agreement prior to the 12.7 mm air gap thickness. For the 6.35 mm air gap, the agreement mirrors that of the 0.0 mm air gap as the model and experimental data both display the same position and behavior throughout the duration of exposure.

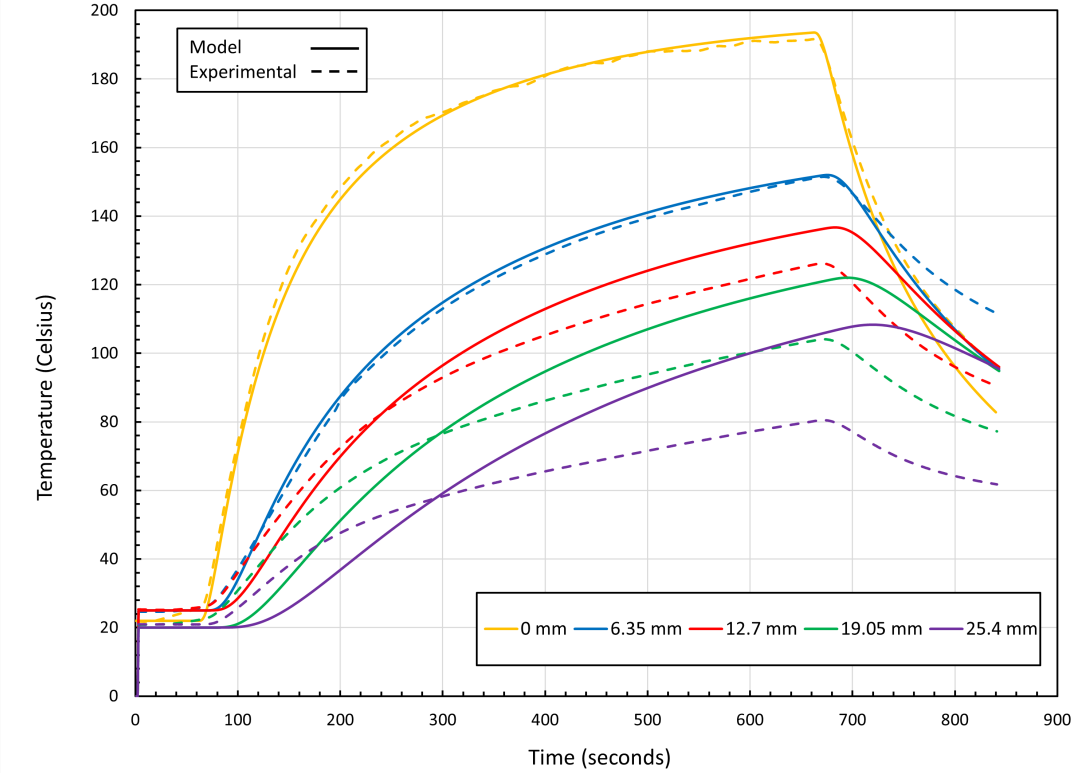

Figure 4.3: Temperature versus Time for the Model and Experimental Data for All PPE Sleeve Assemblies Exposed to a 5 kW/m^2 Heat Flux

From the 12.7 mm to the 25.4 mm air gap sizes, the agreement diminishes with respect to the increasing air gap thickness. The 12.7 mm plot reflects the behavior of the smaller air gap size plots however, prior to 283 seconds the FDS model under predicts the experimental curve and after 283 seconds the model over predicts the temperature of the experimental curve. The 19.05 mm plot furthers the lack of agreement between the two curves and demonstrates that the FDS model also under and over predicts the temperatures prior to and after 283 seconds. The

visible difference between the curves is greater in the 19.05 mm plot than in the 12.7 mm plot. The worst agreement among these plots is seen in the 25.4 mm air gap data. For these curves, the same reoccurring trend is apparent with regard to the under and over prediction of the FDS model before and after the 283 second mark however, the differences between the two curves once the exposure duration is initiated is greater than that of the 19.05 mm plot.

4.1.2.2 10 kW/m^2 Exposure

The temperature-time plots for all PPE sleeve assembly thicknesses under the 10 kW/m^2 heat flux exposure are shown in Figure 4.4. For the 10 kW/m^2 exposure simulations, the trend of the lack of agreement increasing with respect to the increasing air gap thickness is seen from the 12.7 thickness and above. As previously stated, the 0.0 mm plot displays similar behavior between the model and experimental data however the magnitude of these temperatures differ. For the 6.35 mm plot under the 10 kW/m^2 exposure, the visual agreement improves significantly with the two data sets displaying similar trends and magnitudes.

From the 12.7 mm thickness and above, the modeled temperature plots displays the same under and over behavior with the experimental data however, now at varying moments in time. The 12.7 mm FDS curve under predicts the temperature prior to 361 seconds and over predicts the temperature after 361 seconds with the least maximum difference among the 12.7 mm, 19.05 mm, and 25.4 mm plots. The 19.05 mm plot under predicts the temperature prior to 359 seconds and over pre-

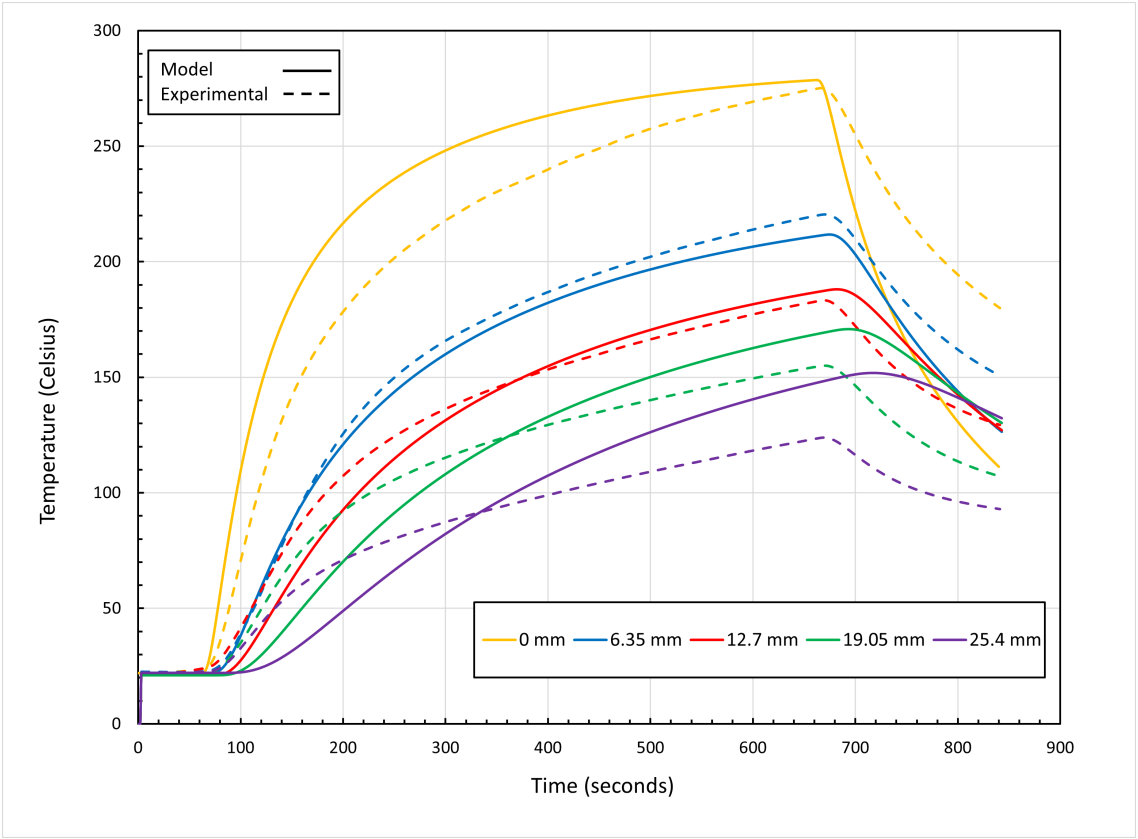

Figure 4.4: Temperature versus Time for the Model and Experimental Data for All PPE Sleeve Assemblies Exposed to a 10 kW/m^2 Heat Flux

dicts the temperature beyond this time. The 25.4 mm plot under and over predicts the temperatures prior to and after 338 seconds, respectively, and shows the largest differences between the curves.

4.2 Discussion of Model Results

The data produced from the FDS simulation serves three main purposes in this study. First, to validate the Cone Heater model using experimental data for the 0.0 mm thicknesses where the heat transfer is thought to be solely conduction dominated through the assembly given the lack of an air gap. The plotted results

in Section 4.1.1 provide the evidence for this analysis specified in Section 4.2.1. Secondly, the validated model can be used to predict the heat transfer through the air gap as the thickness increases. The plotted results in Section 4.1.2 provide the evidence for this analysis also specified in Section 4.2.1. Third and finally, the capability of the FDS model to predict the time to potential burn injury through a PPE-air gap assembly with experimental property inputs is assessed. This is shown in Section 4.2.2 and uses a comparison between the burn injury times to assess the level of agreement between the modeled and experimental data.

4.2.1 Validation and Analysis

The simulated data produced from FDS for the 0.0 mm air gap thickness under the 5 kW/m^2 is validated by the experimental data produced from the Cone Heater. The good agreement found between the experimental and modeled curves in Figure 4.1 entails that the temperature predictions from the cone model are accurate given that FDS has been validated for one-dimensional conduction through solids [58]. While this same validation should stand for the 10 kW/m^2 exposure as well, it is assumed that the leading source of deviation between the experimental and simulated data for the 10 kW/m^2 is material degradation. As shown in Section 3.1.1.2, there was significant thermal degradation not only from the higher exposure but from the repetition of exposure as well, given that the samples used had previously been subjected to the 5 kW/m^2 exposure. Additionally, the deviation between the two 10 kW/m^2 curves was merely in magnitude as the general

behavior of both curves was relatively the same.

Upon the validation of the Cone Heater model, the model was used to gain an understanding of the heat transfer apparent within the air gap assemblies for low level thermal exposures. This was assessed via the agreement between the experimental and modeled curves as the air gap thickness increased. It can be seen by the good agreement shown in both heat flux exposures that the heat transfer through the 0.0 mm and 6.35 mm air gap assemblies is conduction-dominated. From the plots shown in Section 4.1.2, it was concluded that the agreement diminished linearly with respect to an increasing air gap size. To explain the deviations in the agreement, Song's theory of an optimal air gap size should be considered. For short duration flash fire exposure under a single layer of PPE fabric, Song hypothesized and concluded that beyond the optimal air gap size, between 7 to 8 mm, convection is invoked as the larger air gap provides more room for natural convection to occur [37]. This theory holds true as a means of justification for the lack of agreement in these comparisons. The FDS model was designed to only account for conductive heat transfer through the PPE and air gap, so if in reality convection is also influencing the transfer of heat then the modeled conduction curve would surely differ from that of the experimental data. Given that there is no means of proving this theory with the current FDS model capabilities, this is merely a speculation on why the conduction-driven model no longer presents data in good agreement.

There is also the equivalent possibility that the heat transfer shifts from a conduction to a radiation dominant environment within the cavity, in turn causing poor agreement between the model and experimental data. For the 10 kW/m^2

exposure, it can be theorized that the deviations are also a function of the thermal degradation that has been seen to occur on the PPE fabrics in addition to the potential presence of convection in the air gap.

4.2.2 Application

Now that the practicality of the model has been established for smaller air gaps, as agreement below the 6.35 mm gap is visibly sufficient, a further assessment of the capabilities of the model can be conducted. To quantify how good of an agreement is apparent between the data and model, the FDS model's predicted time to burn injury can be compared to the experimental times. This can be done by taking the percent difference between the times to burn injury for each of the two temperature-time curves.

$$P_{Diff} = \frac{\mid t_{model} - t_{exp} \mid}{\frac{1}{2}(t_{model} + t_{exp})} \times 100 \tag{4.1}$$

The absolute percent difference was calculated using Equation 4.1: where t_{model} is the time to burn injury output from the simulations and t_{exp} is the experimental time to burn injury from the Cone Heater series. The absolute value of the difference in times is calculated given that the model both under and over predicts the experimental data, and this is divided by the average of the two times as the "true value" for these exact configurations is unknown.

These percent differences are calculated and shown in Table 4.1 for the 5 kW/m^2 exposure and shown in Table 4.2 for the 10 kW/m^2 exposure. In this

analysis, a 15% difference threshold will be defined and used to assess accuracy between the modeled and experimental data. In both of these tables, the actual potential times to burn injury, for first through third degree, are also specified for each assembly size and data acquisition method.

Table 4.1: Time to Burn Injury Comparison for 5 kW/m^2 Exposure

Air Gap Thickness (mm)	**Degree of Burn Injury**	**Modeled Time (s)**	**Experimental Time (s)**	**Percent Difference (%)**
0.0	First	83	78	6.21
	Second	90	85	5.71
	Third	101	97	4.04
6.35	First	112	113	0.89
	Second	130	134	3.03
	Third	162	168	3.64
12.7	First	134	117	13.6
	Second	159	146	8.52
	Third	204	197	3.49
19.05	First	175	137	24.4
	Second	210	174	18.8
	Third	274	263	4.10
25.4	First	228	177	25.2
	Second	277	262	5.57
	Third	368	507	31.8

From these times it can be reconfirmed that the 6.35 mm assembly displays the best agreement between the model and experimental data. The percent difference between the times to burn injury for all three degrees of severity of the 6.35 mm air gap for both exposure levels are within 6%. In addition to the 6.35 mm assembly, several other assembly sizes also demonstrate relatively good accuracy, remaining under a 15% difference. For the 0.0 mm of the 5 kW/m^2 exposure, the times are

within 7% and for the 0.0 mm of the 10 kW/m^2 exposure, the times are within 15%. The 12.7 mm assembly also displays percent differences within 15% for the 5 kW/m^2 heat flux only. For the remaining assembly sizes in either exposure, the percentages are greater than the established criteria for reasonable accuracy and should not be considered as sound predictions. From these percentages it can be seen that the current FDS model is most accurately predicting the time to burn injury for the 6.35 mm air gap assembly, but additional small air gap sizes under relatively low heat flux exposures will also hold in accuracy. Predicting the time to burn injury under these conditions alone should remain the model's primary function at this point in time if it is to be used for future analysis in regard to varying PPE fabrics and orientations.

Table 4.2: Time to Burn Injury Comparison for 10 kW/m^2 Exposure

Air Gap Thickness (mm)	**Degree of Burn Injury**	**Modeled Time (s)**	**Experimental Time (s)**	**Percent Difference (%)**
0.0	First	76	84	10.0
	Second	80	90	11.8
	Third	86	99	14.1
6.35	First	103	104	0.97
	Second	90	85	5.71
	Third	130	134	3.03
12.7	First	122	101	18.8
	Second	137	115	17.5
	Third	162	136	17.4
19.05	First	146	111	27.2
	Second	167	126	28.0
	Third	201	152	27.8
25.4	First	184	119	42.9
	Second	215	143	40.2
	Third	264	203	26.1

4.2.3 Takeaways

The model demonstrates 15% accuracy in predicting burn injury times for low heat flux exposures and small air gap sizes. At higher temperatures and increased air gap sizes it is reasoned that the discrepancy between modeled and experimental results increases with heat flux due to the thermal decomposition of the materials and an increased significance of convective and radiative heat transfer within the air cavity. It should also be noted that the constant material properties input in the model may also influence the discrepancies at the greater heat flux exposure. Given that these parameters are constant properties and not temperature-dependent, the validity of the properties decrease as the temperatures increase beyond the limits of

the constant property assumptions.

This model, as it is currently configured, is a sufficient resource in calculating the time to burn injury for PPE assemblies with an incorporated air gap thickness of up to 6.35 mm as the heat transfer is theorized to be conduction-dominated and follow the behavior of a conduction-driven model. However, improvements to accuracy may be realized by incorporating more complex physical phenomenon such as in-cavity convection or radiation and moisture transport. It is recommended that future work explore the construction of a FDS model with these capabilities and considerations.

Chapter 5: Conclusions and Future Research

5.1 Conclusions

Understanding the influence of the air gap within firefighter PPE on skin temperature under pre-flashover thermal exposures is important, especially as firefighters continue to fall victim to burn injuries as a result of prolonged exposure within seemingly non-hazardous fire environments. Furthering the understanding of the heat transfer within an air cavity establishes the conceptual principles in providing additional thermal protection to structural firefighting coats and trousers.

The presence of an air gap within firefighter PPE was shown to not only prolong the time to burn injury but reduce the maximum temperatures reached at the skin surface as well, under both 5 and 10 kW/m^2 exposures. As the air gap thickness increases, the time to burn injury also increases and the maximum temperatures at the skin depth decrease for both thermal exposures. These findings fundamentally suggest that the larger the air gap is, the more thermal insulation is provided for the firefighter wearing the PPE. Based on comparisons of the conduction-driven model with the experimental temperature data, the model was demonstrated to be accurate to within 15% of the experiment in the prediction of burn injury times for low heat flux exposures and small air gap sizes. From the agreement of the model,

the heat transfer is confirmed to be conduction-dominated for air gap sizes leading up to 6.35 mm. At larger air gap thicknesses, additional modes of heat transfer are apparent however, the quantification of this heat transfer is beyond the capabilities of the numerical model and the scope of this study.

5.2 Future Research

For future research, refinements to the numerical model can be made both in the specifications of heat transfer as well as the thermal decomposition. The current conduction-driven model displayed poor agreement among the larger air gap sizes indicating that convection and radiation might be present, and future work should explore the construction of a FDS model that incorporates an air gap with these forms of heat transfer. This future model should be validated with the experimental data collected in the current study. In addition to the heat transfer, thermal decomposition should also be considered in the model for the PPE fabrics, especially at higher heat fluxes. Significant thermal degradation found in the experimental samples justifies the discrepancies in the model apparent under the 10 kW/m^2 exposure, and this lack of consideration in the current model should be rectified for future numerical solvers. Additional properties not specifically mentioned in this analysis but relevant to future FDS models include moisture transport and experimentally-measured emissivity values for the radiative boundary conditions.

While this research establishes that more air is thermally advantageous from a protective standpoint, it does not align with the current ideologies of structural

firefighting PPE. In regard to practicality, incorporating a large air gap may prove detrimental to the firefighter in the form of additional bulk or a further reduction in mobility. Future work should be conducted to determine the optimal balance between firefighter safety and the practical reality of gear construction. This can be further investigated by assessing how large of an air gap can truly be integrated into current PPE, and how can this gear be altered to allow for larger air gap sizes to be incorporated as a means of protection.

Additional variables should be considered in their inclusion in this discussion of an air gap in firefighter PPE and skin temperatures. Further analysis of PPE-air gap assemblies under pre-flashover exposures should be conducted with varying properties such as moisture content, PPE fabric brands, and heat flux magnitudes. The incorporation of a computational skin model would also provide a useful means for simulating the temperature increase with regard to the body's thermal regulative attributes, such as blood circulation and perspiration, on the skin surface.

Chapter A: Additional Information and Results

A.1 PPE Fabric Brand Choice

In order to determine the specific brands used for each of the PPE fabric layers, outreach was conducted at a local fire station. An inspection of the firefighter PPE revealed that the brands of PPE fabric currently used are specified on the interior surface of the turnout gear. The specific brands of PPE fabric found on the inside of two turnout coats from the College Park Volunteer Fire Department (CPVFD) Co. 12, are shown in Figure A.1 for a tan turnout coat and in Figure A.2 for a black turnout coat, courtesy of Adam Quiat.

A.2 Effective Thickness of PPE-Air Gap Assembly

The effective thickness for the entire PPE assembly was measured and output as an additional parameter in the Heat Flow Meter series experiments. These thicknesses are shown in Table A.1 and were used as experimental inputs within the FDS model to define the exact depth of the assembly and location of the thermocouple device.

(a) Exterior Turnout Coat

(b) Interior Turnout Coat

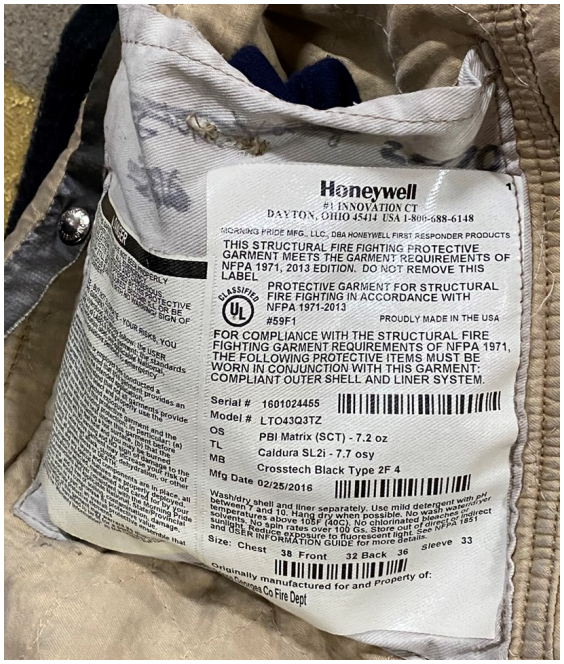

(c) Fabric and Material Specifications

Figure A.1: Tan Firefighter Turnout Coat

(a) Exterior Turnout Coat

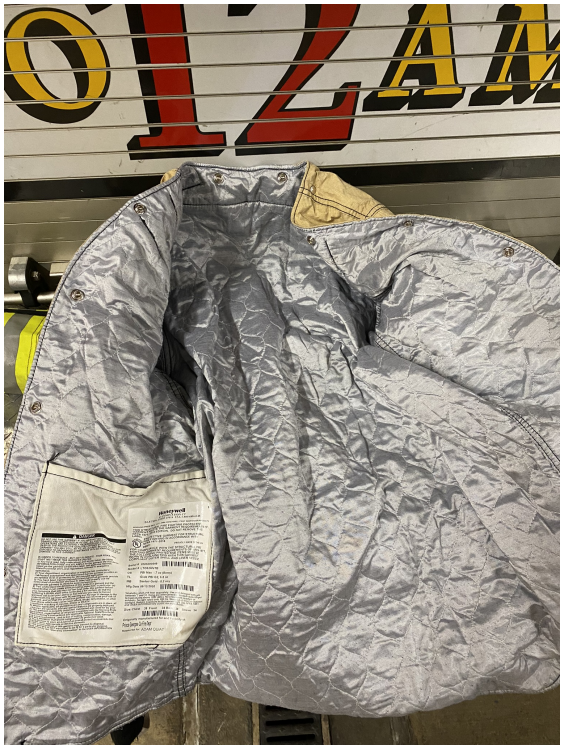

(b) Interior Turnout Coat

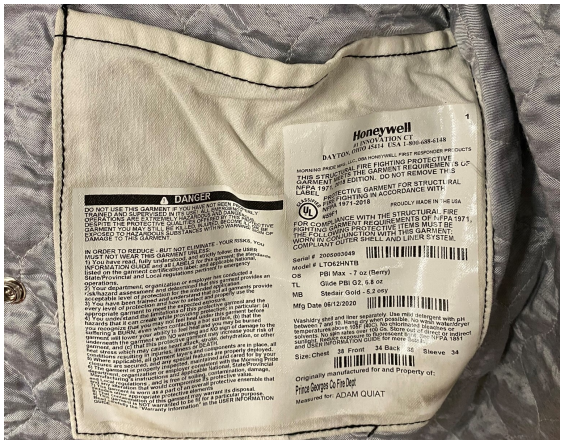

(c) Fabric and Material Specifications

Figure A.2: Black Firefighter Turnout Coat

Table A.1: Output Thicknesses for PPE-Air Gap Assemblies

Air Gap Thickness (mm)	Assembly Thickness (mm)
0.0	3.18
6.35	9.72
12.7	15.5
19.05	21.6
25.4	28.6

A.3 Volumetric Heat Capacity of PPE-Air Gap Assembly

The raw volumetric heat capacities for the triplicate trials of the Heat Flow Meter Series were averaged and are reported with their 2 standard errors in Table A.2 prior to being converted into their specific heat capacities.

Table A.2: Volumetric Heat Capacities for PPE-Air Gap Assemblies

Air Gap Thickness (mm)	Volumetric Heat Capacity ($J/m^3 \cdot K$)
0.0	$3.55 \times 10^5 \pm 9.89 \times 10^3$
6.35	$1.20 \times 10^5 \pm 1.90 \times 10^3$
12.7	$8.15 \times 10^4 \pm 9.50 \times 10^2$
19.05	$6.98 \times 10^4 \pm 3.82 \times 10^3$
25.4	$6.78 \times 10^4 \pm 8.18 \times 10^2$

A.4 FDS Input File Example

The FDS input file for the 6.35 mm PPE assembly under the 5 kW/m^2 heat flux is shown below in Figure A.3. The material and surface properties are denoted in Figure A.3(a) and the associated FDS ramp functions for the temperature-dependent properties of the ceramic fibreboard insulation are shown in Figure A.3(b). The FDS ramp functions for the external heat source are shown in Figure A.3(c) along with the vent specifications and the thermocouple device definition.

```
&HEAD CHID='PPE_5_2', TITLE='PPE Assembly at 5 kW/m2 with 6.35 mm' /

&MESH IJK=3,3,3, XB=-0.15,0.15,-0.15,0.15,0.0,0.30 /

&TIME T_END=840., WALL_INCREMENT=1, DT=0.01 /
&MISC  SOLID_PHASE_ONLY=T /
&MISC  TMPA=25. /

&MATL ID='PPEASSEMBLY'
      CONDUCTIVITY = 0.04316
      SPECIFIC_HEAT = 0.346856
      DENSITY = 345.3858 /

&MATL ID='FIBREBOARD'
      CONDUCTIVITY_RAMP = 'k_fibreboard'
      SPECIFIC_HEAT_RAMP = 'c_fibreboard'
      DENSITY = 224. /

&SURF ID='PPE'
      COLOR='BROWN'
      MATL_ID='PPEASSEMBLY','FIBREBOARD','FIBREBOARD'
      THICKNESS=0.009717,0.0127,0.0127
      HEAT_TRANSFER_COEFFICIENT=7.0469
      EXTERNAL_FLUX=5
      STRETCH_FACTOR=1.
      RAMP_EF='CONE RAMP' /
```

(a) Material and Surface Properties

```
&RAMP ID='k_fibreboard', T=0.0, F=0.04248 /
&RAMP ID='k_fibreboard', T=25.0, F=0.046983 /
&RAMP ID='k_fibreboard', T=50.0, F=0.051485 /
&RAMP ID='k_fibreboard', T=75.0, F=0.055988 /
&RAMP ID='k_fibreboard', T=100.0, F=0.06049 /
&RAMP ID='k_fibreboard', T=125.0, F=0.064993 /
&RAMP ID='k_fibreboard', T=150.0, F=0.069495 /
&RAMP ID='k_fibreboard', T=175.0, F=0.073998 /
&RAMP ID='k_fibreboard', T=200.0, F=0.0785 /
&RAMP ID='k_fibreboard', T=225.0, F=0.083003 /
&RAMP ID='k_fibreboard', T=250.0, F=0.087505 /
&RAMP ID='k_fibreboard', T=275.0, F=0.092008 /
&RAMP ID='k_fibreboard', T=300.0, F=0.09651 /

&RAMP ID='c_fibreboard', T=0.0, F=0.097025 /
&RAMP ID='c_fibreboard', T=25.0, F=0.299307 /
&RAMP ID='c_fibreboard', T=50.0, F=0.342866 /
&RAMP ID='c_fibreboard', T=75.0, F=0.368346 /
&RAMP ID='c_fibreboard', T=100.0, F=0.386425 /
&RAMP ID='c_fibreboard', T=125.0, F=0.400448 /
&RAMP ID='c_fibreboard', T=150.0, F=0.411905 /
&RAMP ID='c_fibreboard', T=175.0, F=0.421592 /
&RAMP ID='c_fibreboard', T=200.0, F=0.429984 /
&RAMP ID='c_fibreboard', T=225.0, F=0.437386 /
&RAMP ID='c_fibreboard', T=250.0, F=0.444007 /
&RAMP ID='c_fibreboard', T=275.0, F=0.449996 /
&RAMP ID='c_fibreboard', T=300.0, F=0.455464 /
```

(b) Temperature-Dependent Ramp Function

```
&RAMP ID='CONE RAMP', T=0.0, F=0.0 /
&RAMP ID='CONE RAMP', T=59.0, F=0.0 /
&RAMP ID='CONE RAMP', T=60.0, F=1.0 /
&RAMP ID='CONE RAMP', T=659.0, F=1.0 /
&RAMP ID='CONE RAMP', T=660.0, F=0.0 /

&VENT MB='XMIN', SURF_ID='OPEN' /
&VENT MB='XMAX', SURF_ID='OPEN' /
&VENT MB='YMIN', SURF_ID='OPEN' /
&VENT MB='YMAX', SURF_ID='OPEN' /
&VENT MB='ZMIN', SURF_ID='PPE' /
&VENT MB='ZMAX', SURF_ID='OPEN' /

&DUMP DT_DEVC=1. /

&DEVC XYZ=0.0,0.0,0.0, IOR=3, QUANTITY='INSIDE WALL TEMPERATURE', DEPTH=0.009717  ID='TC1' /

&TAIL /
```

(c) Ramp, Vent, and Device Specification

Figure A.3: FDS Input File for 6.35 mm Assembly for 5 kW/m^2 Exposure

Chapter B: Additional Figures and Plots

B.1 Outer Shell Fabric Results from Cone Heater Series

The outer shell fabric tests shown here were used as a comparative measure of the temperatures recorded through one layer of PPE fabric. This was done to ensure that the temperatures recorded under the top layer of the PPE for the PPE sleeve assembly tests was equivalent to that recorded for the top outer shell layer alone, which was achieved for these experiments. Additionally, these tests ensured that the thermocouples and DAQ system were functioning properly prior to PPE sleeve assembly exposure. The temperature data of the outer shell fabric tests for the 5 kW/m^2 heat flux is shown in Figure B.1 and the 10 kW/m^2 heat flux in Figure B.2. Given that these outer shell fabric tests were also conducted in duplicate, the averaged data is denoted with the solid color lines and the maximum and minimum values are denoted with the dashed lines.

B.2 Baseline Cotton Fabric Results from Cone Heater Series

The cotton sleeve assembly tests were also conducted to establish a reference point or baseline assessment for the PPE experiments. The tests were conducted

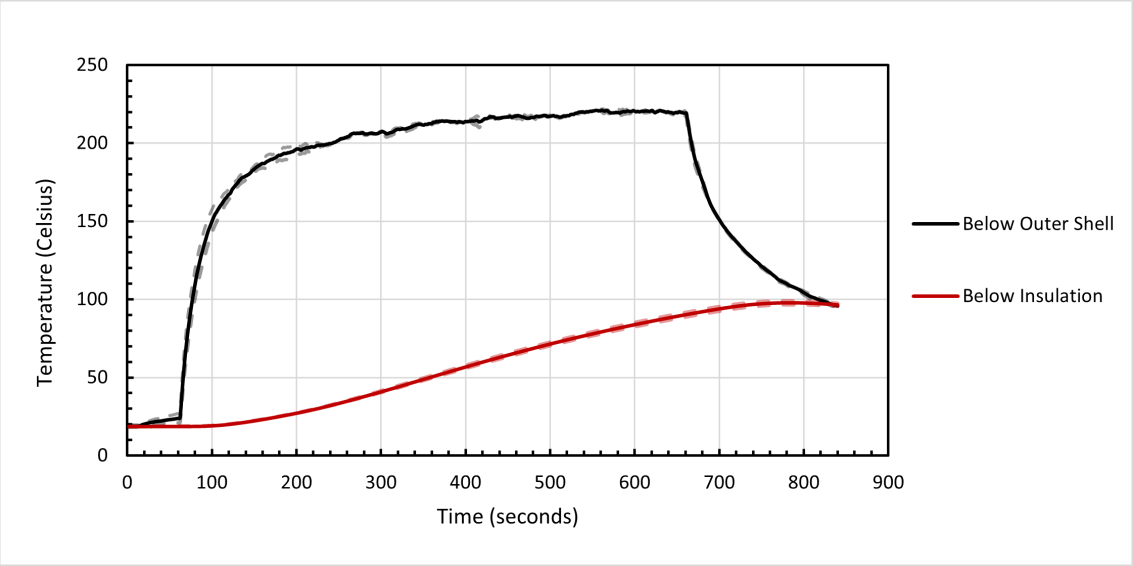

Figure B.1: Temperature versus Time for the Outer Shell Fabric at 5 kW/m^2 Heat Flux

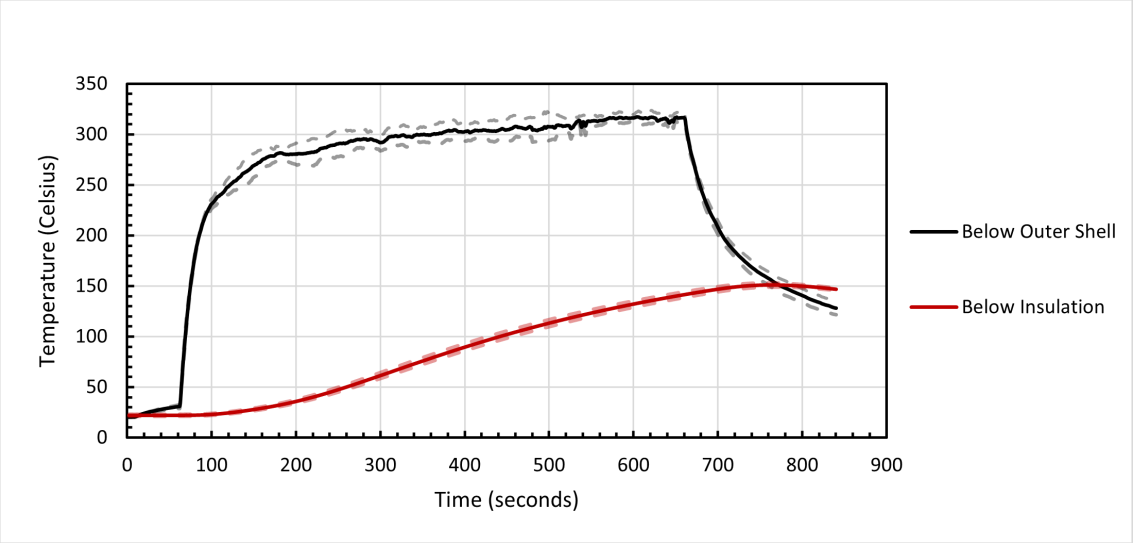

Figure B.2: Temperature versus Time for the Outer Shell Fabric at 10 kW/m^2 Heat Flux

for all five air gap thicknesses for one trial, given the primary purpose of these tests was strictly to observe qualitative over quantitative behavior.

B.2.1 5 kW/m^2 Exposure

Figure B.3 shows the temperature-time data of the 0.0 mm cotton sleeve assembly. Figures B.4 shows the temperature-time plots of the 6.35 mm, 12.7 mm, 19.05 mm, and 25.4 mm cotton sleeve assemblies. The general trend among these curves are that the temperatures recorded on the opposing side of the air gap, denoted as the "Below Bottom Cotton" curve, decrease with the increasing air gap size, demonstrating similar behavior to the PPE sleeve assembly tests.

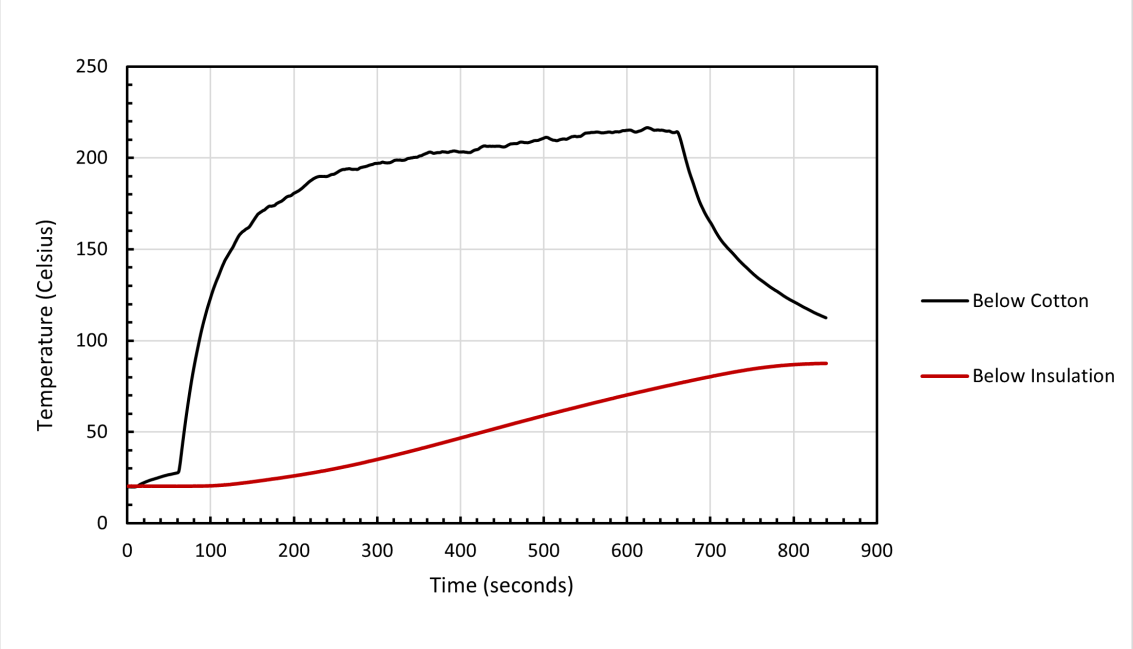

Figure B.3: Temperature versus Time for the Cotton Sleeve Assembly with a 0.0 mm Air Gap at 5 kW/m^2 Heat Flux

B.2.2 10 kW/m^2 Exposure

Figure B.5 shows the temperature-time data of the 0.0 mm cotton sleeve assembly. The erratic spike in the data for this test is a result of ignition occurring

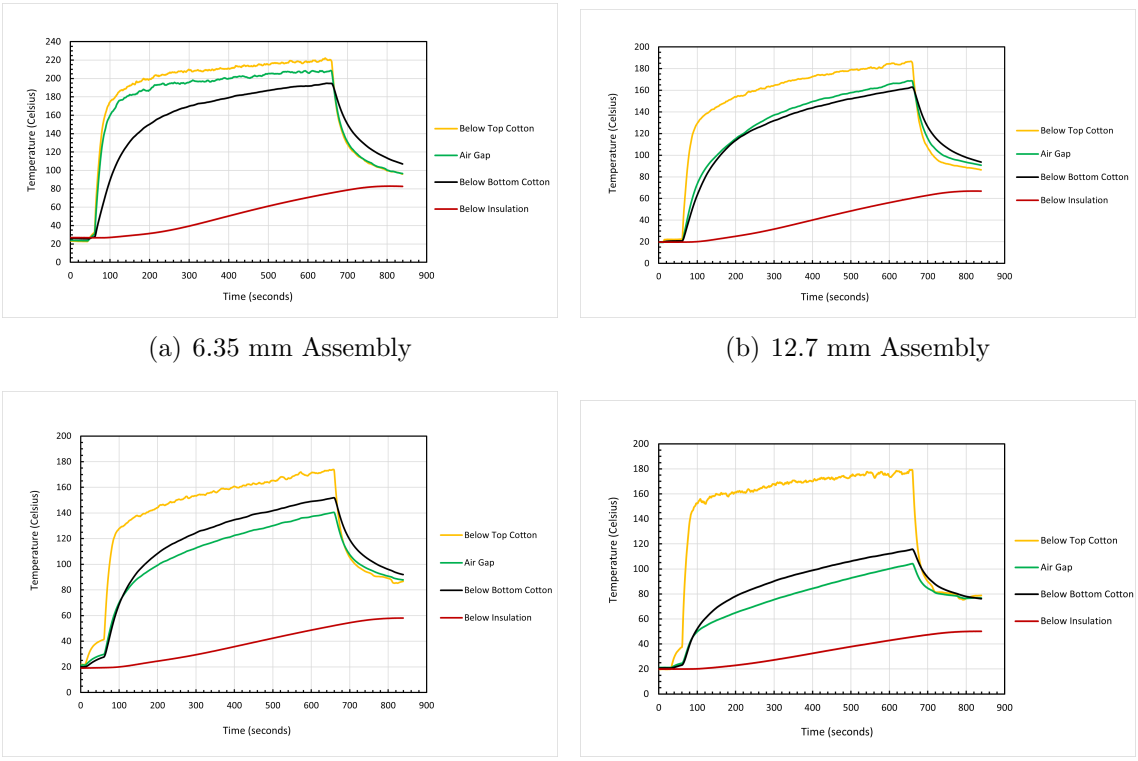

(a) 6.35 mm Assembly

(b) 12.7 mm Assembly

(c) 19.05 Assembly

(d) 25.4 mm Assembly

Figure B.4: Temperature versus Time for the Cotton Sleeve Assemblies with an Air Gap at 5 kW/m^2 Heat Flux

on the cotton fabric. The smoldering ignition of the fabric led to a jump in the recorded temperatures and a qualitative data set unusable for this analysis. Figures B.6 shows the temperature-time plots of the 6.35 mm, 12.7 mm, 19.05 mm, and 25.4 mm cotton sleeve assemblies. Qualitative data was gathered from these tests and the general trend among these curves also show that the temperatures recorded on the opposing side of the air gap, denoted as the "Below Bottom Cotton" curve, decrease with the increasing air gap size, demonstrating similar behavior to the PPE sleeve assembly tests. The fluctuations in the "Air Gap" data is most likely a function of the improper placement and orientation of the thermocouple within the air gap, for example potentially touching either of the surrounding cotton surfaces

or the air gap spacer.

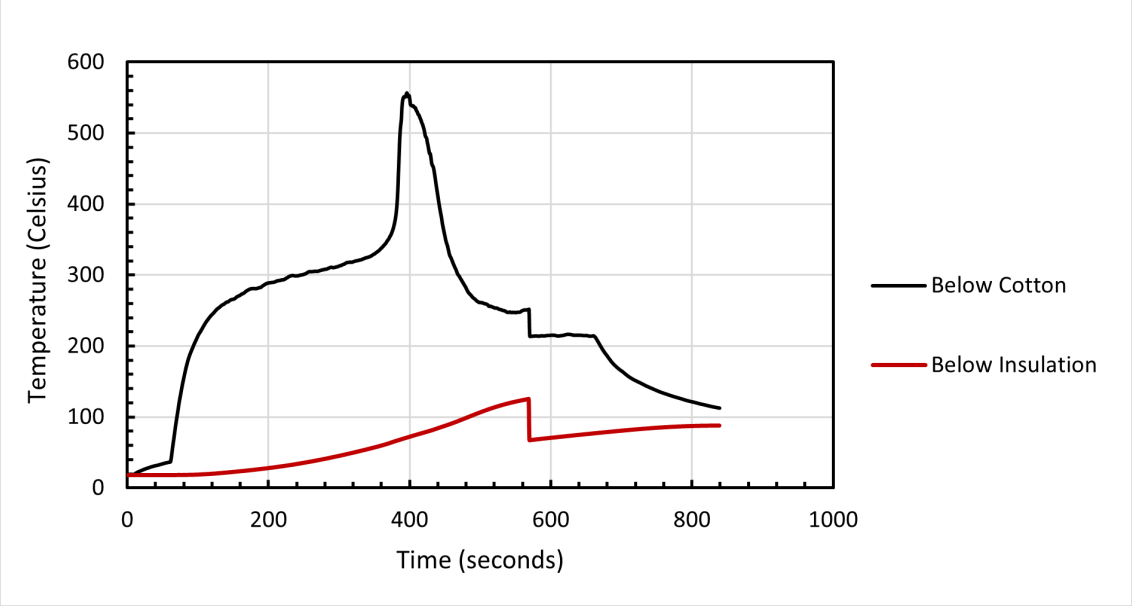

Figure B.5: Temperature versus Time for the Cotton Sleeve Assembly with a 0.0 mm Air Gap at 10 kW/m^2 Heat Flux

B.3 Large Air Gap Assembly Results from Cone Heater Series

B.3.1 5 kW/m^2 Exposure

The temperature-time plots for the 12.7 mm, 19.05 mm, and 25.4 mm air gap assemblies under the 5 kW/m^2 heat flux are shown in Figure B.7, Figure B.8, and Figure B.9, respectively, and are detailed further in Section 3.1.1.1.

B.3.2 10 kW/m^2 Exposure

The temperature-time plots for the 12.7 mm, 19.05 mm, and 25.4 mm air gap assemblies under the 10 kW/m^2 heat flux are shown in Figure B.10, Figure B.11, and Figure B.12, respectively, and are detailed further in Section 3.1.1.2.

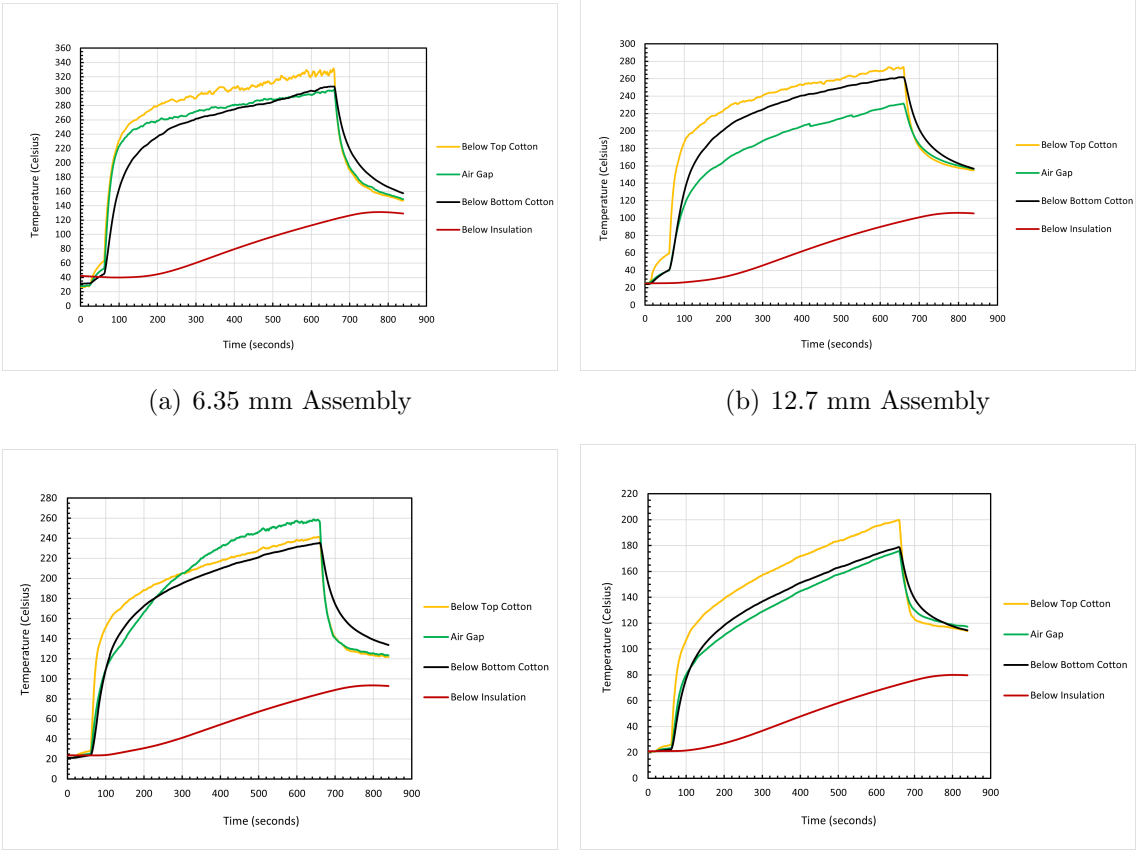

(a) 6.35 mm Assembly

(b) 12.7 mm Assembly

(c) 19.05 Assembly

(d) 25.4 mm Assembly

Figure B.6: Temperature versus Time for the Cotton Sleeve Assemblies with an Air Gap at 10 kW/m^2 Heat Flux

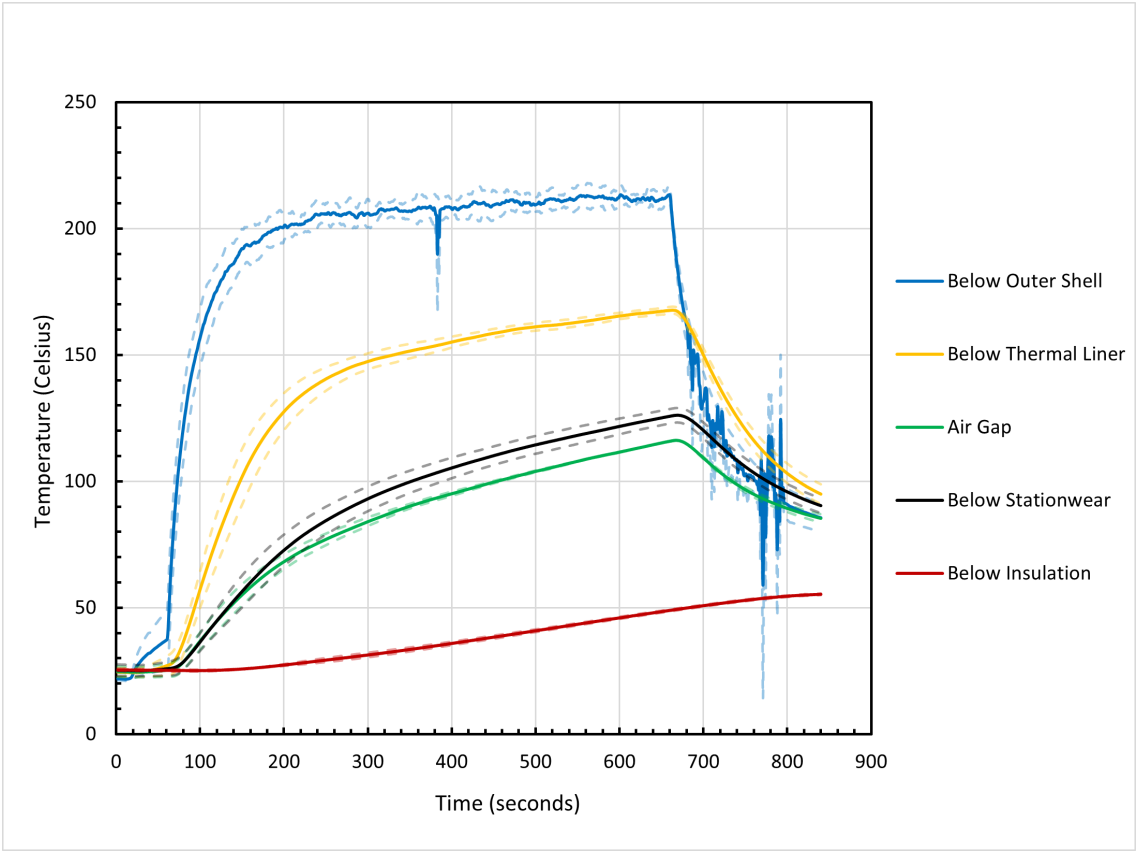

Figure B.7: Temperature versus Time for the PPE Sleeve Assembly with a 12.7 mm Air Gap at 5 kW/m^2 Heat Flux

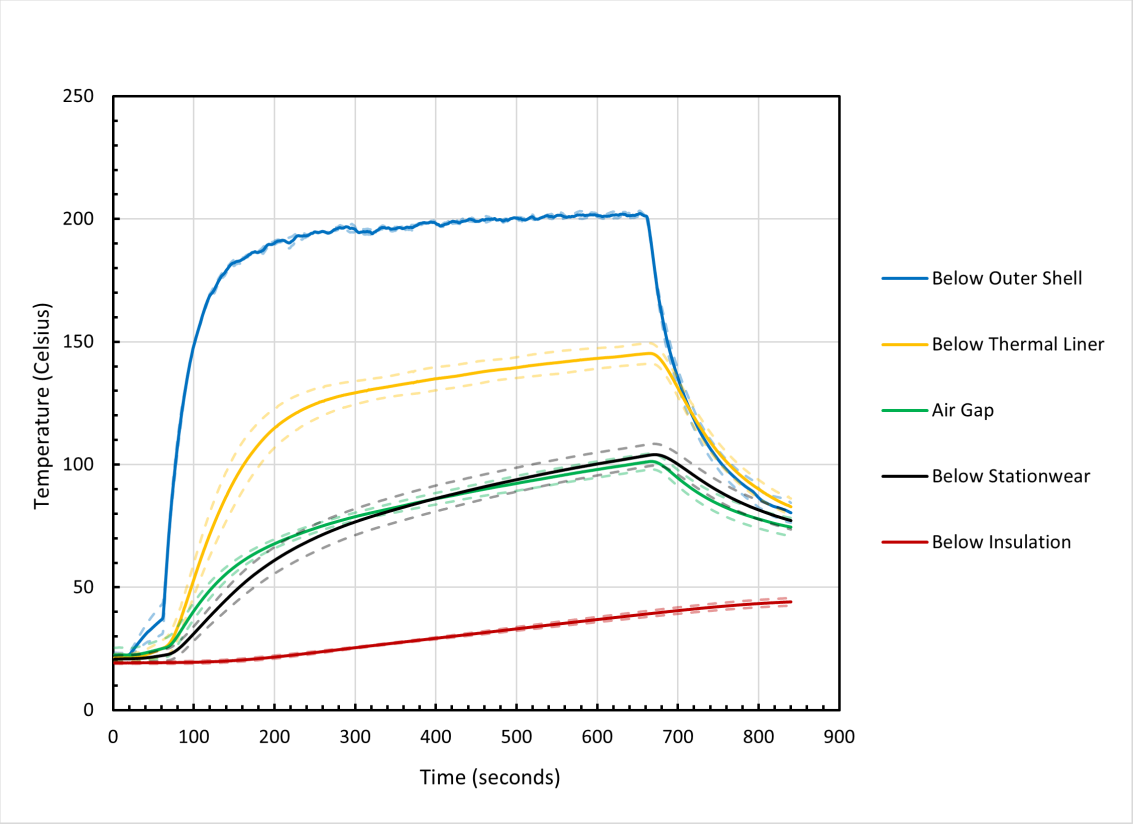

Figure B.8: Temperature versus Time for the PPE Sleeve Assembly with a 19.05 mm Air Gap at 5 kW/m^2 Heat Flux

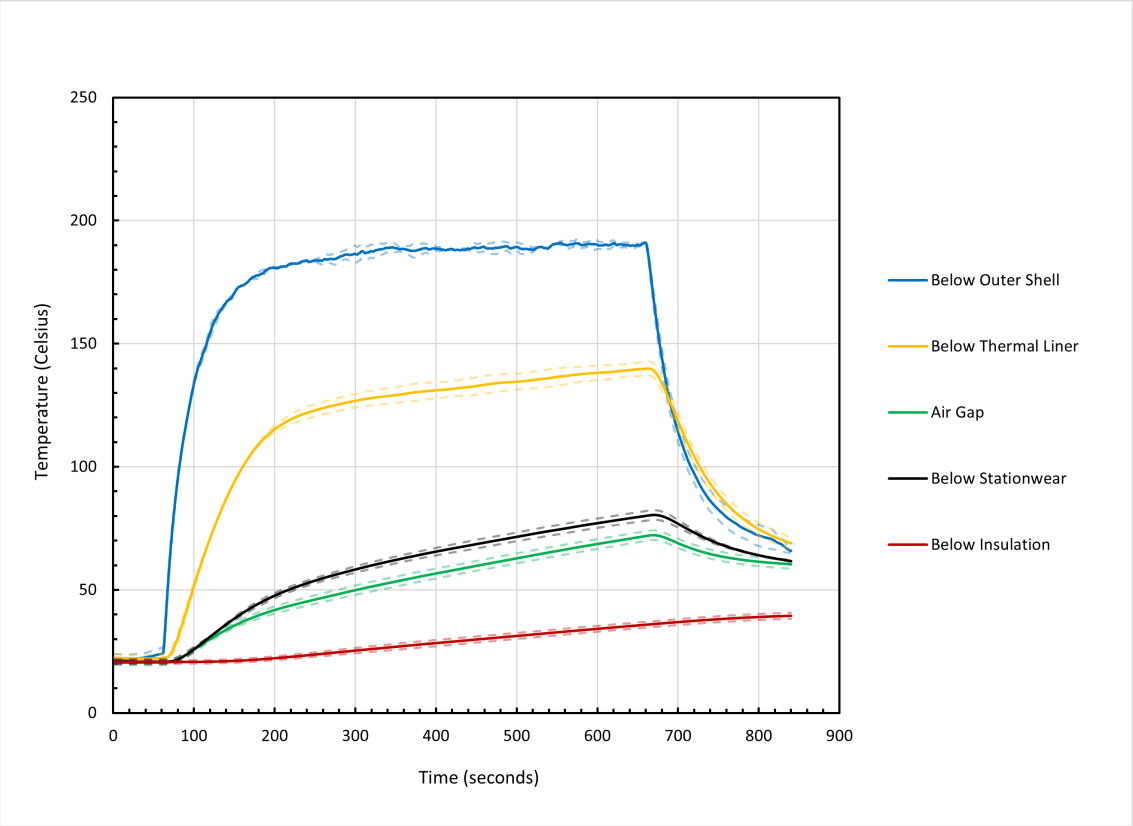

Figure B.9: Temperature versus Time for the PPE Sleeve Assembly with a 25.4 mm Air Gap at 5 kW/m^2 Heat Flux

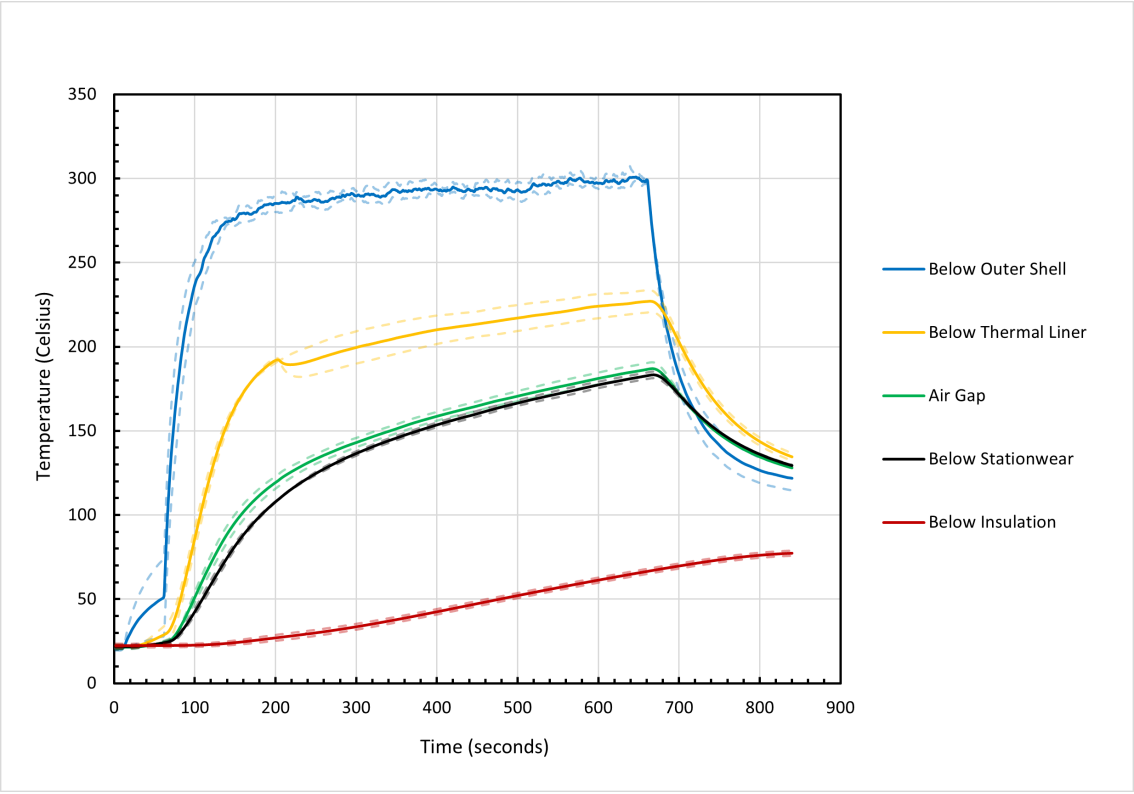

Figure B.10: Temperature versus Time for the PPE Sleeve Assembly with a 12.7 mm Air Gap at 10 kW/m^2 Heat Flux

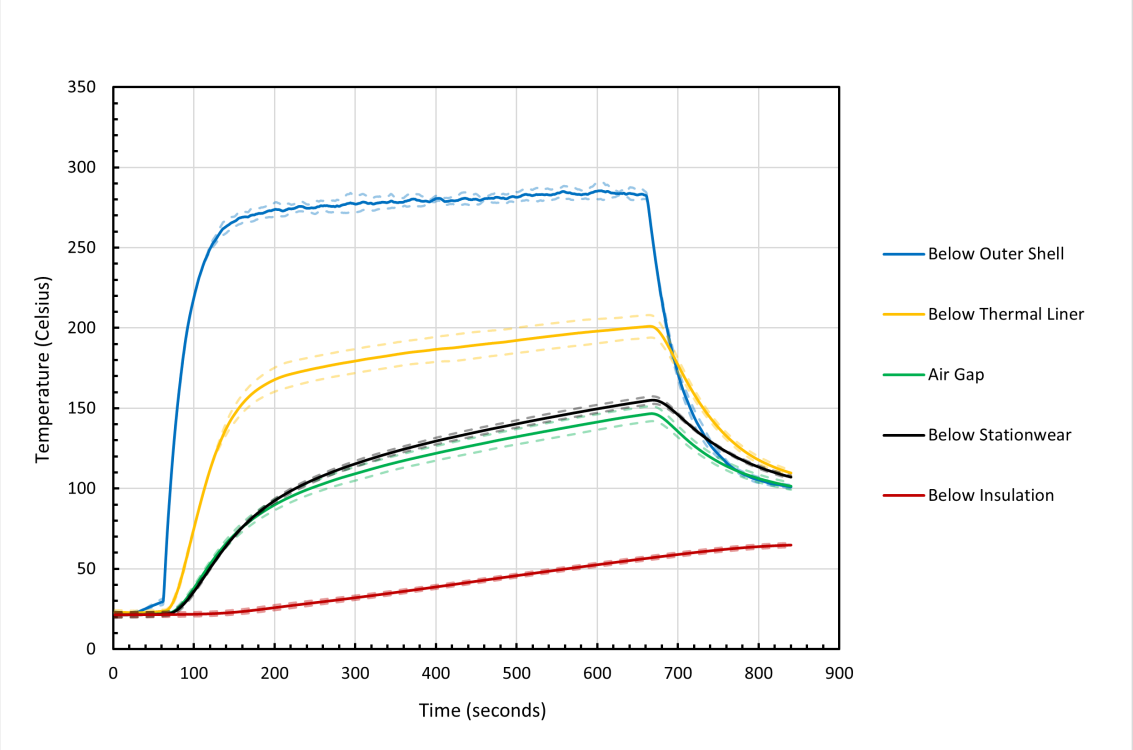

Figure B.11: Temperature versus Time for the PPE Sleeve Assembly with a 19.05 mm Air Gap at 10 kW/m^2 Heat Flux

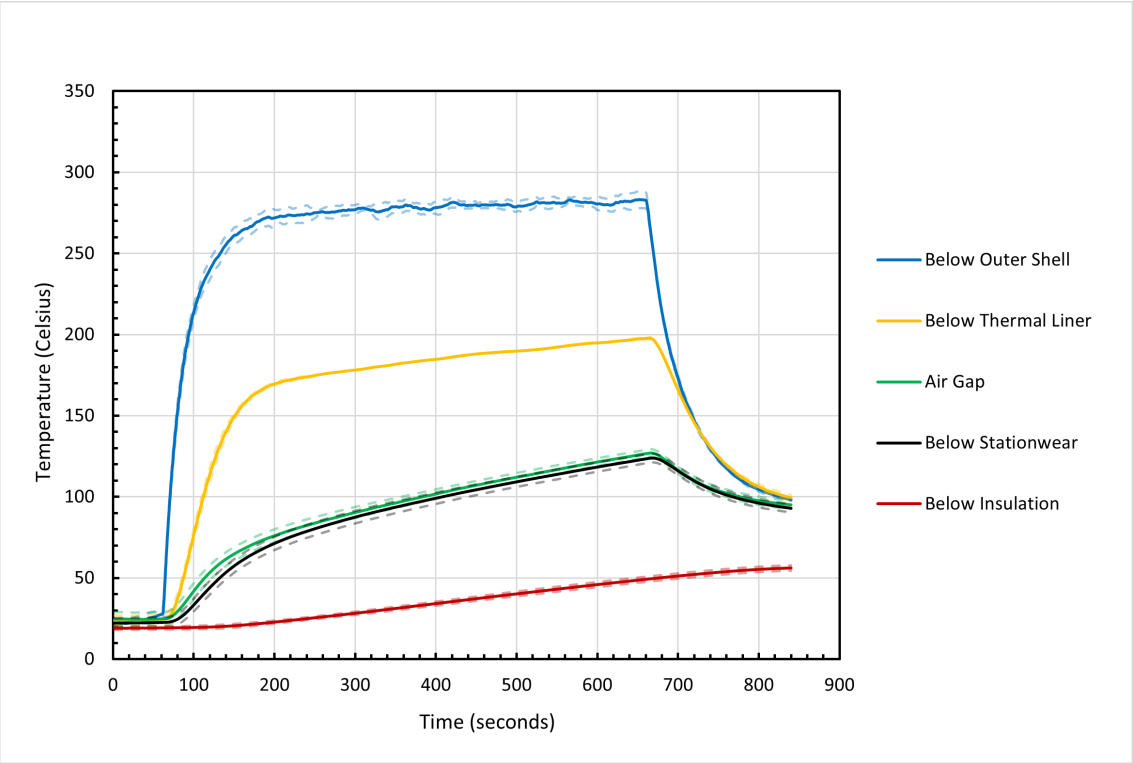

Figure B.12: Temperature versus Time for the PPE Sleeve Assembly with a 25.4 mm Air Gap at 10 kW/m^2 Heat Flux

Bibliography

[1] Fire-Related Firefighter Injuries Reported to the National Fire Incident Reporting System (2015-2017). 20(2), 2019.

[2] D.T. Butry, D. Webb, S. Gilbert, and J. Taylor. The Economics of Firefighter Injuries in the United States. NIST Technical Note 2078, National Institute of Standards and Technology, December 2019.

[3] Fire Dynamics. National Institute of Standards and Technology, Retrieved April 25, 2022, From https://www.nist.gov/el/fire-research-division-73300/firegov-fire-service/fire-dynamics, 2021.

[4] D. Madrzykowski. Standards in Biologic Lesions: Cutaneous Thermal Injury and Inhalation Injury Working Group 2018 Meeting Proceedings. 41(3):604–611, 2019. doi: https://doi.org/10.1093/jbcr/irz207.

[5] J.M. Willi, G.P. Horn, and D. Madrzykowski. Characterizing a Firefighter's Immediate Thermal Environment in Live-Fire Training Scenarios. 52(6):1667–1696, 2016. doi: https://doi.org/10.1007/s10694-015-0555-1.

[6] G. Song, S. Paskaluk, R. Sati, E.M. Crown, J.D. Dale, and M. Ackerman. Thermal Protective Performance of Protective Clothing Used for Low Radiant Heat Protection. 81(3):311–323, 2011. doi: https://doi.org/10.1177/0040517510380108.

[7] *NFPA 1971: Standard on Protective Ensembles for Structural Fire Fighting and Proximity Fire Fighting*. National Fire Protection Association, 2018.

[8] Turnout Gear. Firefighter One, Retrieved April 25, 2022, From https://www.ff1.com/collections/ppe/products/fxr-custom-turnout-gear-set, 2022.

[9] Turnout Gear Composition. PR Web, Retrieved April 25, 2022, From http://www.prweb.com/releases/dupont_protection_tech/lion_turnout_gear/prweb10362363.htm, 2013.

[10] Turnout Gear Materials. Globe Holding Company, LLC., Retrieved April 25, 2022, From https://globe.msasafety.com/materials#:

~:text=Turnout%20Gear%20Materials%20NFPA-certified%20turnout%20gear%20consists%20of,liner%20with%20each%20layer%20performing%20a%20critical%20function, 2021.

[11] Celazole® PBI (polybenzimidazole). Performance Plastics, Retrieved April 25, 2022, https://performanceplastics.com/materials/pbi/#:~:text=PBI%20is%20an%20engineered%20thermoplastic%20that%20has%20exceptional,be%20molded%20for%20use%20in%20high%20performance%20applications.

[12] Nomex® for Turnout Gear. DuPont, Retrieved April 25, 2022, From https://www.dupont.com/personal-protection/firefighter-turnout-gear.html, 2021.

[13] Nomex® and Kevlar® for Emergency Response. DuPont, Retrieved April 25, 2022, From https://www.dupont.com/personal-protection/emergency-response-protective-equipment.html, 2021.

[14] Material Selection Guide. Fire-Dex, LLC., Retrieved April 25, 2022, From https://www.firedex.com/materialselection/#Moisture, 2021.

[15] Understanding Key Turnout Gear Tests. Fire Rescue 1, Retrieved April 25, 2022, From https://www.firerescue1.com/fire-products/fire-eyewear/articles/understanding-key-turnout-gear-tests-NZfvEL0uE27iYnEp/, 2006.

[16] What is ePTFE? Gallagher Fluid Seals, Inc., Retrieved April 25, 2022, From https://www.gallagherseals.com/blog/what-is-eptfe, 2021.

[17] W.L. Hosch. Aramid. Britannica, Retrieved April 25, 2022, From https://www.britannica.com/science/aramid/additional-info#history, 2009.

[18] G. Song, S. Mandal, and R.M. Rossi. *Thermal Protective Clothing for Firefighters*. Woodhead Publishing, 2017. ISBN 978-0-08-101285-7.

[19] T.L. Bergman and A.S. Lavine. *Fundamentals of Heat and Mass Transfer*. Wiley, 8th edition, 2017. ISBN 978-1-119-35388-1.

[20] Convective Heat Transfer-Natural and Forced Convection. Smlease Design, Retrieved April 25, 2022, From https://www.smlease.com/entries/thermal-design/convection-convective-heat-transfer/, 2018.

[21] C.J. Wieczorek and N.A. Dembsey. *Predicting 1st and 2nd Degree Skin Burns from Thermal Radiation*. Society of Fire Protection Engineers, 2000. ISBN 978-0-925223-01-2.

[22] J.R. Lawson, W.D. Walton, N.P. Bryner, and F.K. Amon. Estimates of Thermal Properties for Fire Fighters' Protective Clothing Materials. NISTIR 7282, National Institute of Standards and Technology, Gaithersburg, Maryland, June 2005.

[23] A.M. Stoll and M.A. Chianta. A Method and Rating System for Evaluation of Thermal Protection. 40(11):1232–1237, November 1969.

[24] *ISO17492: Clothing for protection against heat and flame-determination of heat transmission on exposure to both flame and radiant heat*. International Organization for Standardization, 2nd edition, 2019.

[25] *ASTMF1868: Standard Test Method for Thermal and Evaporative Resistance of Clothing Materials Using a Sweating Hot Plate*. American Society for Testing and Materials, 2017.

[26] J.R. Lawson and W.H. Twilley. Development of an Apparatus for Measuring the Thermal Performance of Fire Fighters' Protective Clothing. NISTIR 6400, National Institute of Standards and Technology, Gaithersburg, Maryland, October 1999.

[27] D.W. Stroup, R.A. McLane, and W.H. Twilley. Full Ensemble and Bench Scale Testing of Fire Fighter Protective Clothing. NISTIR 7467, National Institute of Standards and Technology, Gaithersburg, Maryland, November 2007.

[28] K. Prasad, W.H. Twilley, and J.R. Lawson. Thermal Performance of Fire Fighters' Protective Clothing. 1. Numerical Study of Transient Heat and Water Vapor Transfer. NISTIR 6881, National Institute of Standards and Technology, Gaithersburg, Maryland, August 2002.

[29] K. Prasad, H.M.H. Dac, and S. Kukuck. Thermal Performance of Fire Fighters' Protective Clothing. 2. Protective Clothing Performance Simulator - User's Manual. NISTIR 6901, National Institute of Standards and Technology, Gaithersburg, Maryland, January 2003.

[30] S. Kukuck and K. Prasad. Thermal Performance of Fire Fighters' Protective Clothing. 3. Simulating a TPP Test for Single-Layered Fabrics. NISTIR 6993, National Institute of Standards and Technology, Gaithersburg, Maryland, January 2003.

[31] D.A. Torvi and Dale J.D. Heat Transfer in Thin Fibrous Materials Under High Heat Flux. 35(3):210–231, 1999. doi: https://doi.org/10.1023/A:1015484426361.

[32] J.R. Lawson and Mell W.E. A Heat Transfer Model for Firefighters' Protective Clothing. 36(1):39–68, 2000. doi: https://doi.org/10.1023/A:1015429820426.

[33] P. Chitrphiromsri and Kuznetsov A.V. Modeling Heat and Moisture Transport in Firefighter Protective Clothing During Flash Fire Exposure. 41:206–215, 2005. doi: https://doi.org/10.1007/s00231-004-0504-x.

[34] H.H. Pennes. Analysis of Tissue and Arterial Blood Temperatures in the Resting Human Forearm. 1(2):93–122, 1948. doi: https://doi.org/10.1152/jappl.1998.85.1.5.

[35] F.C. Henriques Jr and A.R. Moritz. The Predictability and the Significance of Thermally Induced Rate Processes Leading to Irreversible Epidermal Injury. 43(5):489–502, 1947.

[36] G. Song, R.L. Barker, H. Hamouda, A.V. Kuznetsov, P. Chitrphiromsri, and R.V. Grimes. Modeling the Thermal Protective Performance of Heat Resistant Garments in Flash Fire Exposures. 74(12):1033–1040, 2004. doi: https://doi.org/10.1177/004051750407401201.

[37] G. Song. Clothing Air Gap Layers and Thermal Protective Performance in Single Layer Garment. 36(3):193–205, 2007. doi: https://doi.org/10.1177/1528083707069506.

[38] G. Song, P. Chitrphiromsri, and D. Ding. Numerical Simulations of Heat and Moisture Transport in Thermal Protective Clothing Under Flash Fire Conditions. 14(1):89–106, 2008. doi: https://doi.org/10.1080/10803548.2008.11076752.

[39] A. Ghazy and Bergstrom D.J. Numerical Simulation of Transient Heat Transfer in a Protective Clothing System During a Flash Fire Exposure. 58(9):702–724, 2010. doi: https://doi.org/10.1080/10407782.2010.516691.

[40] A. Ghazy and Bergstrom D.J. Numerical Simulation of Heat Transfer in Firefighters' Protective Clothing with Multiple Air Gaps During Flash Fire Exposure. 61(8):569–593, 2012. doi: https://doi.org/10.1080/10407782.2012.666932.

[41] A. Ghazy. Numerical Study of the Air Gap Between Fire-Protective Clothing and the Skin. 44(2):257–274, 2014. doi: https://doi.org/10.1177/1528083713483784.

[42] L.K. McCarthy. Evaluation of the Thermal Performance of Fire Fighter Protective Clothing with the Addition of Phase Change Material. Master's thesis, University of Maryland, College Park, Maryland, 2010.

[43] B.W. Hendrickson. The Impact of a Variable Air Gap on the Thermal Performance of Firefighter Protective Clothing. Master's thesis, University of Maryland, College Park, Maryland, 2011.

[44] J.A. Perry. Thermal Degradation of Firefighter Turnout Gear Due to the Effects of Moisture. Master's thesis, University of Maryland, College Park, Maryland, 2011.

[45] J.P. White. An Experimental Analysis of Firefighter Protective Clothing: The Influences of Moisture and a Thermally Activated Expanding Air-Gap. Master's thesis, University of Maryland, College Park, Maryland, 2012.

[46] D.A. Yates. Design and Evaluation of a Thermally Responsive Firefighter Turnout Coat. Master's thesis, University of Maryland, College Park, Maryland, 2012.

[47] M. Fu, M.Q. Yuan, and W.G. Weng. Modeling of Heat and Moisture Transfer Within Firefighter Protective Clothing with the Moisture Absorption of Thermal Radiation. 96:201–210, 2015. doi: https://doi.org/10.1016/j.ijthermalsci.2015.05.008.

[48] D. Madrzykowski and A. Makitka. Thermal Conductivity Measurements of Fabrics Measured Using the Linseis Transient Hot Bridge (THB). Technical report, UL Firefighter Safety Research Institute, 2018.

[49] SG-200 Fiberglass Composite. Röchling Glastic Composites, Inc., Retrieved April 25, 2022, From https://www.mcmaster.com/5308N15/, 2022.

[50] FiberFrax Duraboard 2600. Unifrax, Retrieved April 25, 2022, From https://www.unifrax.com/product/fiberfrax-duraboard-2600-insulation/, 2022.

[51] M. DiDomizio. *Experimental Study of Thermal Degradation of Fire Resisting Compartment Partitions in Fires)*. PhD thesis, University of Waterloo, Waterloo, Ontario, 2017.

[52] M.T. Wilson, B.Z. Dlugogorski, and E.M. Kennedy. Uniformity of Radiant Heat Fluxes in Cone Calorimeter. 7:815–826, 2003. doi: http://dx.doi.org/10.3801/IAFSS.FSS.7-815.

[53] Self-Adhesive Polyimide Fast Response Surface Thermocouples. Omega, Retrieved April 25, 2022, From https://www.omega.com/en-us/temperature-measurement/temperature-surface-sensors/p/SA1, 2022.

[54] *ASTME1354: Standard Test Method for Heat and Visible Smoke Release Rates for Materials and Products Using an Oxygen Consumption Calorimeter*. American Society for Testing and Materials, West Conshohocken, PA, 2017.

[55] Fox 200. TA Instruments, Retrieved April 25, 2022, From https://www.tainstruments.com/fox-200/, 2022.

[56] K.B. McGrattan, R.J. McDermott, C.G. Weinschenk, and G.P. Forney. *Fire Dynamics Simulator User's Guide*. Gaithersburg, Maryland, 6th edition, November 2021.

[57] K.B. McGrattan, R.J. McDermott, C.G. Weinschenk, and G.P. Forney. *Fire Dynamics Simulator Technical Reference Guide Volume 1: Mathematical Model*. Gaithersburg, Maryland, 6th edition, November 2021.

[58] K.B. McGrattan, R.J. McDermott, C.G. Weinschenk, and G.P. Forney. *Fire Dynamics Simulator Technical Reference Guide Volume 2: Verification*. Gaithersburg, Maryland, 6th edition, November 2021.